Decadal Evolution of Atmospheric Ozone and Remote Sensing of Tropospheric Ozone

Thesis by

Yibo Jiang

In Partial Fulfillment of the Requirements

for the Degree of

Doctor of Philosophy

Caltech

Pasadena, California

1997

(Submitted May 20, 1997)

Acknowledgements

First I would like to thank my advisor Professor Yuk L. Yung, for all of his patient guidance, encouragement, support, creativity, humor, editorial advice, and many enjoyable conversations. His fundamental understanding of the problems, encouragement for new ideas and advice were essential to this work. I would like to thank Professor Andrew P. Ingersoll, who served as my academic advisor, for his advise over the years. I would also like to thank Mark Allen for his guidance in the developing and debugging of the Caltech/JPL model. Thanks go to Stan Sander, Rich Cageao, Rich Zurek, Glory Manney at JPL for all the discussions and reviewing of the papers. In addition, I would like to thank Kay Campbell, Irma Betters, and Tammie Henderson for their gracious assistance during my stay here.

And of course, I would like to thank all the other people I have been fortunate to know in the time I have been here: Rich Dissly, Steven Leroy, Hari Nair, Albert Haldmann, David Kass, Frank Mills, Anthony Lee, Adam Showman, Rob Kursinski, Charle Qi, Jimmy Kuang, and many more. Thanks for all the good times we have shared, it was memorable and fun. I hope you have found my acquaintance as rewarding as I have found yours.

I can never express all the love and encouragement from my parents, my wife Ruiqian Li and my lovely daughter Sue Jiang who has been counting on her fingers when I can graduate.

Overview

Monitoring and preservation of the Earth's ozone layer has engaged scientists intensively in th 20th century especially after the discovery of the Antarctic ozone hole by Farman *et al.* (1985). There is increasing evidence that ozone depletion occurs on a global scale such as in the Arctic and at midlatitudes. Following the understanding of the the catalytic destruction of ozone in the stratosphere by chlorine derived from chlorofluorocarbons (CFC's), there is a growing realization that the consequences of anthropogenic pollution can be felt in unpredictable ways in near and faraway places.

The atmosphere is a complex mixture of more than a thousand trace chemicals that are constantly reacting and redistributing. The need to understand the sources and distribution of these chemicals, along with the mechanisms by which they are transformed, transported, and ultimately removed from the atmosphere, has grown in parallel with the increased concern about air pollution and its consquences. Therefore, the exploration of the mechanism controlling both spatial and temporal variation of the atmosphere is a key component of the atmosphere science research (as part of the global change) and it requires an interdisciplinary approach and innovative application of the traditional techniques of chemistry, physics, and meteorology.

Monitoring the composition of the troposphere and stratosphere globally is particularly interesting in this context for ozone which is the key component regulating the photochemistry of the atmosphere.

In chapter 1, the decadal evolution of the Antarctic ozone hole is studied by using ozone column amounts obtained by the total ozone mapping spectrometer (TOMS) in the southern polar region during late austral winter and spring (Days 240 – 300) for

1980 – 1991 using area-mapping techniques and area-weighted vortex averages. The vortex here is defined using the -50 PVU (1 PVU $= 1.0 \times 10^{-6}$K $kg^{-1}\, m^2\, s^{-1}$) contour on the 500 K isentropic surface. The principal result is that there is a distinct change after 1985 in the vortex averaged column ozone depletion rate during September and October, the period of maximum ozone loss. The mean ozone depletion rate in the vortex between Day 240 and the day of minimum vortex-averaged ozone is about 1 DU/day at the beginning of the decade, increasing to about 1.8 DU/day by 1985, and then apparently saturating thereafter. The vortex-average column ozone during September and October has declined at the rate of 11.3 DU/yr (3.8%) from 1980 to 1987 (90 DU over 8 yrs), and at a smaller rate of 2 DU/yr (0.9%) from 1987 to 1991 (10 DU over 5 years, excluding the anomalous year 1988). We interpret the year-to-year trend in the ozone depletion rate during the earlier part of the decade as due to the rise of anthropogenic chlorine in the atmosphere. The slower trend at the end of the decade indicates saturation of ozone depletion in the vortex interior, in that chlorine amounts in the mid-80s were already sufficiently high to deplete most of the ozone in air within the isolated regions of the lower stratospheric polar vortex. In subsequent years, increases in stratospheric chlorine may have enhanced wintertime chemical loss of ozone in the south polar vortex even before major losses during the Antarctic spring.

In chapter 2, we will show that standard deviation of column ozone from the zonal mean (COSDZ) provides a measure of the longitudinal inhomogeneity in column ozone and dynamical wave activities in the atmosphere. We point out that simulation of this quantity by three-dimensional (3-D) models could provide a sensitive check on the wave activities in the stratosphere that are responsible for ozone transport. Analysis of the Total Ozone Mapping Spectrometer (TOMS) data shows a profound secular change in COSDZ from 1979 to 1992. The changes are not symmetric between the

southern and northern atmospheres. In the southern higher latitudes, COSDZ shows a significant increase around 65° in August and September, while the changes are much smaller in the northern higher latitudes in the boreal spring. We interpret most of the observed changes to be caused by enhanced ozone losses in the polar vortices in the springtime of the two respective hemispheres. There is also evidence for secular dynamical changes at mid-latitudes.

In chapter 3, an estimate of tropospheric ozone levels over tropical pacific south America is obtained from the difference in the TOMS (Total Ozone Mapping Spectrometer) data between the high Andes and the Pacific Ocean. From 1979 to 1992 tropospheric ozone apparently increased by 1.47 ± 0.40 %/yr or 0.21 ± 0.06 DU/yr over South America and the surrounding oceans. An increase in biomass burning in the Southern Hemisphere can account for this trend in tropospheric ozone levels.

Due to larger multiple scattering effects in the troposphere compared to that in the stratosphere, the optical path of tropospheric ozone is markedly enhanced (as compared with that of stratospheric ozone) in the Huggins bands from 310 nm to 345 nm. By using this principle, we model the direct and diffuse solar fluxes on the ground shows differences between tropospheric and stratospheric ozone in chapter 4. The characteristic signature of tropospheric ozone enables us to distinguish a change in tropospheric ozone from that of stratospheric ozone. A simple retrieval algorithm is used to recover the tropospheric column ozone from simulated data.

Light reflected or transmitted by a planetary atmosphere contains information about the particles and molecules in the atmosphere. Therefore, accurately calculating the radiation field is necessary. In the appendix, the doubling-adding method for plane-parallel polarized radiative transfer model is studied in detail. A special Fourier expansion leading to a compact notation is developed for the azimuth-dependent quantities. The multi-layer model for a vertically inhomogeneous atmosphere is im-

plemented and several numerical results are presented for verification and comparison. Preliminary runs from this model in the Huggins bands show the distinct features of linear polarization in the reflection spectrum due to the multiple Rayleigh scattering in the troposphere.

Contents

List of Figures

List of Tables

Chapter 1 Decadal Evolution of the Antarctic Ozone Hole

Yibo Jiang, Yuk L. Yung

Division of Geological and Planetary Sciences

California Institute of Technology

Pasadena, CA 91125

and

Richard W. Zurek

Earth and Space Sciences Division

Jet Propulsion Laboratory

California Institute of Technology

Pasadena, CA 91109

Published in modified form in *J. Geophys. Res.* **101**, 8985-8999, 1996.

Contribution number 5465 from the Division of Geological and Planetary Sciences,

California Institute of Technology.

Abstract

Ozone column amounts obtained by the total ozone mapping spectrometer (TOMS) in the southern polar region are analyzed during late austral winter and spring (Days 240 – 300) for 1980 – 1991 using area-mapping techniques and area-weighted vortex averages. The vortex here is defined using the -50 PVU (1 PVU = 1.0×10^{-6}K $kg^{-1}\,m^2\,s^{-1}$) contour on the 500 K isentropic surface. The principal result is that there is a distinct change after 1985 in the vortex averaged column ozone depletion rate during September and October, the period of maximum ozone loss. The mean ozone depletion rate in the vortex between Day 240 and the day of minimum vortex-averaged ozone is about 1 DU/day at the beginning of the decade, increasing to about 1.8 DU/day by 1985, and then apparently saturating thereafter. The vortex-average column ozone during September and October has declined at the rate of 11.3 DU/yr (3.8%) from 1980 to 1987 (90 DU over 8 yrs), and at a smaller rate of 2 DU/yr (0.9%) from 1987 to 1991 (10 DU over 5 years, excluding the anomalous year 1988). We interpret the year-to-year trend in the ozone depletion rate during the earlier part of the decade as due to the rise of anthropogenic chlorine in the atmosphere. The slower trend at the end of the decade indicates saturation of ozone depletion in the vortex interior, in that chlorine amounts in the mid-80s were already sufficiently high to deplete most of the ozone in air within the isolated regions of the lower stratospheric polar vortex. In subsequent years, increases in stratospheric chlorine may have enhanced wintertime chemical loss of ozone in the south polar vortex even before major losses during the Antarctic spring.

1.1 Introduction

The dramatic decrease of the total column of ozone over Antarctica in southern late winter and spring (August through November), a phenomenon known as the Antarctic ozone hole, was first described using observations made with Dobson spectrophotometer on the ground [*Farman et al.*, 1985] and later by satellite observations [*Stolarski et al.*, 1986]. It is now understood that the Antarctic ozone depletion is caused by catalytic chlorine chemistry in the lower stratosphere, where low temperatures prevail due to the special geography and meteorology of the Antarctic regions (e.g., Fig. 1.1). This cold air in the lower stratosphere at high southern latitudes permits the formation and persistence of polar stratospheric clouds (PSCs). Heterogeneous chemistry on these ice clouds, followed by the action of sunlight, converts reservoir species of chlorine (HCl and $ClONO_2$) into very reactive radicals such as Cl and ClO [*McElroy et al.*, 1986a, 1986b; *Molina et al.*, 1987b; *Toon et al.*, 1986; *Tolbert et al.*, 1987]. The presence of these chlorine radicals [*de Zafra et al.*, 1987], particularly of ClO and its anti-correlation with O_3, has been confirmed by *in situ* measurements from aircraft [*Anderson et al.*, 1989a, 1989b, 1991] and by remote sensing from the Upper Atmosphere Research Satellite (UARS) [*Manney et al.*, 1993a; *Waters et al.*, 1993a, 1993b]. While there is little doubt of the key role played by heterogeneous chemical reactions involving stratospheric chlorine, the quantitative aspects of the mechanisms involved in producing the Antarctic ozone hole are still the subjects of intense study and observation. This is due principally to the effects of dynamics on the temperature (and thus the ice cloud microphysics) and on the distributions of chemical trace gases and their exposure to sunlight [*Solomon et al.*, 1986; *Bojkov*, 1986; *Mahlman et al.*, 1986; *Tung et al.*, 1986; *Garcia* and *Solomon*, 1987; *McIntyre*, 1989; *Solomon*, 1990; *Schoeberl et al.*, 1991, 1992; *Tung* and *Yang*, 1994a, 1994b; *Yang* and *Tung*, 1994]. These effects vary from year to year and thus complicate attempts to interpret the

observed 30% to 60% decline in total column ozone amounts during the last decade. A thorough discussion of the Antarctic ozone hole was given by Solomon [1988, 1990] and WMO [1988, 1989, 1991]

In this paper we examine the record of total column ozone variations observed by the Total Ozone Mapping Spectrometer (TOMS) over the period 1980 – 1991. Past analyses of the Antarctic ozone depletion have tended to use the ozone minimum values or zonal averages when examining decadal trends [*Bowman*, 1985, 1988, 1990; *Herman et al.*, 1991,1993; *Krueger et al.*, 1992; *Stolarski et al.*, 1991, 1992]. Other analyses have focused on interannual variations in the ozone minimum values and have found potential links to phenomena associated with the Quasi-Biennial Oscillation (QBO) [e.g., *Garcia* and *Solomon*, 1987; *Lait et al.*, 1989]. More recently, Randel and Wu [1995] examined trends in ozone by first averaging TOMS data along potential vorticity (PV) contours in order to account for displacement and longitudinal asymmetries of the polar vortex. Another natural coordinate for these purposes is ozone itself. Here we will use the ozone area-mapping technique first applied to Antarctic ozone by Yung *et al.* [1990] to re-examine the decline rates of Antarctic springtime column ozone from 1980 to 1991, emphasizing both general and year-to-year changes over that period. A key modification of the previous application of this technique is to constrain the ozone area mapping to the south polar vortex using values of potential vorticity (PV) derived from National Meteorological Center (NMC) data for the same period.

In section II, we first briefly describe the data we used. The area-mapping method is described in section III. Then, in section IV, we present our main results obtained from the TOMS ozone data using the area-mapping method in combination with the use of PV and of area-mapped NMC temperatures in the polar vortex. Two

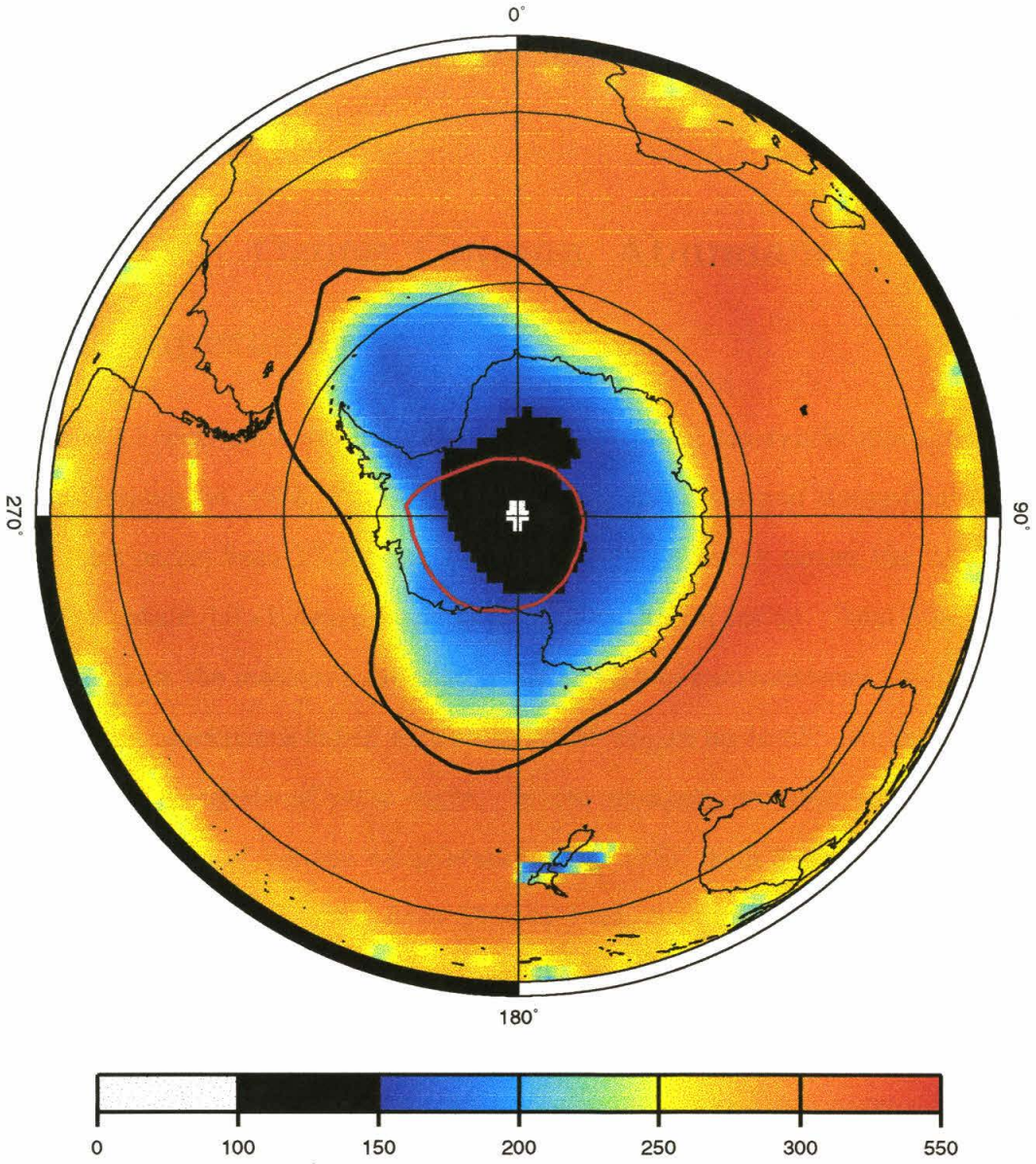

Figure 1.1: Southern polar orthographic projection of ozone column abundance (DU) on Day 275 (October 2) 1987. There are no TOMS data in the white area. The area bound by the 300 DU contour is 13% of the area of the southern hemisphere. The smaller and larger circles are located at $-60°$ and $-30°$ latitudes, respectively. The heavy red line indicates regions where the temperature is below 195 K on the 500 K isentropic surface and PSCs may form. The -50 PVU contour of PV (heavy dark line) at 500 K, used to define the polar vortex, is also shown.

important features emerging from the analysis are a distinct change in the decline rate of vortex-averaged column ozone after 1986 and the anomaly represented by the 1988 Antarctic spring.

1.2 TOMS Ozone Column Abundance, PV and Temperature

The Nimbus 7 spacecraft was launched into a local-noon, sun-synchronous, near-polar orbit on October 24, 1978. Its TOMS instrument has measured the spatial distribution of total ozone from 1978 until May 6, 1993 by scanning across the track of the satellite to obtain data between successive satellite orbital tracks. Total column ozone is retrieved from the measured differential absorption of backscattered ultraviolet irradiance using observations taken with solar zenith angles up to 88°. No measurements are available in regions of polar night. In our analysis, we used the daily TOMS gridded ozone data of Version 6.0 [*Herman et al.*, 1991] from NASA (on a 1° × 1.25° grid in latitude and longitude) from 1980 to 1991. The 1979 data were not used in our analysis mainly due to frequently missing data (e.g. Day 277, 278, 279) in this year.

The other two data sets used are NMC temperatures and Rossby-Ertel PV [*Manney* and *Zurek*, 1993b] derived from NMC analyses of temperature and geopotential heights [e.g., *Gelman et al.*, 1986]. The PV and temperature fields are gridded at 2.5° × 5.0° in latitude and longitude. In our study, we will use temperature and PV fields on the 500 K isentropic surface to help interpret variations in the total column ozone. This level is in the lower stratosphere near the ozone number density peak in early August, prior to the formation in recent years of the ozone hole during the austral spring.

1.3 Area-Mapping Method

The ozone area-mapping method used here was described by Yung *et al.* [1990] and is similar to that used in area mapping of Ertel's potential vorticity on an isentropic surface [*Butchart* and *Remsberg*, 1986; *Baldwin et al.*, 1988]. Let $A(t, \Omega^*)$ be the area enclosed by any contour value $\Omega^*(\vec{r}, t)$ of ozone column abundance, as a function of time (t) and position ($\vec{r}$) on the surface of the Earth. A convenient unit for the area bound by an ozone isopleth is the area of the southern hemisphere, $2\pi R^2$ (R is the radius of Earth). For comparison, the areas out to the Antarctic circle and -60° latitude circle are 0.079 and 0.13, respectively, while the area of the Antarctica continent, including the ice shelf, is 5.5% of the area of the southern hemisphere.

Since total column ozone generally changes monotonically outward from a minimum in the interior to the edge of the polar vortex, an area increase (decrease) of a total column ozone isopleth with time implies that the ozone hole (i.e., the region of lowest column ozone) is expanding (shrinking). This result holds no matter where the center of ozone hole is. Thus, to first order, this method filters out planetary-scale (i.e., low longitudinal wavenumber) perturbations of the Antarctic polar vortex such as distortions of the vortex or displacements away from the pole. We assume that the ozone column abundance in the south polar night region is smaller than that in the daylight region and only include daytime data in the area averages, adjusting the area weighting to include just the sunlit portions of the south polar regions. This has little effect on our analyses as we focus on the late winter and spring period when the area with no TOMS measurements is very small (e.g., Fig. 1.1).

The assumption of monotonic variation breaks down beyond the edge of the polar vortex, in the region of the total column ozone maxima in high mid-latitudes sometimes called the polar "collar" region. For some contours near the vortex boundary,

area-mapping would mix data points from outside of the vortex with that inside the vortex. Vortex-averaged quantities have been shown to be useful in examining the relationships between, for instance, ozone , temperature and ClO, at various heights in the lower stratosphere [e.g., *Manney et al.*, 1994a]. Randel and Wu [1995] recently mapped column ozone by averaging the TOMS data around PV contours at 520 K. The issue is how to apply a vortex constraint given that a definition of the polar vortex in terms of PV contours will vary with height and from year to year.

Because the total column ozone value is heavily weighted to the lower stratosphere [e.g., *Manney et al.*, 1994b; *Froidevaux et al.*, 1994], we have chosen to define the vortex using PV values there. By inspection, we have chosen a single value, namely -50 PVU (1 PVU $= 1.0 \times 10^{-6}\mathrm{K\,kg^{-1}}\,m^2\,s^{-1}$). In later years (1992 and 1993, not considered here), Chen [1994] found that this value, which was toward the poleward edge of the region of large PV gradients, defined an isolated inner vortex at 500 K. For the years and season considered here the -50 PVU contour is typically in the middle of the region of strong PV gradients on the 500 K isentropic surface and is outside the region of large ozone loss (Fig. 1.1), which makes it suitable for limiting the ozone area-mapping. Interannual variations of the area within this PV contour are representative of changes in vortex size and reflect at least indirectly variations in planetary wave activity, including minor warmings; these can affect both ozone transport and heterogeneous chemistry. To assess these effects more quantitatively requires consideration of vertical, as well as horizontal, variations in both ozone and PV and is beyond the scope of this paper.

1.4 Area Mapping of Ozone, PV and Temperature: Results and Discussion

1.4.1 Average column ozone: The ozone hole period

We will first investigate variations of area-averaged ozone column abundance inside the polar vortex. Figure 1.2 shows the temporal variations of the area-weighted average of ozone column abundance inside the polar vortex (solid line), as constrained by the location of the -50 PVU contour at 500 K. The time interval chosen for each year is from Day 240 (August 28 for non-leap year) to Day 300, corresponding to the period of maximum ozone depletion in each year. These vortex-constrained area-averages of column ozone are significantly larger than the minimum ozone column abundance [*e.g., Lait et al.*, 1989, Fig. 2a], as they include large regions of the vortex close to the boundary, where ozone values are higher (Fig. 1.1).

The dotted lines in Figure 1.2 indicates the area-weighted average of ozone column abundance, except for the region between 60°S and 90°S. Differences between this zonal and the vortex-limited average reflect the longitudinal asymmetry of the polar vortex and its seasonal decrease in area during southern spring. The latter is evident as a tendency for the zonal and vortex delimited averages to separate after September. As the vortex shrinks seasonally, the zonal average includes more of the higher ozone values outside the vortex. The short-period fluctuations (i.e., on the order of a few to several days) are more pronounced in the high-latitude zonal average. Similar, but smaller amplitude, fluctuations appear in the vortex-limited area-weighted column ozone. These fluctuations, often correlated with those of the zonal average, suggest that synoptic-scale disturbances of the vortex, of ozone in the vortex or of both are not totally filtered out by averaging within the vortex.

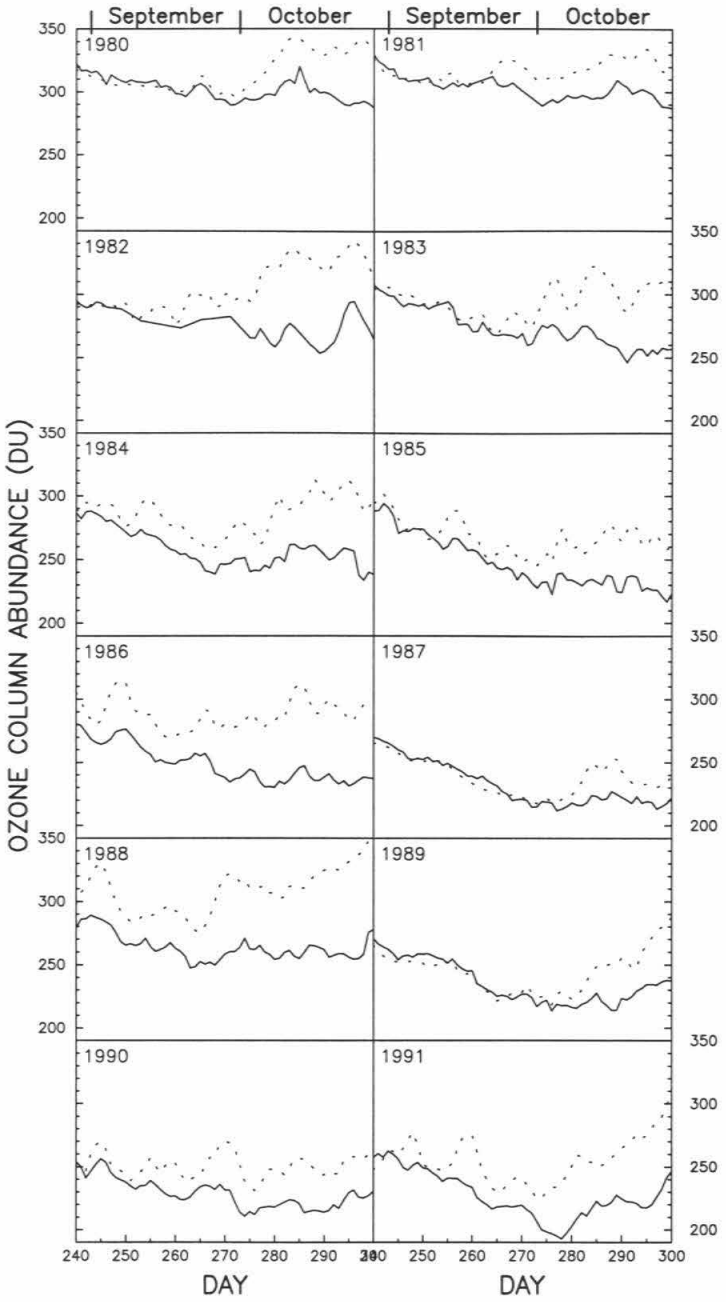

Figure 1.2: Area-weighted average ozone column abundance (DU) inside the polar vortex bound by PV contour of -50 PVU from day 240 to 300 for 1980 – 1991. Dotted lines denote area-weighted average ozone column abundance (DU) between 60°S and 90°S.

Both averages show the decline of column ozone in September – October over the last decade . The years 1986 and 1988 are notable in that the 60° latitude and vortex limited averages differ even in early September. These years were dynamically active [*Krueger et al.*, 1989; *Schoeberl et al.*, 1989; *Kanzawa* and *Kawaguchi*, 1990]: the vortex and ozone hole were, by southern hemisphere standards, often greatly distorted and displaced away from the geographic south pole. By contrast, the polar zonal and vortex averaged column ozone averages are remarkably similar in 1987 and 1989, indicating that in those years the vortex was nearly zonally symmetric and extended at least to 60°S.

Similar differences extend to other years as well, with the polar zonal and vortex area-weighted averages of column ozone agreeing more closely in September during odd, than during even, years. Furthermore, as seen in Figure 1.3, the vortex-limited average of column ozone tends to decrease significantly from 1981 to 1982, and 1983 to 1984, but with the column ozone averages relatively unchanged from 1980 to 1981, 1982 to 1983 and, until October, 1984 to 1985 . A different pattern follows in 1986, with ozone average values similar to those in 1985. These are followed by a significant decrease in September – October of 1987 but substantially increased values in 1988, when vortex-limited column ozone values are as high, or higher than, those for the same months in 1984. After the anomaly of 1988, the vortex-limited ozone average again declines, with the lowest averaged values occurring in October, 1991. In September the years 1990 and 1991 are reminiscent of the pattern in vortex-limited averaged column ozone before 1986. The lowest vortex-average ozone column abundance occurs in 1991. This result is consistent with that based on an analysis of the ozone minimum value in October [*Krueger et al.*, 1992]. Hofmann *et al.* [1992] argued that the penetration of volcanic aerosols from Pinatubo and Hudson into the polar vortex might have enhanced the depletion of ozone. However, Schoeberl *et al.* [1993]

showed that the polar vortex and the mid-latitude regions were nearly isolated from each other during the late August period. The issue of what caused the unusually low ozone in 1991 remains unresolved.

Figure 1.4 shows the vortex-average value of column ozone on Day 240, the minimum value before Day 290 (mid-October), and the day on which the minimum occurred for each year. As seen here and in Table 1.1, the minimum vortex-average column amount occurred in all years during the last week of September and the first week of October, except for 1988, when it occurred nearly a week earlier in mid-September.

The divergence of the Day 240 and the minimum value curves indicates that the average loss of ozone during this season early in the decade is about half that at the end of the decade, except for the anomalous year 1988. The "initial value" of vortex-average column ozone on Day 240 has declined by 20% over the decade. Recent observations by the Microwave Limb Sounder (MLS) on board UARS of higher ClO and lower ozone as early as mid-July [*Waters et al.*, 1993a, 1993b; *Santee et al.*, 1995] indicate that some chlorine activation and photochemical ozone loss occur in southern mid-winter. The depletion of ozone at this early time (while the geographic south pole is still in the dark) can occur because the south polar vortex is sufficiently large that its outer regions are in sunlight even during the period of polar night. Air there may be exposed to polar stratospheric clouds in the same regions or can move into the sunlit regions following exposure to PSCs in areas of polar night. The ensuing chemical loss of ozone in the sunlit portions of the vortex due to chlorine photochemistry could account, then, for the downward trend of vortex-average column ozone at the end of August.

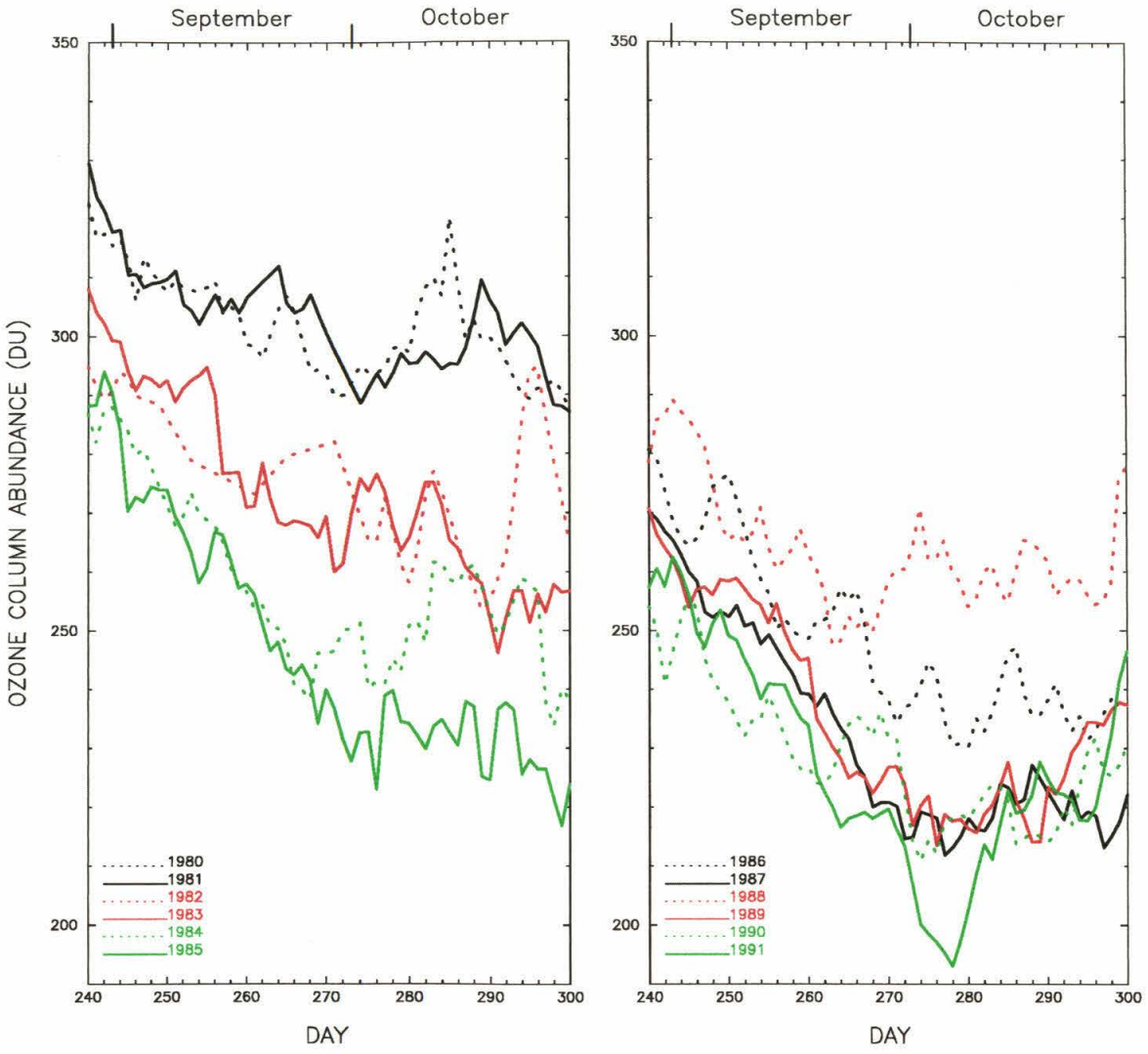

Figure 1.3: Alternative display of the solid lines from Figure 1.2. The solid lines are for the odd years; the dotted lines are for the even years.

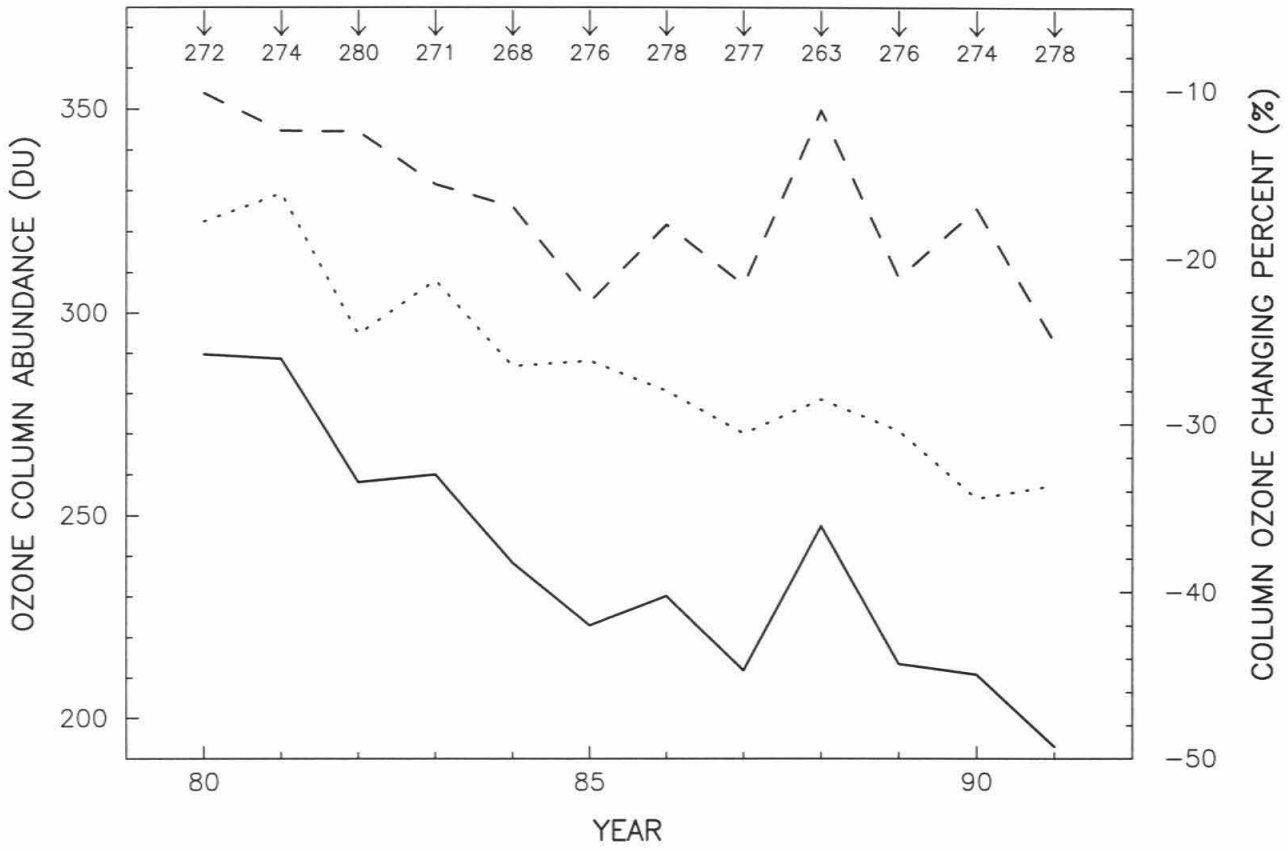

Figure 1.4: The area-weighted average ozone column abundance (DU) on Day 240 of each year (dotted curve); same for the minimum value attained in each year between Days 240 and 290 (solid curve). Dashed line gives the percent loss of ozone (relative to Day 240). The days on which the minimum value for the area-weighted average ozone column abundance occurred are indicated.

Table 1.1: Column Ozone Depletion Rate (DU/day) as Computed by Three Methods

	Method 1[a]				Method 2[b]		Method 3[c]
Year	(240)	(Minimum)	Minimum	Rate	(240)	Rate	Rate
1980	324	293	272	1.06	320	0.90	0.76
1981	332	291	274	1.20	323	0.98	0.64
1982	297	261	280	0.92	293	0.85	0.63
1983	309	262	271	1.55	303	1.37	1.36
1984	288	241	268	1.73	288	1.70	1.74
1985	289	225	276	1.81	292	1.83	1.73
1986	286	233	278	1.26	277	1.09	1.14
1987	271	214	277	1.57	269	1.49	1.55
1988	283	251	263	1.35	289	1.65	1.45
1989	271	217	276	1.59	266	1.42	1.50
1990	256	213	274	1.27	251	1.11	0.84
1991	259	198	278	1.70	262	1.75	1.76

Mean column ozone depletion rate (DU/day) in the polar vortex:

[a] Method 1 uses ozone values on Day 240 and the day of minimum ozone.

[b] Method 2 is based on a 5 day average of the initial value of ozone from Days 240 to 244.

[c] Method 3 is based on a linear least squares fit to the ozone values between Day 240 and the day of minimum ozone.

Figure 1.5 shows the decadal variation in the the mean ozone depletion rate from Day 240 to the day when the minimum area-averaged column ozone is found in the polar vortex (solid line). In the first three years the ozone depletion rate during this September-October period is only about 1 DU/day. After 1982, the ozone depletion rate increases to a value of 1.8 DU/day in 1985. Since then, the ozone depletion rate has fluctuated around 1.5 DU/day and shows a possible QBO signature. The dashed line in Figure 1.5 is obtained in the same way as for the solid line, except that the mean of 5 days (Days 240 – 244) is used for the initial value. The dotted line is obtained by using a linear least squares fit to the data. Detailed information related to the computation of various rates is summarized in Table 1.1. The depletion rates are particularly difficult to estimate in 1988 and 1990, because the variation during the season is more non-linear in those years (Fig. 1.3).

The likely explanation for the rapid increase in the ozone depletion rate is the rapid rise of total chlorine (Cly) in the lower stratosphere in the early part of the decade. The dominant effect of chlorine chemistry on ozone loss is quadratic in ClO [*Molina* and *Molina*, 1987a; *Sander et al.*, 1989; *Anderson et al.*, 1991], with smaller contributions from coupling to bromine and HOx chemistry. The latter effects are linear in ClO. Figure 1.6 (solid line) shows the rate of ozone loss (relative to 1980) as estimated using the model of Sander *et al.* [1989]. The values of Cly in the stratosphere are taken from a model [*Weisenstein et al.*, 1992], which is based on the release of chlorofluorocarbons, atmospheric observations and modeling. This shows that the chemical forcing on the ozone hole has increased from 1980 to 1985 by about 40%, which is about 60% of the increase in ozone depletion rate in the same period (see Figure 1.5). For comparison, we also compute the chemical forcing if it were linear in Cly (dashed line) or quadratic in Cly (dotted line). We should point out

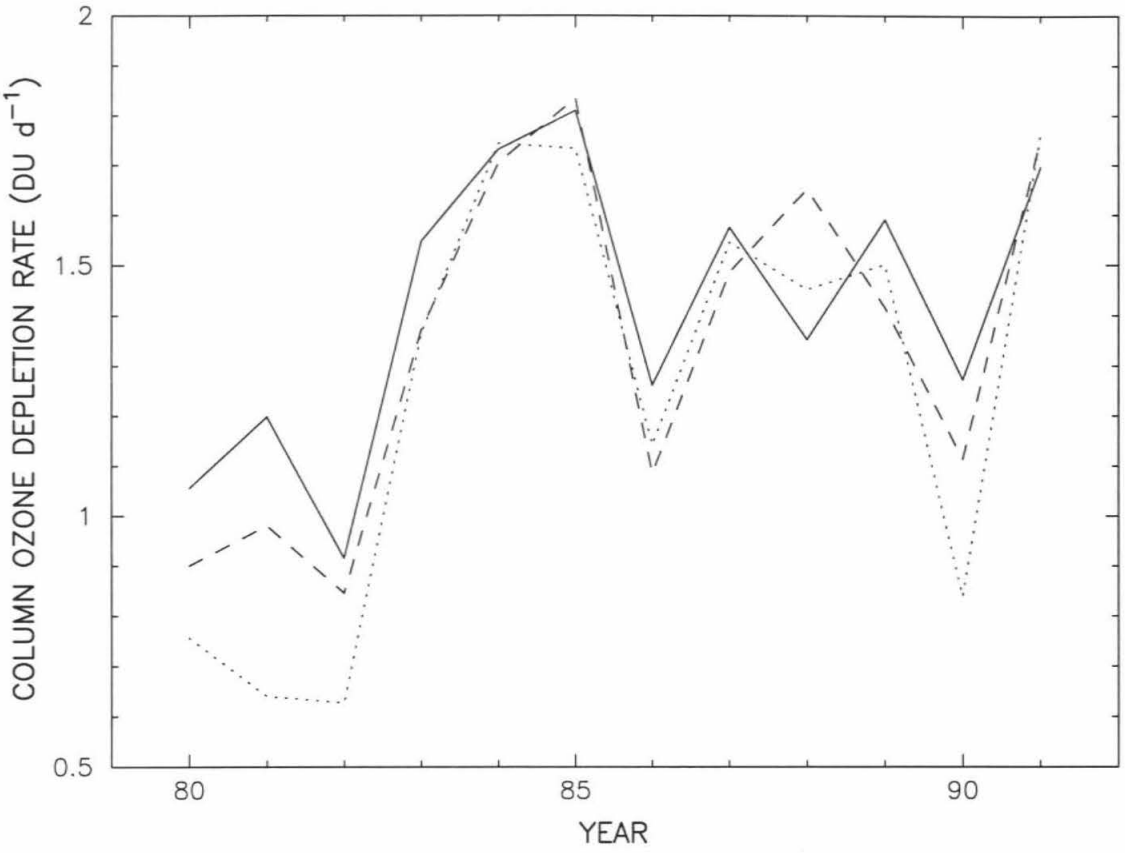

Figure 1.5: Mean ozone column depletion rate (DU/day) in the polar vortex. The solid line denotes the rate computed using ozone values on Day 240 and the day of minimum ozone. The dashed line is based on a 5 day average of the initial value of ozone from Day 240 to 244. The dotted line is based on a linear least squares fit to the average ozone values between Day 240 and the day of minimum ozone. Details are summarized in Table 1.1.

that despite the dominance of the Molina-Molina catalytic cycle that is quadratic in ClO the chemical forcing is not quadratic in Cly. The reason is that as Cly increases, part of the reactive chlorine is sequestered in the Cl_2O_2 dimer, thus lowering its efficiency for the destruction of ozone.

After 1985, the depletion of ozone apparently reached saturation, in that the ozone depletion rates did not increase with increasing chlorine and, in fact, were probably moderated in later years by dynamical processes. These could horizontally modulate the region of photochemical loss within the vortex (i.e., the chemically perturbed region) or the area of the vortex itself; they could also affect the rate of vertical motion and so the seasonal downwelling of air with higher ozone mixing ratios from the middle stratosphere in the polar vortex [*Manney et al.*, 1995].

The moderated depletion rate after 1985 for column ozone may also be due to the fact that the loss rate depends on ozone itself, and ozone amounts during this later period are already very low during this season. This effect can be illustrated by dividing for each year the difference between the day of minimum vortex-average column ozone and Day 240 by the vortex-average amount on Day 240. As seen in Figure 1.4 (dash line), the 1985 loss rate is sustained in later years, with 1988 again being a most exceptional year.

We can compare the loss rates of the vortex-average area-weighted column ozone of Figure 1.5 to those computed by Lait *et al.* [1989]. They used the minimum TOMS column ozone value found poleward of 30°S on any given day to estimate linear decline rates D for the late August to September period. They then estimated the change over the period 1979 – 1987 by least squares fitting of the September variations and obtained:

D [DU/day] = -0.19 * (year – 1980) – 0.65

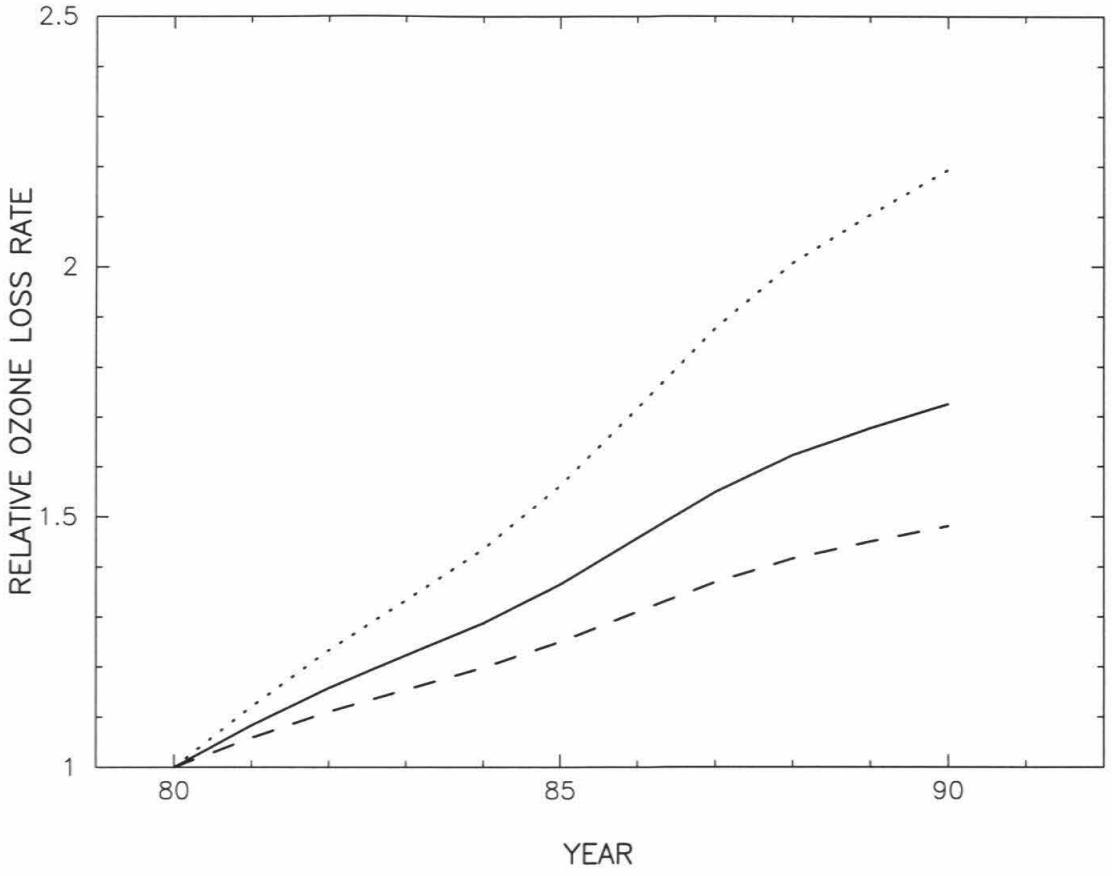

Figure 1.6: The relative rate of ozone loss in October (solid line) as estimated using the model of Sander *et al.* (1989). The total chlorine (Cly) in the stratosphere from 1980 to 1990 is taken from the model of Weisenstein *et al.* [1992]. The dashed and dotted lines give the rate of ozone loss if it were proportional to Cly and Cly^2, respectively. All values are normalized to that of 1980, the year with Cly = 1.44 ppbv.

This can be compared to comparable linear least squares fitting of the values shown in Figure 1.5 for 1980 – 1987:

D [DU/day] = -0.14 * (year – 1980) – 0.71

As noted above, the distinct change in decline rates for the vortex-average column ozone occurs after 1985. A linear least squares fitting for the September decline rates for 1980 – 1985 yields:

D [DU/day] = -0.25 * (year – 1980) – 0.51

which translates into an increase over those years by a factor of 3 or more. This would reduce to a factor of 2 using the decline rates computed in Figure 1.5 as simple differences. Both these factors are larger than that suggested by the growth in stratospheric chlorine (Fig. 1.6).

Lait *et al.* [1989] found that the residuals of the September decline rates of minimum column ozone values from the interannual linear fit showed a distinct Quasi-Biennial Oscillation (QBO) signature. This is consistent with the September decline rates of the vortex-average column ozone shown in Figure 1.5 for years before 1986, except for 1984. Oscillations in September decline rates after 1985 have the character and magnitude of those during September in 1980 – 1982. However, the distinctive QBO-like pattern shown in Fig. 1.3 for vortex-averaged column ozone in 1980 – 1985 is not apparent in later years.

Figure 1.7 shows the vortex-average area-weighted column ozone for the period when the ozone hole is deepest from 1980 to 1991. The change in trend from year-to-year for the years before and after 1986 is clearly seen, as is the anomaly of the 1988 column ozone variation. The area-averaged ozone column abundance decreases with a slope of 3.8% (11.3 DU) per year before 1987 and 0.9% (2.0 DU) per year after that (the year 1988 is anomalous and is not included in the trend analysis). The average

rate of decline is 25% per decade from 1980 to 1991. These rates of decline of the vortex-averaged column ozone during one month (mid-September to mid-October) of lowest ozone may be compared to the value 30% per decade obtained on the basis of zonal averages in the southern polar regions from 1979 to 1990 [*Herman et al.*, 1993]; similar rates of decline were also obtained when column ozone was mapped as a function of PV within the Antarctic polar vortex for September over the same period [*Randel* and *Wu*, 1995]. However, the distinct break in trend after 1985 has not been previously noted.

1.4.2 Growth of the ozone hole

The results presented above utilized area-weighted averages of column ozone over the entire polar vortex. Here, the area-mapping technique is used to examine the evolution of the ozone hole in more detail. Figure 1.8 shows the area enclosed by contours of ozone column abundance, again plotted versus enclosed area in units of $2\pi R^2$. As before, the period covered is from Days 240 to 300 for 1980 – 1991, and the domain of integration is confined inside the polar vortex by PV contour of -50 PVU at 500 K. In these plots, we have used 5-day smoothing to remove high frequency variations. Since there are no ozone data for the part of the vortex in the dark, the lower left parts of these figures are blank. Note that the areas bounded by column ozone contours less than 250 DU increase rapidly around Day 260 (mid-September), implying that the ozone hole is expanding and the column ozone is decreasing inside the vortex. By Day 280 (early October), the ozone hole has reached its greatest extent and depth. Typically, the area remains constant then for a few days before it begins to shrink. This reflects first the warming of the vortex air and eventually the seasonal weakening of the vortex itself, which has generally broken up by November.

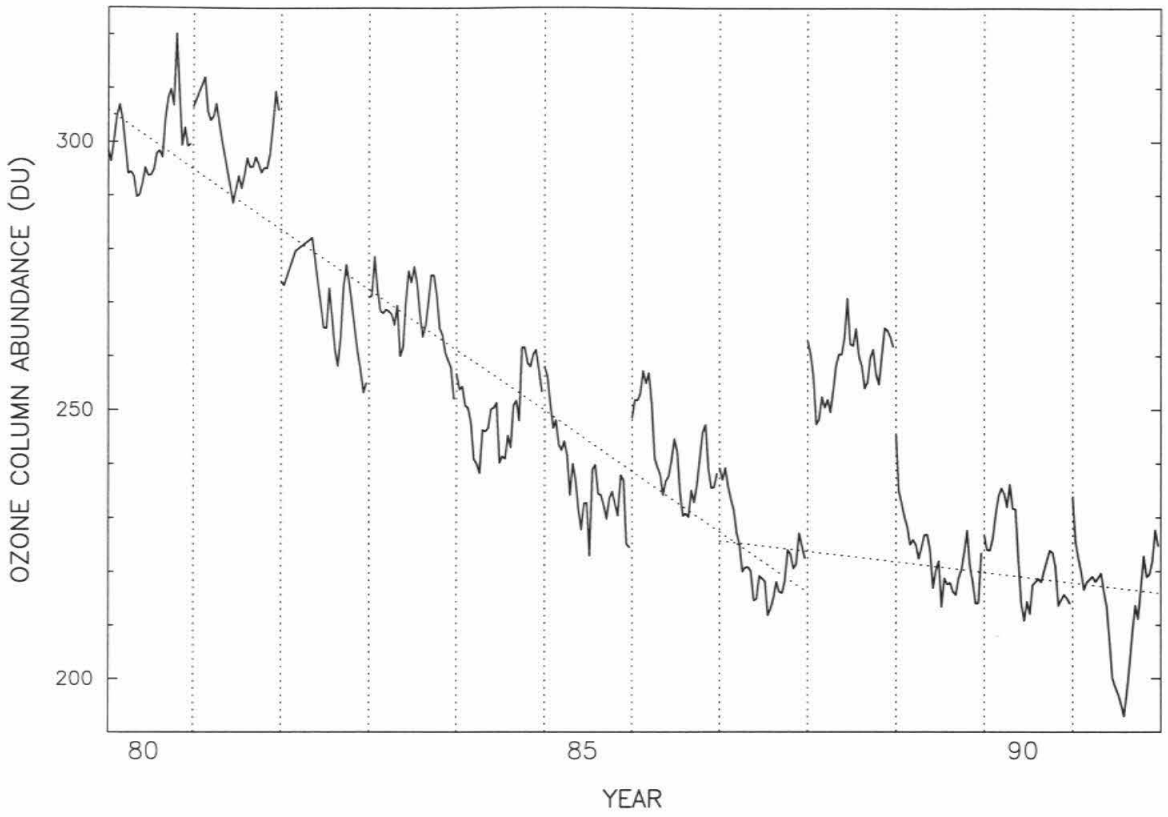

Figure 1.7: The vortex-averaged area-weighted column ozone abundance (DU) in the vortex from Days 260 to 290 (mid September to mid October), the season of minimum column ozone each year. The steep dotted line is the linear least squares fit to the data during this month from 1980 and 1987. The slope is 3.8% (11.3 DU) per year with the averaged ozone value 300 DU during this time in 1980 as reference. The shallow dotted line is a similar fit to the data from 1987 to 1991 but excluding 1988. The slope is 0.9% (2.0 DU) per year by using the averaged ozone value 222 DU during this time in 1987.

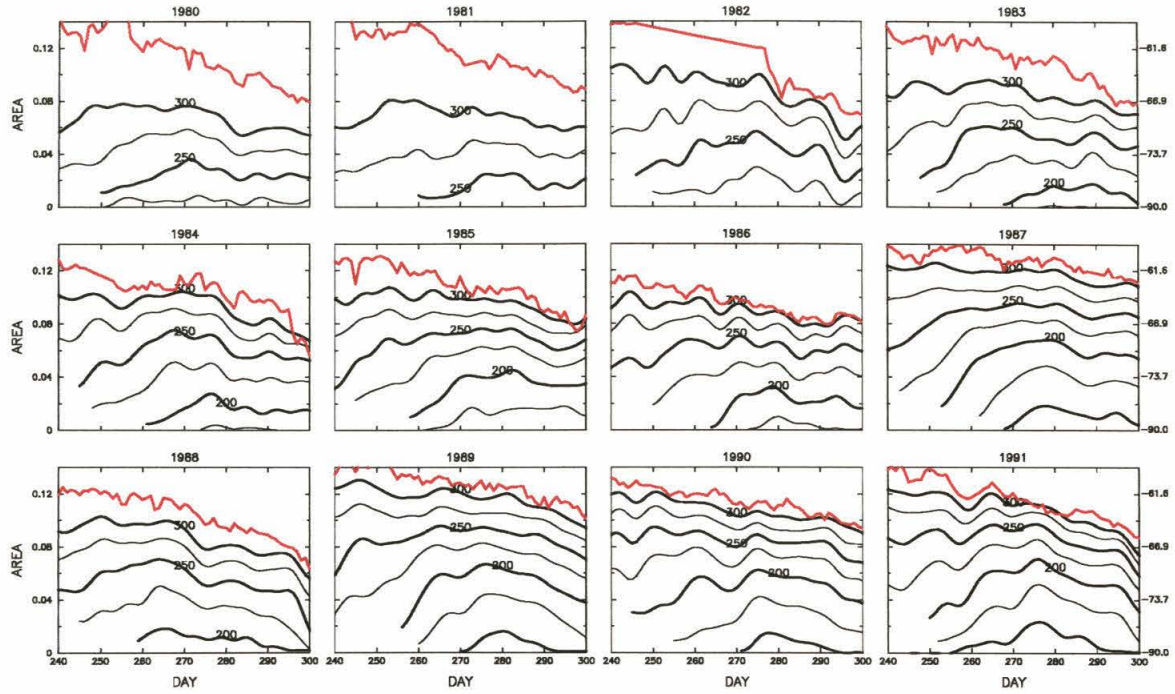

Figure 1.8: Contours of ozone column abundance (DU) plotted versus enclosed area in units of $2\pi R^2$ (R is the radius of Earth) from Day 240 to Day 300 for 1980 – 1991. The area mapped is confined within the vortex as defined by the -50 PVU contour (red line). Areas greater than the vortex area reflect computational uncertainty due to using different grids for PV and O_3 and to different gradients in these fields at the vortex edge. The blank space in the lower left corner is caused by the lack of data. Positive slopes indicate ozone decrease, negative slopes indicate ozone increase. Contour increment is 25 DU. The equivalent latitude is indicated on the right hand axis.

As can be seen from Figure 1.8, the ozone column abundance contour of 200 DU, does not appear until 1983, but occupies a maximum area of 7% of the southern hemisphere in 1991. The 150 DU contour appears in 1987. These regions are well inside the polar vortex. On the vortex boundary, where the ozone column abundance is usually greater than 300 DU, the seasonal change of area reflects the area of the vortex. In this region (e.g., the 300 DU contour), there is a little increase during the seasonal formation of the ozone hole, but mostly the area is constant until the vortex begins to decrease in area. As seen in Figure 1.8, the ozone hole develops during late August to mid-September and is largely independent of day-to-day variations near the vortex boundary. These different trends and the general steepening of the gradients at the vortex boundary indicate that the air within the vortex is isolated in the lower stratosphere from air at similar levels outside the vortex. The steepening of ozone gradients at the vortex boundary results from the spatial expansion , as well as the deepening, of the ozone hole over that period.

The anomalous behavior of 1988 is clearly seen by comparing the areas bound by the 200 DU contour in the successive years 1987, 1988 and 1989. The maximum areas in 1987 and 1989 exceed 6% of the southern hemisphere, whereas in 1988 the maximum area is only about 2% of the southern hemisphere. Similar area mapping results were obtained by Stolarski *et al.* [1990, Fig. 3] for these years.

In Figure 1.8 the increasing areas in successive years of the ozone contours inside the vortex on Day 240 indicates that the ozone column abundance must have already begun to decrease earlier in the season. The area-mapping (not shown here) of column ozone from Day 220 to 320 (early-August to mid-November) shows ozone depletion even before Day 220. This is consistent with the trends in the vortex-averaged column ozone (Figs. 1.3, 1.4) and, as discussed earlier, with recent observations by UARS.

Area mapping provides a convenient measure of the magnitude of maximum ozone depletion each year. Consider the area bounded by a low ozone contour, such as the 250 DU contour (Fig. 1.8). Figure 1.9 shows the maximum area enclosed by this contour between Days 260 and 300 (mid-September to late October) and the days on which the maximum area is attained in each year. Except in 1981 and 1986, the increase of the maximum area before 1987 is roughly linear. The linear least squares fit shows a slope of 8.36×10^{-3} per year from 1980 to 1987. The same fitting procedure shows no trend for 1987 – 1991 (with 1988 excluded); the average over the whole period is 5.49×10^{-3} per year from 1980 to 1991. From the definition of equivalent latitude θ_{E},

$$\Delta A(t, \Omega^*) = \sin(90^0 + \theta_{\mathrm{E}})\, \Delta\theta_{\mathrm{E}}$$

we can express the change in the maximum area of the 250 DU contour as an equatorward expansion at a rate of approximately 1.35° per year before 1987 and at a rate for the full 1980 – 1991 period of 0.84° per year (see Table 1.2). The maximum area of the ozone hole usually occurs in late September or early October, consistent with the vortex-average trends discussed earlier, and also near or before the time when the minimum ozone column amounts (not shown) are found.

One may ask whether this rapid growth in the chemical ozone hole is accompanied (or partly driven) by climatological changes in the stratosphere [e.g., *Mahlman et al.*, 1986; *Angell*, 1993, *Mahlman et al.*, 1994]. To address this question qualitatively, we compute the areas of the polar vortex using the -52 PVU contour and the 195 K isotherm, both on the 500 K isentropic surface. Figure 1.9 shows these areas on the same days of maximum area of the 250 DU column ozone contour. The vortex (PV) area has little trend over the decade (only 0.05°/yr; see Table 1.2), although it

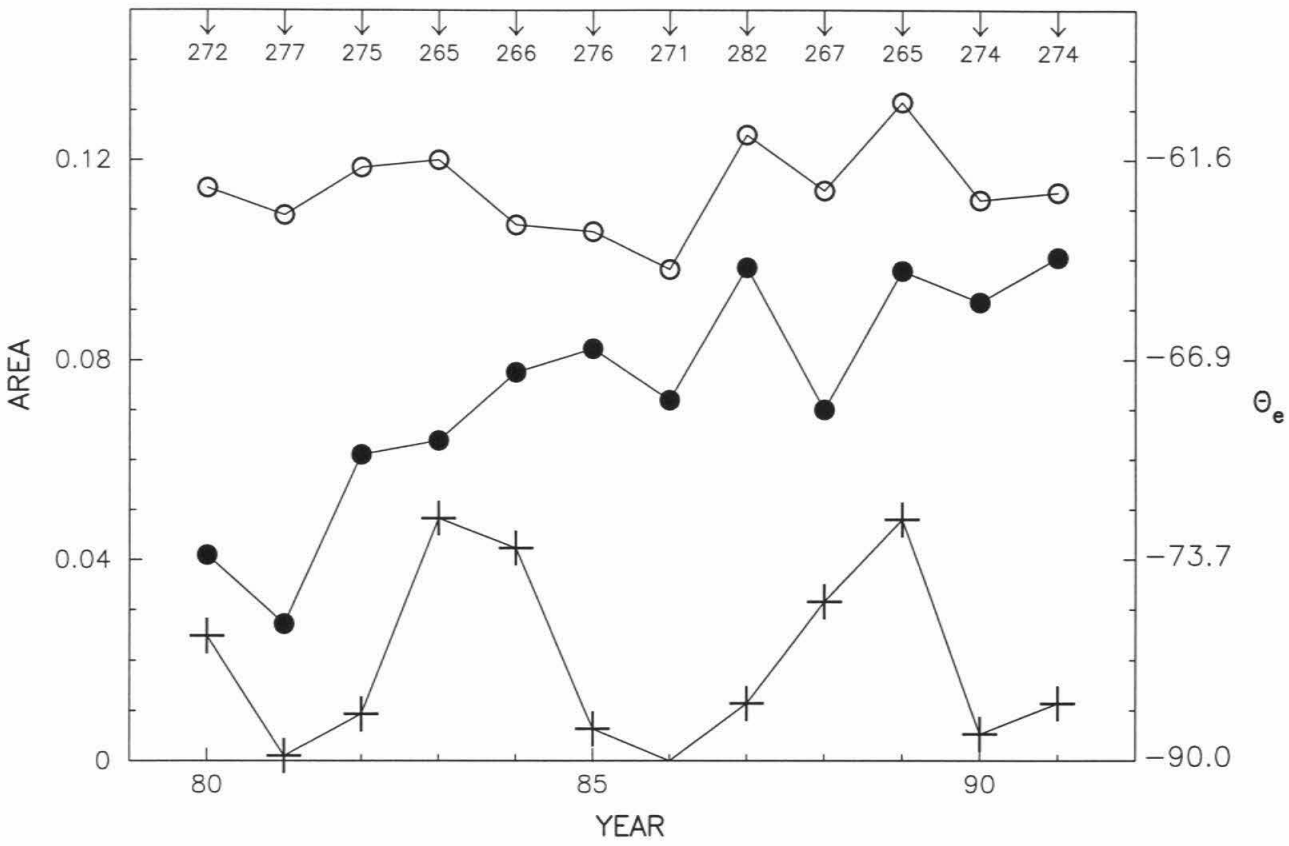

Figure 1.9: The maximum area (dots) enclosed by the 250 DU contour in each year between Days 260 and 300. The days on which the maximum area is attained are indicated. Also shown for the same days are the areas of the vortex, as indicated by the -52 PVU contour (o) on the 500 K isentropic surface and of the 195 K isotherm (+), also at 500 K. The equivalent latitude is indicated on the right hand axis.

Table 1.2: Decadal Growth Rates (Degree/yr) of Areas Bound by Isopleths of O_3 (250 DU), PV (-52 PVU) and T (195 K)

	1980-1987	1987–1991	1980–1991	Reference
O_3	1.35 ± 0.27	0.00 ± 0.28^a	0.84 ± 0.16	Figure 1.9
PV	–	–	0.05 ± 0.10	Figure 1.9
T	–	–	0.05 ± 0.19	Figure 1.9

[a] The year 1988 is not included in the calculation.

fluctuates interannually about a more or less constant value. In 1980 the vortex area at 500 K is nearly twice that of the 250 DU contour, but the latter increases until it fills more than 70% of the entire vortex by 1985. After 1985 the fluctuations in the area of the 250 DU contour reflect those of the vortex area itself, which limits the size of the 250 DU area and thus of the ozone hole.

The lack of correlation in Figure 1.9 between the areas enclosed by the 195 K temperature, an indicator of the horizontal extent of PSCs, and the 250 DU TOMS column ozone contour, on the days when the latter is a maximum, is not surprising given that much of the processing of polar air would have occurred earlier. Furthermore, stratospheric winds can expose most of the vortex interior air to PSCs, even if the latter occupies only part of the vortex. This has been shown most dramatically for the north [*Waters et al.*, 1993a], where PSCs are not as extensive. The more critical factor may be exposure to sunlight. For short time periods that exposure depends critically on details of the air motion within the vortex, but for periods of a few weeks or more that factor depends more crucially on the vortex extent and location and may be reflected in the vortex area shown in Figure 1.9. At least to first order, most of the growth of the ozone hole over the last decade appears driven by chemistry alone, due to increasing stratospheric chlorine. This increase has slowed down, not because the stratospheric chlorine loading or activation has stopped increasing, but simply because the region of ozone-depleted air now fills (horizontally) much of the polar vortex, whose own fluctuations in area reflect interannual variability in dynamical activity.

This limiting of the ozone loss region to the vortex is reflected in the fact that after 1983 high contour values of column ozone (larger than 300 DU) are near the vortex edge as defined here on the 500 K isentropic surface (Fig. 1.8), except in 1988. In that year the chemically perturbed region was distinctly within the vortex (Figs. 1.8, 1.9),

as described by Schoeberl *et al.* [1989] in their analysis of the 1987 Antarctic campaign (AAOE) data. Figures 1.8, 1.9 show that 1988 is not representative in this regard of all other years following 1985. Thus, further chemical ozone loss during this season now depends upon factors that would expand the south polar vortex region horizontally or which would extend the zone of chemical depletion vertically, as happened in 1993 due to heterogeneous chemical effects associated with the entrainment of Mt. Pinatubo aerosols into the south polar vortex [*Hofmann et al.*, 1994].

Figure 1.10 shows the variations in ozone column abundance versus area on the days of maximum area in the 250 DU contour (Fig. 1.9) each year from 1980 to 1991. The greater extent of ozone-poor air in the years after 1985 is again apparent, as is the anomaly of ozone values in 1988. As more ozone gets depleted, the radial gradient of ozone in the vortex gets steeper, as can be seen from Figure 1.11, which shows the average gradient of the transition region between 250 DU and 280 DU, defined as $\frac{280-250(\mathrm{DU})}{\theta_{\mathrm{E}}(280\mathrm{DU})-\theta_{\mathrm{E}}(250\mathrm{DU})}$. Years since 1984 are typically characterized by larger gradients as a result of greater ozone depletion, as discussed earlier, with notable exceptions in 1988 and 1989. As we have remarked repeatedly, 1988 is anomalous in many respects. The relatively weak column ozone gradient in 1989 is partly due to the fact that the vortex area in 1989 was the largest in the record (Fig. 1.9). Although Figure 1.10 shows results for a single day, the area-contours of Figure 1.8 show that the results are representative of the ozone hole period in those years. Finally, as pointed out by previous studies [*McIntyre*, 1989 and *Hartmann et al*, 1989], the steep gradients of PV and ozone indicate relative isolation of the chemically perturbed region from air outside the vortex.

Figure 1.12 shows the time rate of change of ozone column abundance over a period from Days 240 to 300 (late August to late October) for each year from 1980

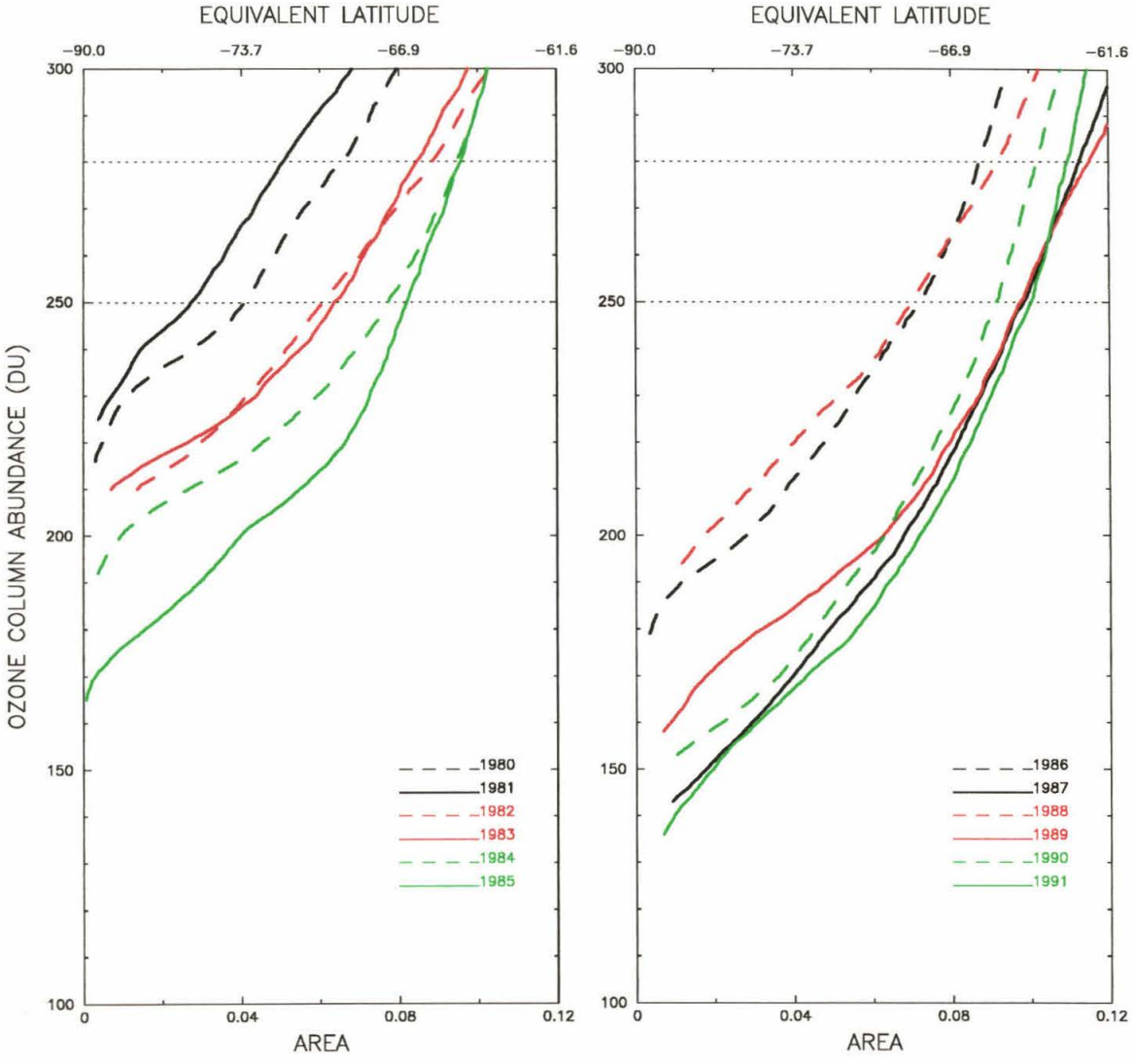

Figure 1.10: Ozone column abundance versus area on the days shown in Figure 1.9 for each year for 1980 – 1991. The equivalent latitude is indicated on the top axis.

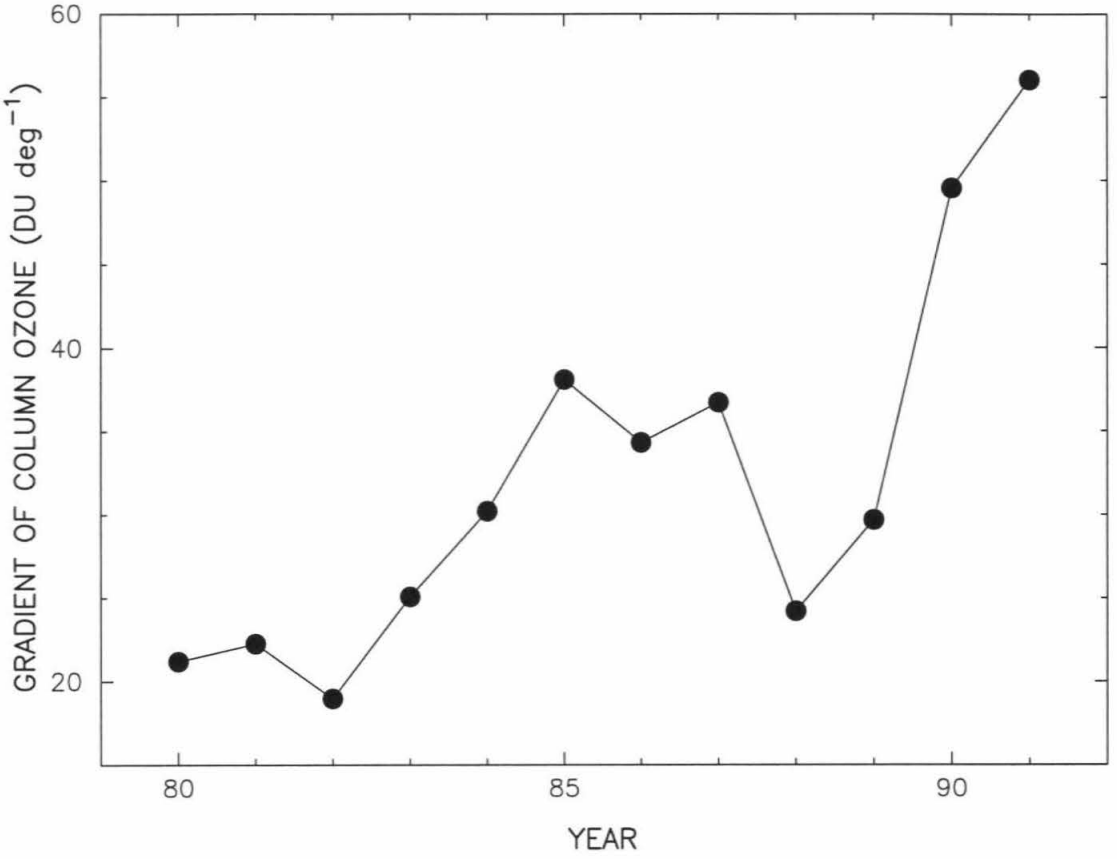

Figure 1.11: Average ozone column gradient with respect to equivalent latitude, computed as described in the text, for the same days as in Figure 1.10.

to 1991. The results for 1987 have been shown previously by Yung *et al.* [1990, Fig. 4]; this figure extends that result to 12 years. The average rate of ozone depletion in the vortex is 1 to 2 DU/day, consistent with that shown in Figure 1.5.

Larger depletion rates (5 DU/day) are prevalent near the center of the vortex (Fig. 1.8). In some of the recent years, such as the dynamically quiescent years 1987 and 1989, large ozone depletion rates can persist for long periods of time. In most years the development of the ozone hole is periodically interrupted by increases of ozone with a period about 10 – 20 days, with the changes being more prominent away from the vortex center. These increases may be due to the action of synoptic scale systems which are known to produce minor warmings in the mid-stratosphere, as these systems have a characteristic time scale of 10 – 20 days [e.g., *Fishbein, et al.*, 1993; *Manney, et al.*, 1993b]. These dynamical events affect ozone in the lower stratosphere within the vortex by moving ozone into the vortex in mid-stratosphere and then down to lower levels [e.g., *Leovy, et al.*, 1985; *Manney, et al.*, 1994b].

Some care needs to be taken when interpreting the area-mapped fields shown in Figs. 1.8 and 1.12, as the area-mapping tends to filter out the planetary-scale features. However, after the ozone hole reaches its maximum depth around Day 280 in early spring, the polar vortex starts to shrink and ozone column abundance starts to recover. Significant warming events and erosion of the vortex are marked in Figure 1.12 by ozone increases extending nearly to the vortex center. Due to the anomalous circulation and extremely cold temperature of 1987 [*Randel*, 1988], the final warming and the break up of the ozone hole was delayed 20 days (as compared with climatology). Figure 1.12 shows that the ozone depletion rate was never as persistent and as extensive as in 1987. This decrease was interrupted by a minor warming around Day 280 and then terminated by the final warming after Day 300.

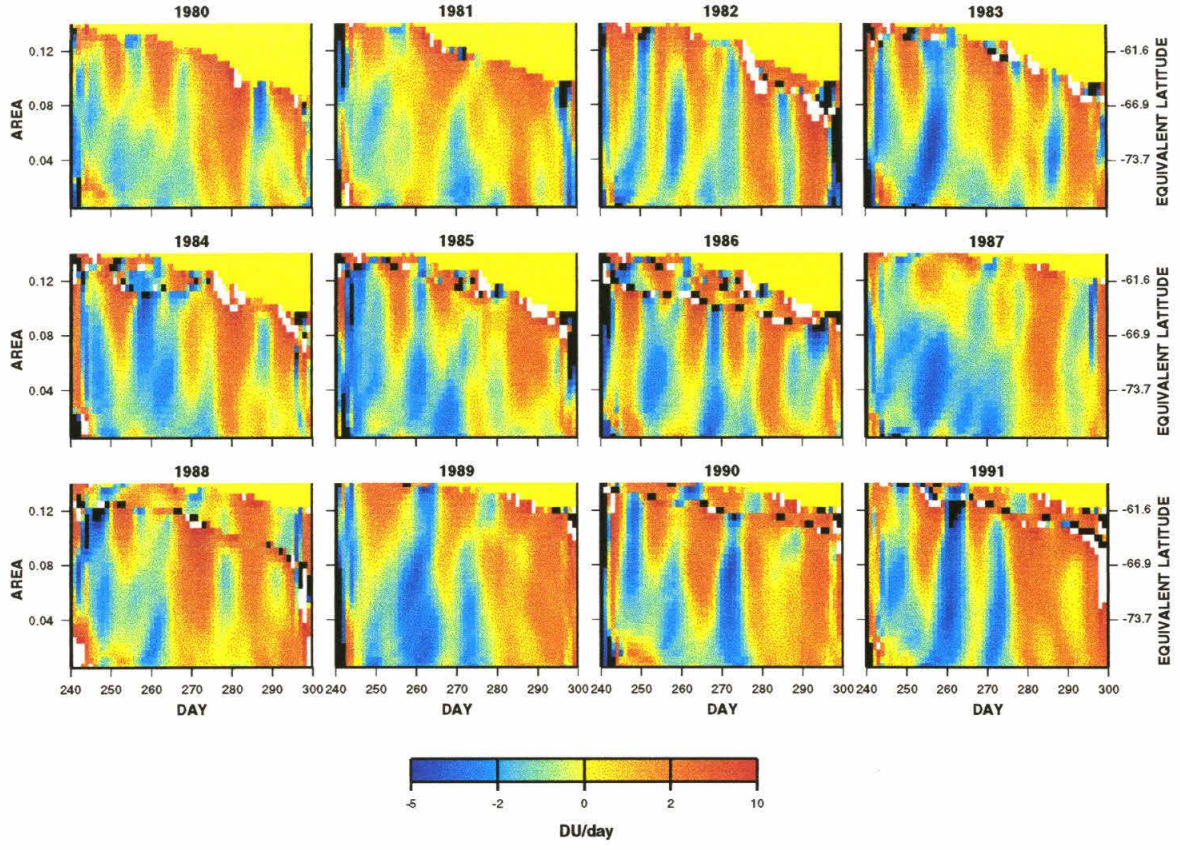

Figure 1.12: Contour plot of the time rate of change of ozone column abundance ($\partial\Omega/\partial t$), in DU/day, plotted versus enclosed area from Day 240 to Day 300 for 1980 - 1991. The horizontal axis is day number and the vertical axis is area in units of $2\pi R^2$ (R is the radius of Earth).

In 1988 on the other hand, stratospheric temperatures had warmed significantly by late September, terminating most decreases in column ozone. The maximum total ozone decline is only 15% during September 1988 compared to nearly 50% during September 1987 [*Schoeberl et al.*, 1989; *Krueger et al.* 1989]. This appears to be the direct result of the brevity of the decline through September. Wave activity at the time was anomalously strong [*Manney et al.*, 1991] and the stratospheric sudden warming in late winter was reminiscent of major winter warmings in the northern hemisphere [*Kanzawa* and *Kawaguchi*, 1990]. The 1988 ozone hole began filling on October 19, nearly six weeks earlier than in 1987, and drifted out of the polar regions in mid-November for the earliest breakup since 1979.

1.5 Conclusions

The area-weighted ozone column abundance averaged over the polar vortex in late August (Day 240), often viewed as the beginning of the ozone hole season, exhibits a steady decline from about 320 DU in 1980 to about 250 DU at the end of the decade. This amounts to a total drop of 70 DU in a decade (Table 1.1) and accounts for a large part of the overall decrease of more than 90 DU in vortex-average October ozone column abundance that has occurred over the same period. Most of that drop occurred before 1987, as the decline since then has been much smaller (Fig. 1.7).

Part of this decadal decline may be due to the recurrent presence of the ozone hole every year. Due to the long lifetime of ozone in the lower stratosphere, there is persistence of depleted ozone from one year into the next. The effect, known as the dilution effect, has been modeled by Sze *et al.* [1989], Prather *et al.* [Chapter 1, WMO, 1989] and Mahlman *et al.* [1994]. These models predict a decline of ozone of 5 – 7 % at polar latitudes in June due to the presence of an ozone hole, or about 15

– 20 DU. That still leaves 50 – 55 DU in the decadal decline unexplained. It is more likely that the result is due to increasing stratospheric chlorine producing increasing chemical loss of ozone in the south polar vortex even during southern winter, as indicated by the recent UARS observations. Photochemical loss can occur because the southern vortex is sufficiently large that it has regions in sunlight even during this period of polar night (such loss could be more heavily weighted in our method because of the area-weighting of our vortex averages).

The mean ozone depletion rate in the vortex between late August (Day 240) and the day of minimum vortex-averaged ozone (typically in late September or early October) has changed from about 1 DU/day at the beginning of the decade, rapidly increasing to about 1.8 DU/day by 1985, and apparently saturating thereafter (Fig. 1.5). This change in ozone depletion rates is qualitatively, but perhaps not quantitatively, consistent with chemical forcing of the ozone hole solely by chlorine (Fig. 1.6). The character and magnitude of fluctuations in the September depletion rates in 1980 – 1982 are comparable to those after 1985, and it is possible that these reflect the extratropical QBO in ozone. A QBO signature in the depletion rates derived here is perhaps not as strong as obtained by Lait *et al.* [1989] who analyzed minimum column ozone abundance and not vortex averages. The QBO signature is evident in the vortex ozone averages themselves for the years 1980 – 1985, but is not readily apparent in later years. That interannual variations can affect ozone abundance during this season is clearly indicated by the anomalously high column ozone values during September 1988, a very active year dynamically.

Area mapping of various column ozone contours provided some insight into the detailed morphology of the ozone depletion rate in the south polar vortex. The time-rate-of-change of column ozone appears to be greater deeper in the vortex (Fig. 1.12). Whether this reflects the exposure of air parcels to sunlight or some other factor

was not investigated here. Many of the regions with the highest rates of change in ozone are cold enough that water-ice PSCs may form; if so, greater dehydration and denitrification of the vortex air may enhance the ozone loss there. Regions near the vortex edge may have greater downwelling of ozone-rich air during this season. The 10 – 20 day modulation of the ozone change rates within the vortex suggests that synoptic activity is affecting the rate of resupply, probably by descent of ozone from mid-stratospheric levels.

Our results suggest that further increases in stratospheric chlorine after 1985 did not significantly increase the horizontal extent of ozone loss, as the area of loss now filled most of the inner (i.e., isolated) region of the polar vortex in the lower stratosphere and was now limited by the area of the vortex. Thus, depletion rates of the vortex-average ozone did not increase further and in fact were not as high as in 1985 until 1991, when volcanic aerosols may have extended the vertical extent of ozone chemical loss.

In summary, our results suggest that chemical loss due to stratospheric chlorine was significant even early in the 1980 – 1991 period studied here, as judged from a vortex average. Increases in ozone depletion rates since 1982 are consistent with increasing chlorine effects approaching saturation in 1985 as the region of ozone loss filled the isolated inner regions of the polar vortex during September. In more recent years, the main effect of increased chlorine may have been to increase the wintertime chemical loss of ozone, thereby lowering the threshold on which the ozone hole develops in August and September. This early loss would occur despite the polar darkness, due mainly to the great size of the southern winter vortex. The dilution effect discussed above may also play a role. This view is necessarily speculative until more quantitative dynamic-chemical simulations of chlorine activation and ozone loss are done.

1.6 Acknowledgements

We would like to express our appreciation to R. S. Stolarski for sharing his insights of the TOMS data with us. The NMC geopotential height and temperature stratospheric analyses were obtained from the National Center for Atmospheric Research as part of an EOS interdisciplinary science investigation; wind and PV fields were derived and provided by Dr. Gloria Manney at JPL. We thank M. Allen, L. Froidevaux, R. Herman, L. Jaegle, R. Salawitch, S. Sander and three anonymous referees for valuable comments. This work was supported principally by NASA grant NAGW 2204 to the California Institute of Technology and was carried out there and at JPL, under contract with NASA. Contribution number 5465 from the Division of Geological and Planetary Sciences, California Institute of Technology.

1.7 References

Anderson, J. G., W. H. Brune, and M. H. Proffitt, Ozone destruction by chlorine radicals within the Antarctic vortex: The spatial and temporal evolution of ClO–O_3 anticorrelation based on *in situ* ER–2 data, *et al., J. Geophys. Res.* **94**, 11465–11479 (1989a).

Anderson, J. G., W. H. Brune, S. A. Lloyd, D. W. Toohey, S. P. Sander, W. L. Starr, M. Loewenstein, and J. R. Podolske, Kinetics of O_3 destruction by ClO and BrO within the Antarctic vortex: An analysis based on *in situ* ER–2 data, *et al., J. Geophys. Res.* **94**, 11480–11520 (1989b).

Anderson, J. G., D. W. Toohey and W. H. Brune, Free radicals within the Antarctic vortex: The role of CFCs in Antarctic ozone loss, *Science* **251**, 39–46 (1991).

Angell, J. K., Reexamination of the relation between depth of the Antarctic ozone hole, and equatorial QBO and SST, 1962–1992, *Geophys. Res. Lett.* **20**, 1559–1562 (1993).

Baldwin, M. P., and J. R. Holton, Climatology of the stratospheric polar vortex and planetary wave breaking, *J. Atmos. Sci.* **45**, 1123–1142 (1988).

Bojkov, R. D., The 1979–1985 ozone decline in the Antarctic as reflected in ground based observations, *Geophys. Res. Lett.* **13**, 1236–1239 (1986).

Bowman, K. P., and A. J. Krueger, A global climatology of total ozone from the Nimbus 7 total ozone mapping spectrometer, *J. Geophys. Res.* **90**, 7967–7976 (1985).

Bowman, K. P., Global trends in total ozone *Science* **239**, 48–50 (1988).

Bowman, K. P., Evolution of the total ozone field during the breakdown of the Antarctic circumpolar vortex, *J. Geophys. Res.* **95**, 16529–16543 (1990).

Butchart, N., and E.E. Remsberg, The area of the stratospheric polar vortex as a diagnostic for tracer transport on an isentropic surface, *J. Atmos. Sci.* **43**, 1319–1339 (1986).

Chen, P., The permeability of the Antarctic vortex edge, *J. Geophys. Res.* **99**, 20563–20571 (1994).

de Zafra, R. L., M. Jaramillo, A. Parrish, P. Solomon, B. Connor, and J. Barrett, High concentrations of chlorine monoxide at low altitudes in the Antarctic spring stratosphere: diurnal variation, *Nature* **328**, 408–411 (1987).

Farman, J. C., B. G. Gardiner, and J. D. Shanklin, Large losses of total ozone in Antarctica reveal seasonal ClOx/NOx interaction, *Nature* **315**, 207–210 (1985).

Fishbein, E. F., L. S. Elson, L. Froidevaux, G. L. Manney, W. G. Read, J. W. Waters, and R. W. Zurek, MLS observations of stratospheric waves in temperature and O_3 during the 1992 southern winter, *Geophys. Res. Lett.* **20**, 1255–1258 (1993).

Froidevaux, L., J. W. Waters, W. G. Read, L. S. Elson, D. A. Flower, and R. F. Jarnot, Global ozone observations from UARS MLS – An overview of zonal-mean results, *J. Atmos. Sci.* **51**, 2846–2866 (1994).

Garcia, R. R., and S. Solomon, A possible relationship between interannual variability in Antarctic ozone and the quasibiennial oscillation, *Geophys. Res. Lett.* **14**, 848–851 (1987).

Gelman, M. E., K. W. Johnson, and R. M. Nagatani, Detection of long-term trends in global stratospheric temperature from NMC analyses derived from NOAA

satellite data, *Adv. Space Res.* **6**, 17–26 (1986).

Hartmann, D. L., K. R. Chan, B. L. Gray, M. R. Schoeberl, P. A. Newman, R. L. Martin, M. Loewenstein, J. R. Podolske, and S. E. Strahan, Potential vorticity and mixing in the south polar vortex during spring, *Geophys. Res. Lett.* **94**, 11625–11640 (1989).

Herman, J. R., R. McPeters, R. S. Stolarski, D. Larko, and R. Hudson, Global average ozone change from November 1978 to May 1990, *J. Geophys. Res.* **96**, 17297–17305 (1991).

Herman, J. R., R. McPeters, and D. Larko, Ozone depletion at northern and southern latitudes derived from January 1979 to December 1991 Total Ozone Mapping Spectrometer Data, *J. Geophys. Res.* **98**, 12783–12793 (1993).

Hofmann, D. J., S. J. Oltmans, J. M. Harris, S. Solomon, T. Deshler, and B. J. Johnson, Observation and possible causes of new ozone depletion in Antarctica in 1991, *Nature* **359**, 283–287 (1992).

Hofmann, D. J., S. J. Oltmans, J. A. Lathrop, J. M. Harris, and H. Vomel, Record low ozone at the south pole in the spring of 1993, *Geophys. Res. Lett.* **21**, 421–424 (1994).

Kanzawa, H., and S. Kawaguchi, Large stratospheric sudden warming in Antarctic late winter and shallow ozone hole in 1988, *Geophys. Res. Lett.* **17**, 77–80 (1990).

Krueger, A. J., R. S. Stolarski, and M. R. Schoeberl, Formation of the 1988 Antarctic ozone hole, *Geophys. Res. Lett.* **16**, 381–384 (1989).

Krueger, A. J., M. R. Schoeberl, P. A. Newman, and R. S. Stolarski, The 1991 Antarctic ozone hole: TOMS observations, *Geophys. Res. Lett.* **19**, 1215–1218 (1992).

Lait, L. R., M. R. Schoeberl, and P. A. Newman, Quasi-Biennial modulation of the Antarctic ozone depletion, *J. Geophys. Res.* **94**, 11559–11571 (1989).

Leovy, C. B., C-R. Sun, M. H. Hitchman, E. E. Remsberg, J. M. Russell III, L. L. Gordley, J. C. Gille, and L. V. Lyjak, Transport of ozone in the middle stratosphere: Evidence for planetary wave breaking, *J. Atmos. Sci.* **42**, 230–244 (1985).

Mahlman, J. D., and S. B. Fels, Antarctic ozone decreases: a dynamical cause ?, *Geophys. Res. Lett.* **13**, 1316–1319 (1986).

Mahlman, J. D., J. P. Pinto, and L. J. Umscheid, Transport, radiative, and dynamical effects of the Antarctic ozone hole: A GFDL "SKYHI" model experiment, *J. Atmos. Sci.* **51**, 489–508 (1994).

Manney, G. L., L. Froidevaux, J. W. Waters, L. S. Elson, E. F. Fishbein, and R. W. Zurek, The evolution of ozone observed by UARS MLS in the 1992 late winter southern polar vortex, *Geophys. Res. Lett.* **20**, 1279–1282 (1993a).

Manney, G. L., and R. W. Zurek, Interhemispheric comparison of the development of the stratospheric polar vortex during fall: A 3-dimensional perspective for 1991-1992, *Geophys. Res. Lett.* **20**, 1275–1278 (1993b)

Manney, G. L., L. Froidevaux, J. W. Waters, R. W. Zurek, W. G. Read, L. S. Elson, J. B. Kumer, J. L. Mergenthaler, A. E. Roche, A. O'Neill, R. S. Harwood, I. MacKenzie, and R. Swinbank, Chemical depletion of ozone in the Arctic lower stratosphere during winter 1992-1993, *Nature* **370**, 429–434 (1994a).

Manney, G. L., R. W. Zurek, A. O'Neill, and R. Swinbank, On the motion of air through the stratospheric polar vortex, *J. Atmos. Sci.* **51**, 2973–2994 (1994b).

Manney, G. L., L. Froidevaux, J. W. Waters, and R. W. Zurek, Evolution of microwave limb sounder ozone and the polar vortex during winter, *J. Geophys. Res.* **100**, 2953–2972 (1995).

McElroy, M. B., R. J. Salawitch, S. C. Wofsy, and J. A. Logan, Reductions of Antarctic ozone due to synergistic interactions of chlorine and bromine, *Nature* **321**, 759–762 (1986a).

McElroy, M. B., R. J. Salawitch, and S. C. Wofsy, Antarctic O_3: Chemical mechanisms for the spring decrease, *Geophys. Res. Lett.* **13**, 1296–1299 (1986b).

McIntyre, M. E., On the Antarctic ozone hole, *J. Atmos. Terr. Phys.* **51**, 29–43 (1989).

Molina, L. T., and M. J. Molina, Production of Cl_2O_2 from the self-reaction of the ClO radical, *J. Phys. Chem.* **91**, 433–436 (1987a).

Molina, M. J., T.-L. Tso, L. T. Molina, and F. C.-Y. Wang, Antarctic stratospheric chemistry of chlorine nitrate, hydrogen chloride, and ice: Release of active chlorine, *Nature* **27**, 1253–1257 (1987b).

Randel, W. J., The anomalous circulation in the southern hemisphere stratosphere during spring 1987, *Geophys. Res. Lett.* **15**, 911–914 (1988).

Randel, W. J., and F. Wu, TOMS total ozone trends in potential vorticity coordinates, *Geophys. Res. Lett.* **22**, 683–686 (1995).

Salawitch, R. J., S. C. Wofsy, and M. B. McElroy, Influence of polar stratospheric clouds on the depletion of Antarctic ozone, *Geophys. Res. Lett.* **15**, 871–874 (1988).

Sander, S. P., R. R. Friedl, and Y. L. Yung, Rate of formation of ClO dimer in the polar stratosphere: Implications for ozone loss, *Science* **245**, 1095–1098 (1989).

Santee, M. L., W. G. Read, J. W. Waters, L. Froidevaux, G. L. Manney, D. A. Flower, R. F. Jarnot, R. S. Harwood, and G. E. Peckham, Interhemispheric differences in polar stratospheric HNO_3, H_2O, ClO, and O_3, *Science* **267**, 849–852 (1995).

Schoeberl, M. R., R. S. Stolarski, and A. J. Krueger, The 1988 Antarctic ozone depletion: Comparison with previous year depletions, *Geophys. Res. Lett.* **16**, 377–380 (1989).

Schoeberl, M. R., and D. L. Hartmann, The dynamics of the stratospheric polar vortex and its relation to springtime ozone depletions, *Science* **251**, 46–52 (1991).

Schoeberl, M. R., L. R. Lait, P. A. Newman, and J. E. Rosenfield, The structure of the polar vortex, *J. Geophys. Res.* **97**, 7859–7882 (1992).

Schoeberl, M. R., S. D. Doiron, L. R. Lait, P. A. Newman, and A. J. Krueger, A simulation of the Cerro Hudson SO_2 cloud, *J. Geophys. Res.* **98**, 2949–2955 (1993).

Solomon, S., R. R. Garcia, F. S. Rowland, and D. J. Wuebbles, On the depletion of Antarctic ozone, *Nature* **321**, 755–758 (1986).

Solomon, S., The Mystery of the Antarctic ozone "Hole", *Rev. Geophys.* **26**, 131–148 (1988).

Solomon, S., Progress towards a quantitative understanding of Antarctic ozone depletion, *Nature* **347**, 347–354 (1990).

Stolarski, R. S., A. J. Krueger, M. R. Schoeberl, R. D. McPeters, P. A. Newman, and J. C. Alpert, Nimbus 7 satellite measurements of the springtime Antarctic ozone decrease, *Nature* **322**, 808–811 (1986).

Stolarski, R. S., M. R. Schoeberl, P. A. Newman, R. D. McPeters, and A. J. Krueger, The 1989 Antarctic ozone hole as observed by TOMS, *Geophys. Res. Lett.* **17**, 1267–1270 (1990).

Stolarski, R. S., P. Bloomfield, R. D. McPeters, and J. R. Herman, Total ozone trends deduced from Nimbus 7 TOMS data, *Geophys. Res. Lett.* **18**, 1015–1018 (1991).

Stolarski, R. S., R. Bojkov, L. Bishop, C. Zerefos, J. Staehelin, and J. Zawodny, Measured trends in stratospheric ozone, *Science* **256**, 342–349 (1992).

Sze, N. D., M. K. W. Ko, D. K. Weisenstein, J. M. Rodriguez, R. S. Stolarski, and M. R. Schoeberl, Antarctic ozone hole: Possible implications for ozone trends in the Southern Hemisphere, *J. Geophys. Res.* **94**, 11521–11528 (1989).

Tolbert, M. A., M. J. Rossi, R. Malhotra, and D. M. Golden, Reaction of chlorine nitrate with hydrogen chloride and water at Antarctic stratospheric temperatures, *Science* **238**, 1258–1260 (1987).

Toon, O. B., P. Hamill, R. P. Turco, and J. Pinto, Condensation of HNO_3 and HCl in the winter polar stratosphere, *Geophys. Res. Lett.* **13**, 1284–1287 (1986).

Tung, K. K., M. K. W. Ko, J. M. Rodriguez, and N. D. Sze, Are Antarctic ozone variations a manifestation of dynamics or chemistry ? *Nature* **322**, 811–814

(1986).

Tung, K. K., and H. Yang, Global QBO in circulation and ozone. Part I: Reexamination of observational evidence, *J. Atmos. Sci.* **51**, 2699–2707 (1994a).

Tung, K. K., and H. Yang, Global QBO in circulation and ozone. Part II: A simple mechanistic model, *J. Atmos. Sci.* **51**, 2708–2721 (1994b).

Waters, J. W., L. Froidevaux, W. G. Read, G. L. Manney, L. S. Elson, D. A. Flower, R. F. Jarnot, and R. S. Harwood, Stratospheric ClO and ozone from the Microwave Limb Sounder on the Upper Atmosphere Research Satellite, *Nature* **362**, 597–602 (1993a).

Waters, J. W., L. Froidevaux, G. L. Manney, W. G. Read, and L. S. Elson, MLS observations of lower stratospheric ClO and O_3 in the 1992 southern hemisphere winter, *Geophys. Res. Lett.* **20**, 1219–1222 (1993b).

Weisenstein, D. K., M. K. W. Ko, and N.-D. Sze, The chlorine budget of the present-day atmosphere: A modeling study, *J. Geophys. Res.* **97**, 2547–2559 (1992).

WMO, Report of the International Ozone Trends Panel: 1988, World Meteorological Organization Report No. 18 (1988).

WMO, Scientific Assessment of Stratospheric Ozone: 1989, World Meteorological Organization Report No. 20 (1989).

WMO, Scientific Assessment of Ozone Depletion: 1991, World Meteorological Organization Report No. 25 (1991).

Wofsy, S. C., M. J. Molina, R. J. Salawitch, L. E. Fox, and M. B. McElroy, Interactions between HCl, NOx, and H_2O ice in the Antarctic stratosphere: Implications for ozone, *J. Geophys. Res.* **93**, 2442–2450 (1988).

Yang, H., and K. K. Tung, Statistical significance and pattern of extratropical QBO in column ozone, *Geophys. Res. Lett.* **21**, 2235–2238 (1994).

Yung, Y.L., M. Allen, D. Crisp, R. W. Zurek, and S. P. Sander, Spatial variation of ozone depletion rates in the springtime Antarctic polar vortex, *Science* **248**, 721–724 (1990).

Chapter 2 Decadal Change of the Standard Deviation of Column Ozone from the Zonal Mean

Yibo Jiang, Yuk L. Yung

Division of Geological and Planetary Sciences

California Institute of Technology

Pasadena, CA 91125

and

Anne R. Douglass

Laboratory for Atmospheres

Goddard Space Flight Center

Greenbelt, Maryland 20771

Submitted to *Geophysical Research Letters*on March 10, 1997

Contribution number 5754 from the Division of Geological and Planetary Sciences,

California Institute of Technology.

Abstract

Standard deviation of column ozone from the zonal mean (COSDZ) provides a measure of the longitudinal inhomogeneity in ozone and dynamical wave activities in the atmosphere. We point out that simulation of this quantity by three-dimensional (3-D) models could provide a sensitive check on the wave activities in the stratosphere that are responsible for ozone transport. Analysis of the Total Ozone Mapping Spectrometer (TOMS) data shows a profound secular change in COSDZ from 1979 to 1992. The changes are not symmetric between the southern and northern atmospheres. In the southern higher latitudes, COSDZ shows a significant increase around 65° in August and September, while the changes are much smaller in the northern higher latitudes in the boreal spring. We interpret most of the observed changes to be caused by enhanced ozone losses in the polar vortices in the springtime of the two respective hemispheres. There is evidence for secular dynamical changes at mid-latitudes.

2.1 Introduction

The atmosphere (including stratosphere and troposphere) is changing both chemically and dynamically in ways that may be subtly coupled [McElroy *et al.*, 1992]. Negative ozone trends at high latitudes in both hemispheres are predominantly due to the heterogeneous chemical losses on polar stratospheric cloud particles and aerosols, stemming ultimately from anthropogenic emissions of chlorofluorocarbons (see e.g. WMO 1994). The direct effect of this ozone trend is to exert a cooling, which varies both spatially and seasonally in the lower stratosphere [Ramaswamy *et al.*, 1996]. How these climatic changes (self-induced or otherwise) feed back on the distribution of ozone is not well understood. We shall argue that the standard deviation of column ozone from the zonal mean (COSDZ) provides another valuable indicator of the variability of the stratosphere.

In this paper, we use the high resolution ($1° \times 1.25°$ in latitude and longitude) Nimbus 7 total ozone mapping spectrometer (TOMS) version 7 data from 1979 to 1992 [McPeters and Labow, 1996]. The total column ozone Ω can be expanded in zonal Fourier harmonics up to some zonal wave number N representing the limit of resolution of the data [Andrews *et al.*, 1987],

$$\Omega(\phi) = \Omega_0 + \sum_{n=1}^{N} \Omega_n \cos(n\phi + \alpha_n) \tag{2.1}$$

Here ϕ is longitude in radians, α_n is the phase for wavenumber n and $\Omega(\phi)$ is column ozone as a function of ϕ. We have zonal-averaged column ozone in each latitude

$$\Omega_0 = \frac{1}{2\pi} \int_0^{2\pi} \Omega d\phi \tag{2.2}$$

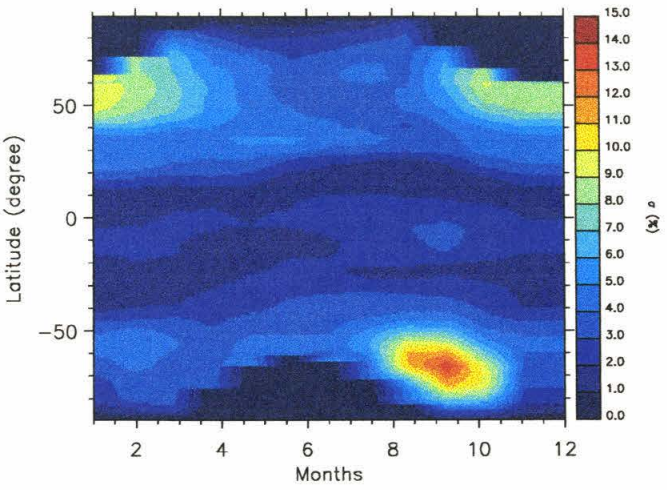

(a)

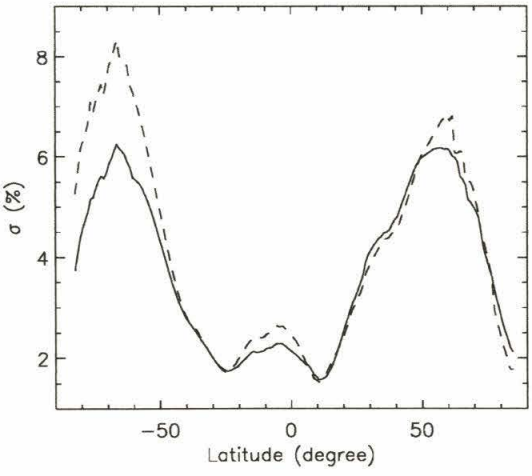

(b)

Figure 2.1: (a) Climatology of COSDZ from 1979 to 1992; (b) Annual average of COSDZ from 1979 to 1992.

Previous studies of zonal-averaged column ozone trend [Stolarski *et al.*, 1991] have focused on Ω_0, which is mainly caused by the chemical effects. All the information in higher wavenumbers (≥ 1) was discarded in this analysis due to zonal averaging. It is known that the higher wavenumbers represent the dynamical wave activities in the atmosphere. In this paper, we will demonstrate the usefulness of the higher wavenumbers for monitoring the change of the dynamical activity of the stratosphere. We define the column ozone standard zonal deviation (COSDZ) and derive the relationship between COSDZ and the higher wave harmonics.

Let

$$\Sigma^2(\Omega) = \frac{1}{2\pi}\int_0^{2\pi}(\Omega - \overline{\Omega})^2 d\phi$$

We have

$$\Sigma^2(\Omega) = \frac{1}{2\pi}\int_0^{2\pi}\left(\sum_{n=1}^{N}\Omega_n\cos(n\phi+\alpha_n)\right)^2 d\phi = \frac{1}{2}\sum_{n=1}^{N}{\Omega_n}^2 \tag{2.3}$$

Thus

$$\Sigma(\Omega) = \sqrt{\frac{1}{2}\sum_{n=1}^{N}{\Omega_n}^2} \tag{2.4}$$

Therefore, COSDZ ($\sigma(\Omega)$) represents the sum of the intensity of all higher wavenumbers in the Fourier harmonics. It is convenient to define the dimensionless quantities

$$\begin{aligned} \omega_n &= \frac{\Omega_n}{\Omega_0} \\ \sigma(\Omega) &= \frac{\Sigma(\Omega)}{\Omega_0} \end{aligned} \tag{2.5}$$

In the following, we will refer $\sigma(\Omega)$ as COSDZ.

2.2 Results and Discussion

The TOMS monthly average data is used in the analysis. Figure 2.1a shows the climatology of COSDZ which averaged from 1979 to 1992 in each latitude. COSDZ is more than 10% in high latitude regions during both Arctic and Antarctic winter/spring. There are at least two reasons. First, there are great wave activities in the winter stratosphere. Second, the formation of the polar vortex followed by ozone depletion inside creates a large gradient in ozone across the vortex boundary. Any excursion of the polar vortex away from the poles will contribute to COSDZ. In the southern hemisphere, the peak value is achieved in October when the ozone hole is well developed and starts to breakup. Similarly, the peak in COSDZ occurs in January and February in the northern hemisphere. The high COSDZ in northern hemisphere extends to midlatitude while it is confined to the polar region in the southern hemisphere. This can also be seen in Figure 2.1b, which gives the annual average of COSDZ based on Figure 2.1a. The peak in the annually averaged COSDZ in the northern hemisphere is wider than that in the southern hemisphere.

COSDZ is low in the tropics, where typical values are about 2%, with little seasonal variation. This may be due to the lack of planetary wave activities at the equator relative to the midlatitudes. Averaged over a year (Figure 2.1b) COSDZ values in both hemispheres are relatively symmetric with COSDZ peaks located at latitude $\pm 65^{\circ}$, though the northern hemisphere peak is broader than that of the southern hemisphere. It is worth noting that COSDZ is low at the summer poles. The reason is the relative lack of planetary wave activities in this season.

The results summarized in Figure 2.1a and 2.1b are generally consistent with those obtained by Randel and Wu [1995], but it is difficult to make a quantitative comparison because all their values for standard deviations were multiplied by the

square root of the cosine of latitude.

We shall argue that COSDZ provides a valuable check for the 3-D models of stratospheric ozone. Unfortunately, there are no published model results for COSDZ to compare with Figure 2.1a and 2.1b. We compute the values for COSDZ from the Goddard 3-D model for stratospheric ozone [Douglass *et al.*, 1996] from September 11, 1991 to September 8, 1992. This model uses winds from the Goddard Earth Observing System Data Assimilation System (GEOS DAS) for transport (Schubert *et al.*, 1993). The results are presented in Figure 2.2a and 2.2b. Compared with Figs. 1a and 1b and TOMS COSDZ, it is clear that the Goddard model simulates correctly the general pattern of COSDZ observed by TOMS, including the high winter polar peaks and the low values in the the summer poles. However, the magnitude of the model COSDZ is about a factor of two larger than the observations.

The minimum in COSDZ in the tropics is not reproduced in the model, in spite of the reasonable agreement between the zonal mean total ozone and TOMS observations as reported by Douglass *et al.* (1996). The COSDZ provides a more quantitative measure of the excess variability found particularly in the model tropics and subtropics. This excess variability is produced not by the chemistry and transport model but by the noisy assimilation wind fields which are input to the model. Efforts are underway both to improve the Goddard assimilation procedure in the tropics, thereby reducing the nonphysical variability, and to improve the usage of the assimilation fields in the model. This diagnostic can be easily applied model ozone fields that are calculated using winds from a general circulation model.

The decadal trend in zonally averaged ozone is well known [e.g. Stolarski *et al.*, 1991], but that for COSDZ is poorly known. The COSDZ trend in each latitude from 1979 to 1992 is shown in Figure 2.3a and 2.3b. [The years after 1992 were not

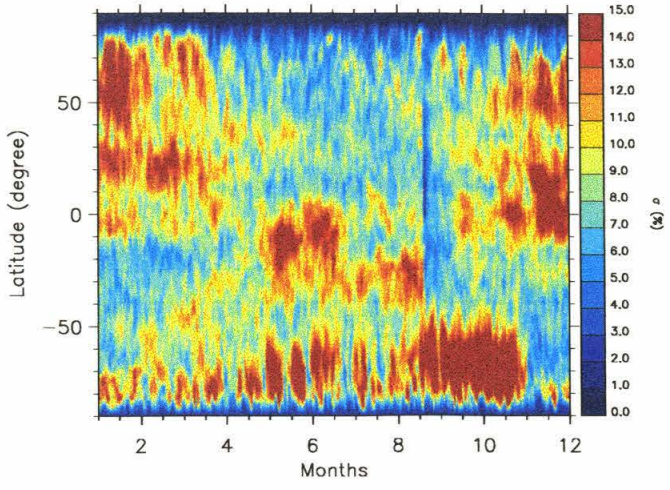

(a)

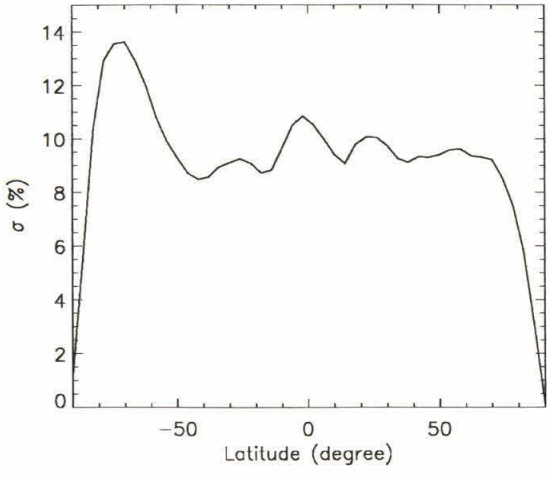

(b)

Figure 2.2: (a) Model COSDZ from September 11, 1991 to September 8, 1992; (b) Annual-average of model COSDZ. Data from output of the Goddard model [Douglass *et al.*, 1996].

used due to complications arising from Pinatubo aerosols.] There is a negative trend in mid-latitude in both hemispheres with a maximum decrease of 0.2%/decade. In the equatorial region the trend is slightly positive or close to zero. There is also a negative trend in November and December in both hemispheres. The trends are small except in the polar region during polar winter. The reason for the significantly high increase (6%/decade) in southern polar region in August and September is due to the deepening of the Antarctic ozone hole. As there is a much smaller peak in the northern high latitudes in the winter. Comparing Figure 2.3a and 2.1a, we cannot see any symmetry in the COSDZ trend in both hemisphere. It remains a challenge to 3-D models of the stratosphere to reproduce the observed trend in COSDZ and to evaluate the chemical and dynamical contributions to that trend.

Comparing Figure 2.3a and 2.1a, we may note that the COSDZ trend peak is two months earlier than the COSDZ peak. This may be caused by a climatological change in the stratosphere in the last decade. As Kodera and Yamazaki (1994) have recently argued, the polar lower stratospheric cooling trends in November and associated accelerations of the polar night jet may have induced significant trends in tropospheric dynamics later in the winter. Included among the expected modifications of tropospheric dynamics are changes in planetary wave propagation that could result in significant indirect perturbations of the tropospheric stationary wave pattern at northern midlatitudes. One possible mechanism is radiative and dynamical heating changes associated with stratospheric ozone depletion.

Figure 2.2b gives the annually averaged COSDZ trend as a function of latitude. The southern polar region stands out with a trend approaching 2% per decade. Most of the other regions show a small increase except in the mid-latitude region where there is a significant decrease in both hemispheres. This may be another piece of evidence

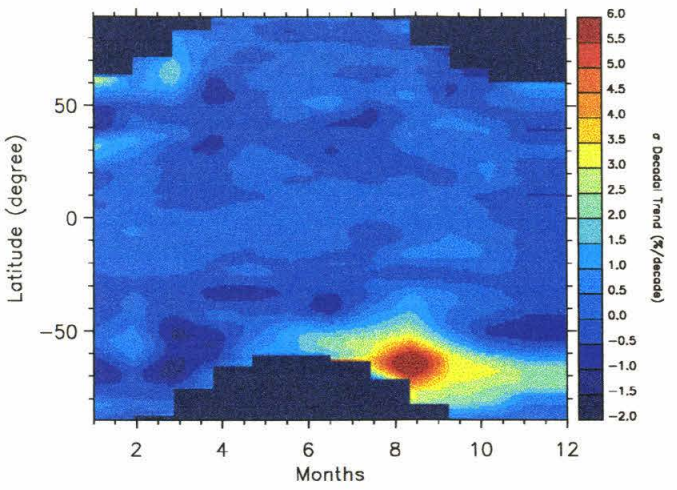

(a)

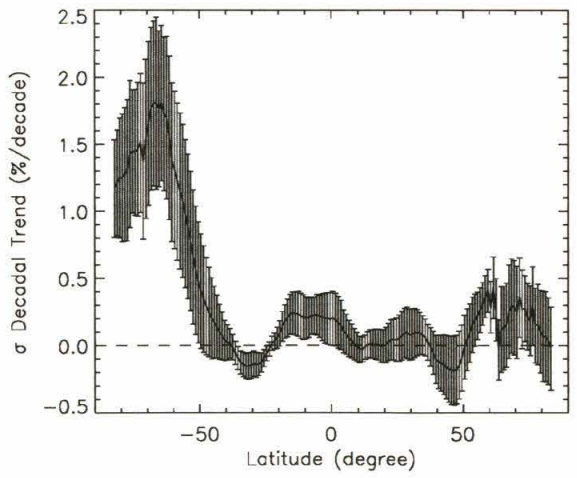

(b)

Figure 2.3: (a) Decadal trend of COSDZ in each month from 1979 to 1992; (b) Annual-averaged decadal trend of COSDZ in each month from 1979 to 1992.

suggesting that the dynamics of the lower stratosphere and upper troposphere may be changing.

Through the analysis of TOMS ozone and geopotential data, Hood and Zaff (1995) have recently showed that the geopotential height deviation at 50° in January at lower stratosphere and troposphere is significantly weaker in 1989-1991 than that in 1980-1982. They concluded that the observed longitude dependence of winter total ozone trends in the northern high latitude during the 1980s is most probably a consequence of decadal climate variability originating in the troposphere. Randel and Cobb (1994) also demonstrated that both ozone and temperature trends resembled a zonal wave 1 pattern, which suggests a dynamical origin for this spatial dependence. These suggestions are consistent with a decrease in COSDZ.

2.3 Conclusions

The intricate coupling between atmospheric chemistry, radiation, climate and dynamics has recently been discussed in a seminal paper by McElroy *et al.* (1992), but there is no definitive evidence for the coupled changes. In this paper we point out the potential usefulness of the standard deviation of column ozone from the zonal mean (COSDZ) as a key index of change of the middle atmosphere.

The pattern of COSDZ extracted from Version 7 of TOMS data (Figure 2.1a and 2.1b) reveals a complex interplay between chemistry and dynamics in determining the distribution of stratospheric ozone. A state of the art 3-D model (Figure 2.2a and 2.2b) captures the essential features of the observed pattern, but the absolute magnitude appears to be too high by a factor of two. The pattern in the decadal trend of COSDZ (Figure 2.3a and 2.3b) indicates that the decadal change of stratospheric ozone is dominated by ozone depletion in the polar winter, with a minor contribution

from dynamical changes, especially at the midlatitudes.

It remains a challenge to 3-D models to reproduce both the climatological mean of the observed COSDZ and its decadal trend.

2.4 Acknowledgements.

We thank M. Allen, L. Hood, A. Ingersoll, J. Kaye, R. Salawitch, R. Stolarski, and R. Zurek for valuable comments. This work was supported by NASA grant NAG1-1806 to the California Institute of Technology. Contribution number 5754 from the Division of Geological and Planetary Sciences, California Institute of Technology.

2.5 References

Andrews, D. G., J. R. Holton, and C. B. Leovy, *Middle Atmosphere Dynamics*, Academic, San Diego, Calif., 1987.

Douglass, A. R., C. J. Weaver, R. B. Rood, and L. Coy, A three-dimensional simulation of the ozone annual cycle using winds from a data assimilation system, *J. Geophys. Res.*, **101**, 1463-1474, 1996.

Hood, L. L., and J. P. McCormack, Components of interannual ozone change based on Nimbus 7 TOMS data, *Geophys. Res. Lett.*, **19**, 2309-2312, 1992.

Hood, L. L., and D. A. Zaff, Lower stratospheric stationary waves and the longitude dependence of ozone trends in winter, *J. Geophys. Res.*, **100**, 25791-25800, 1995.

Kaye, J. A., A. R. Douglass, R. B. Rood, R. S. Stolarski, P. A. Newman, D. J. Allen, and E. M. Larson, Spatial and temporal variability of the extent of chemically processed stratospheric air, *Geophys. Res. Lett.*, **18**, 29-32, 1991.

Kurzeja, R. J., Spatial variability of total ozone at high latitudes in winter, *J. Atmos. Sci.*, **41**, 695-697, 1984.

McElroy, M. B., R. S. Salawitch, and K. Minschwaner, The changing stratosphere, *Planet Space Sci.*, **40**, 373-401, 1992.

McPeters, R. D., G. J. Labow, An assessment of the accuracy of 14.5 years of Nimbus-7 TOMS version 7 ozone data by comparison with the dobson network, *Geophys. Res. Lett.* **23**, 3695-3698, 1996.

Pawson, S., T. Kubitz, Climatology of planetary waves in the northern stratosphere, *J. Geophys. Res.* **101**, 16987-16996, 1996.

Randel, W. J., and J. B. Cobb, Coherent variations of monthly mean total ozone and lower stratospheric temperature, *J. Geophys. Res.*, **99**, 5433-5447, 1994.

Randel, W. J., and F. Wu, Climatology of stratospheric ozone based on SBUV and SBUV/2 data: 1978-1994, *NCAR Technical Note*, 1995.

Rood, R. B., and A. R. Douglass, Interpretation of ozone temperature correlations, *J. Geophys. Res.*, **90**, 5733-5743, 1985.

Ramaswamy, V., M. D. Schwarzkopf, and W. J. Randel, Fingerprint of ozone depletion in the spatial and temporal pattern of recent lower-stratospheric cooling, *Nature*, **382**, 616-618, 1996.

Schubert, S., R. Rood, J. Pfaendtner, An assimilated dataset for earth science applications, *Bull. Am. Meteorol. Soc.* **74**, 2331-2342, 1993.

Stolarski, R. S., P. Bloomfield, R. D. McPeters, J. R. Herman, Total ozone trends deduced from Nimbus 7 TOMS data, *Geophys. Res. Lett.* **18**, 1015-1018, 1991.

Chapter 3 Tropospheric Ozone from 1979 to 1992 Over Tropical Pacific South America from TOMS data

Yibo Jiang, Yuk L. Yung

Division of Geological and Planetary Sciences

California Institute of Technology

Pasadena, CA 91125

Published in modified form in *Science* **272**, 714-716, 1996.

Contribution number 5644 from the Division of Geological and Planetary Sciences, California Institute of Technology.

Abstract

An estimate of tropospheric ozone levels is obtained from the difference in the TOMS (Total Ozone Mapping Spectrometer) data between the high Andes and the Pacific Ocean. From 1979 to 1992 tropospheric ozone apparently increased by 1.48 $\pm$ 0.40 %/yr or 0.21 $\pm$ 0.06 DU/yr over South America and the surrounding oceans. An increase in biomass burning in the Southern Hemisphere can account for this trend in tropospheric ozone levels.

3.1 Introduction

Tropospheric ozone is known to play a key role in regulating the chemical composition and climate of the troposphere [Logan it et al., 1981]. Ozone is photolyzed to form $O(^1D)$, which reacts with H_2O to form reactive HO_x radicals in the troposphere. These radicals are in turn involved in a series of chemical reactions that are important for the lifetimes of a large number of gases (e.g. CH_4, CO, CH_3X, where X is a halogen or nitrile). Ozone is also part of air pollution. Its increase in the atmosphere is of concern because it has a deleterious effects on vegetation and human health.

There is general agreement that tropospheric ozone levels have increased in recent decades in the temperate zones in the Northern Hemisphere, but trends seem to vary geographically and temporally. A regional increase in tropospheric ozone levels was first documented by Warmbt (1979), who analysed a 20-year record of surface ozone measurements at stations in Germany between the mid-1950s and 1970s. Analyses of the vertical dependence of the ozone levels were then attempted, using the record of ozonesonde readings [Angell and Korshover, 1983; Logan, 1985; Tiao it et al., 1986; Staehelin and Schmid, 1991]. These studies typically showed an increase in ozone levels of about 1% per year in the lower troposphere. However, detailed analysis revealed that ozone levels from 1979 to 1982 in the layer from 0 to 5 km varied from year to year by -2 to 3% per year among 12 ozonesonde stations at mid- and high-latitudes in the Northern Hemisphere [Tiao it et al., 1986]. Recently, Tarasick *et al.* (1995) found that tropospheric ozone levels had decreased over Canada from 1980 to 1993. On the other hand, there have been few measurements in the Southern Hemisphere. In this study, we use space-borne measurements of tropospheric ozone to show that tropospheric ozone levels have increased over Pacific South America from 1979 to 1992.

The Total Ozone Mapping Spectrometer (TOMS) instrument on the Nimbus 7 spacecraft has measured the spatial distribution of total ozone from 1978 until 6 May 1993. By scanning across the track of the satellite, TOMS obtained data between successive satellite orbital tracks. We used the daily TOMS gridded ozone data of Version 7 [Herman *et al.*, 1991] (on a $1^\circ \times 1.25^\circ$ grid in latitude and longitude) from 1979 to 1992. The improvements of Version 7 over Version 6 that are essential for this work are as follows: (1) improved ISCCP cloud height climatology and higher resolution terrain height maps, (2) use of a more accurate model for partially-clouded scenes, and (3) improved radiative transfer calculations for table generation.

3.2 Results and Discussions

The high Andes along the west coast of Central South America and the nearby oceans, provides a topographic contrast in which the TOMS data can be used to examine ozone levels in the lower troposphere by difference. The highest mountains are 6768 m above sea level in Peru and 6908 m above sea level in Chile. Therefore the total column ozone measurement by TOMS in these regions will be above the bulk of the troposphere. For a region spanning only a few degrees in latitude and longitude, we assume that the ozone vertical distribution does not change. Taking the January, 1980 column ozone map as an example, as shown in Figure 3.1, the column ozone is relatively smooth in the east-west direction over South America, except for the region near the Andes, where ozone levels are low. Because TOMS measured column ozone from the top of the atmosphere to the surface of the Earth, the difference of TOMS column ozone from the mountains to surrounding oceans gives us the column ozone value from sea level to the top of the mountains about 6 km above sea level. According to Hudson *et al.* (1995), the TOMS algorithm is not very sensitive in

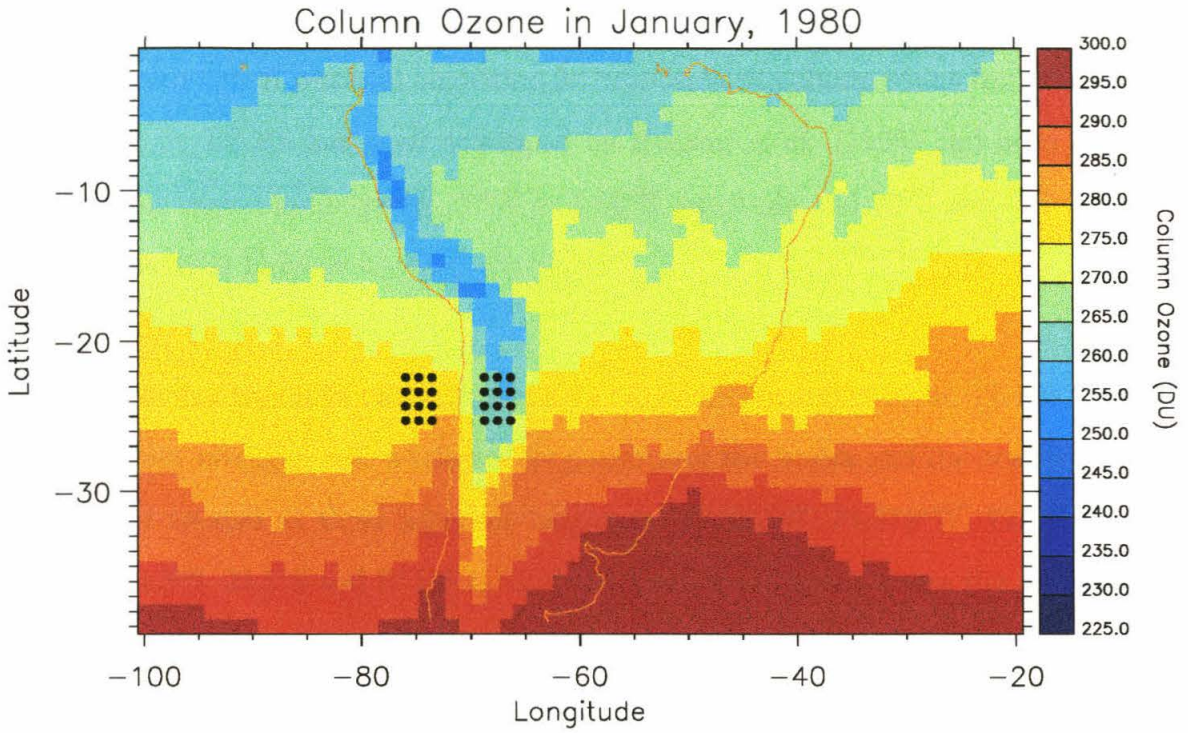

Figure 3.1: Monthly averaged column ozone of January, 1980 from TOMS with color code from 220 DU to 300 DU. Solid black square encloses the region we consider. The black dots are the 24 points used in the analysis. The TOMS data are from Herman *et al.* (1993).

detecting O_3 in the lower troposphere (about 60% efficiency in detecting O_3 in this layer). The a priori column O_3 between 1000 and 500 mb as in the TOMS algorithm is about 13 DU. Thus, if a value of 20 DU for the tropospheric O_3 is derived, this value must be corrected by the efficiency factor, about 60%, to get the right value (20 DU - 13 DU)/0.6 + 13 DU = 24.7 DU - giving a trend of 2.30 $\pm$ 0.62% per year relative to the initial value of 15.23 DU. In this paper, the correction proposed above was not adopted. A retrieval algorithm for tropospheric column ozone from radiances measured by TOMS has been developed by Hudson *et al.* (1995) had been applied only to the region bounded by 20°W and 60°E longitude and 20°S and 0°S latitude during the 1989 biomass burning season.

To examine trends in this difference, we analysized monthly mean TOMS column ozone values averaged over a selected 24 points over the Andes and the oceans. These points are located at three adjacent longitude (75.625°W, 74.375°W, 73.125°W) at 25.5°S, 24.5°S, 23.5°S and 22.5°S latitude for the column ozone above the sea surface, and three adjacent longitude (68.125°W, 66.875°W, 65.625°W) at 25.5°S, 24.5°S, 23.5°S and 22.5°S latitude for the column ozone above mountains. There are a total of 24 data points in each monthly averaged TOMS data file in the respective region we considered. From 1979 to 1992, the ocean (higher) ozone shows no obvious trend (Figure 3.2A) which is consistent with results in the equatorial region [Herman *et al.*, 1993]. However, the difference, the tropospheric column ozone in the 0–6 km layer (Figure 3.2B) has increased by about 1.48 $\pm$ 0.40 % per year relative to the reference tropospheric column ozone of 14.34 DU in 1979, which is consistent with the trend obtained through the use of the tropospheric residual technique [Fishman *et al.*, 1990, 1993]. This is equivalent to an increase of 0.21 $\pm$ 0.06 DU per year. The years with El Nino (1982–83, 1986–87) are marked by lower ozone values. Some comparison of

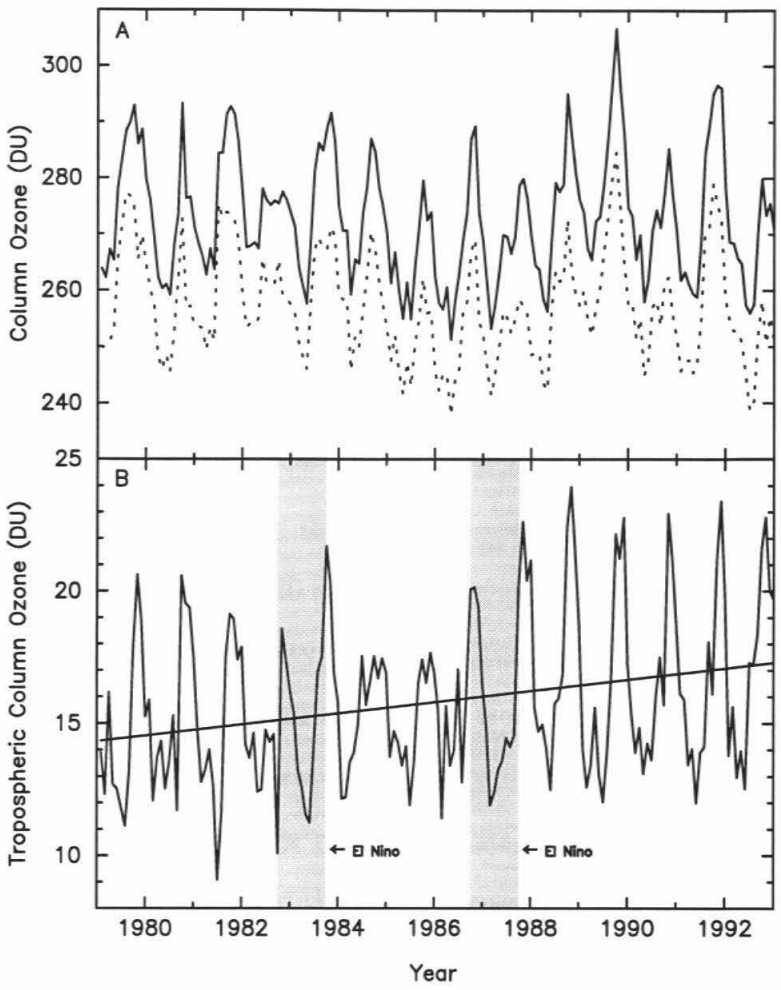

Figure 3.2: (a) Averaged column ozone over the mountain region (low ozone, dotted line) and the nearby oceans (higher ozone, solid line). (b) Tropospheric column ozone from sea level to 6 km is shown with a straight line as a linear least squares fit to the data. The slope of the line is 1.48 $\pm$ 0.40%/yr. Two major El Nino events are indicated by shaded regions.

these results is possible using the ozonesonde measurements nearby at Natal, Brazil (6°S, 35°W) [Kirchhoff *et al.*, 1989, 1991]. Data have been obtained here from 1978 to 1988, but these are relatively sparse and unevenly distributed in time of the ozone soundings [Fishman *et al.*, 1990], and are not adequate to study ozone trends, but can be used to assess our tropospheric column ozone calculation. Our estimate shows an ozone column of 20.29 DU in 0–6 km layer in September 1987 as compared to about 16.33 DU at Natal. In addition both data sets show high levels of ozone from August to November in each year. Considering the roughness in the calculation of column ozone at Natal, the two datasets agree.

A likely cause of the increase in ozone levels is an increase in biomass burning [Fishman *et al.*, 1990, 1993]. As shown in Figure 3.3A, which plots the biomass burning [Hao and Liu, 1994] from 20 to 30°S, the seasonality of the tropospheric ozone is well correlated with the seasonality of the biomass burning. Ozone column amounts and rates of biomass burning were both high from August to November in each year. Although it is hard to separate the stratospheric sources from anthropogenic sources of tropospheric ozone, this result suggests that the higher values of ozone between August and November are the direct consequences of biomass burning. The anomalous low O_3 concentration in El Nino years may be a result of a decrease in biomass burning during these wetter years [1].

[1] Other factors could contribute to the deviation of tropospheric O_3 from the linear trend during El Nino years, such as higher level clouds (due to deep convection) or less cloud in the lower troposphere, which would cause an underestimation of tropospheric O_3. Reflectivity and cloud height data can be examined in this region, but these analyses are beyound the scope of this paper.

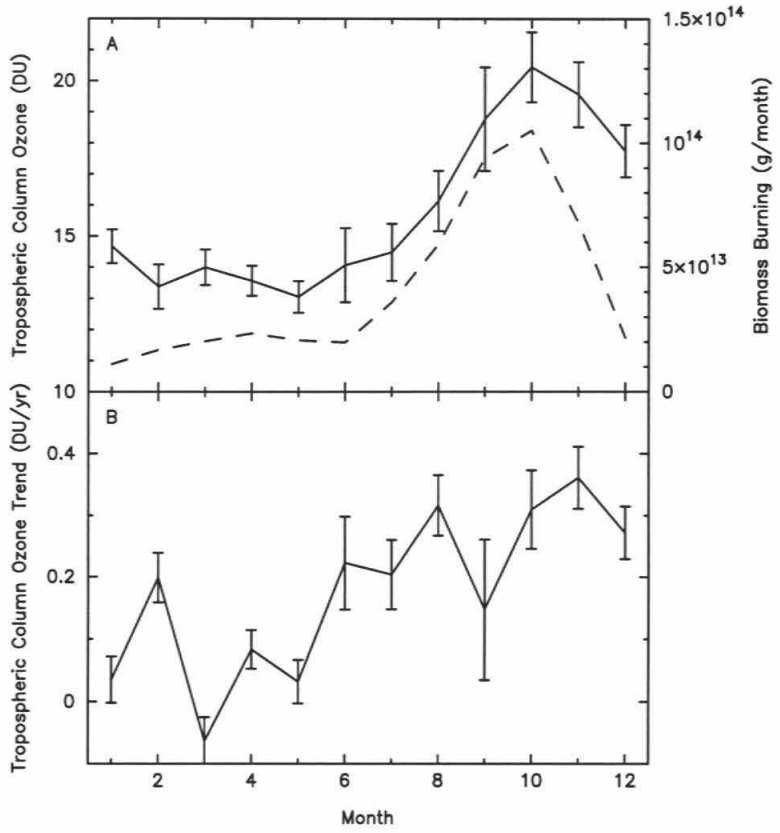

Figure 3.3: (a) Climatological tropospheric ozone (solid line) averaged from 1979 to 1992 and biomass burning (dash line) in 20–30°S latitude belt. To convert from g-biomass to g-carbon, multiply by 0.5. (b) Tropospheric ozone trends (DU/yr) in each month from 1979 to 1992. The biomass burning data is from Hao and Liu (1994).

3.3 Conclusions

Analysis of tropospheric ozone trends from 1979 to 1992 for each month (Figure 3.3B) supports the conclusion that the biomass burning causes the tropospheric ozone increasing. Ozone trends are higher around 0.35 DU/yr, between August and November versus about 0.15 DU/yr at other times.

3.4 Acknowledgements

We thank R. S. Stolarski for sharing his insights of the TOMS data and thank M. Allen, Wei Min Hao, A. Ingersoll, J-H Kim, R. Salawitch and S. Sander for valuable comments. We thank the Goddard Ozone Processing Team for kindly allowing us to use their data prior to publication. This work was supported by NASA grant NAGW 2204 and NSF grant ATM 9526209 to the California Institute of Technology. Contribution number 5644 from the Division of Geological and Planetary Sciences, California Institute of Technology.

3.5 References

Angell, J. K. and J. Korshover, Global variation in total ozone and layer-mean ozone: an update through 1981, *J. Clim. Appl. Meteorol.* **22**, 1611-1627, 1983.

Fishman, J., C. E. Watson, J. C. Larsen, J. A. Logan, Distribution of tropospheric ozone determined from satellite data, *J. Geophys. Res.* **95**, 3599-3617, 1990.

Fishman, J., *et al.*, in *Fire in the Environment: The Ecological Atmospheric, and Climatic Importance of Vegetation Fires,* P. J. Crutzen and J. G. Goldammer, Eds. (Wiley, New York, 1993), pp. 345-356.

Hao, W.and M. Liu, Spatial and temporal distribution of tropical biomass burning, *Global Biogeochem. Cycles* **8**, 495-503, 1994.

Herman, J. R., R. McPeters, R. Stolarski, D. Larko, R. Hudson, Global average ozone change from November 1978 to May 1990, *J. Geophys. Res.* **96**, 17297-17305, 1991.

Herman, J. R., R. McPeters, D. Larko, Ozone depletion at northern and southern latitudes derived from January 1979 to December 1991 Total Oozone Mapping Spectrometer data, *J. Geophys. Res.* **98**, 12783-12793, 1993.

Hudson, R. D., J.-H. Kim and A. M. Thompson, On the derivation of tropospheric column ozone from radiances measured by the total ozone mapping spectrometer, *J. Geophys. Res.* **95**, 11137-11145, 1995.

Kirchhoff, V. W. J. H., A. W. Setzer, M. C. Pereira, Biomass burning in Amazonia: seasonal effects on atmospheric O_3 and CO, *Geophys. Res. Lett.* **16**, 469-472, 1989.

Kirchhoff, V. W. J. H., R. A. Barnes, A. L. Torres, Ozone climatology at Natal, Brazil, from in situ ozonesonde data, *J. Geophys. Res.* **96**, 10899-10909, 1991.

Logan, J. A., M. J. Prather, S. C. Wofsy, M. B. McElroy, Tropospheric chemistry: a global perspective, *J. Geophys. Res.* **86**, 7210-7254, 1981.

Logan, J. A., Tropospheric ozone: seasonal behavior, trends, and anthropogenic influence, *J. Geophys. Res.* **90**, 10463-10482, 1985. *Geophys. Res. Lett.* **22**, 409-412, 1995.

Staehelin, J. and W. Schmid, Trend analysis of tropospheric ozone concentrations utilizing the 20-year data set of ozone ballon sounding over Payerne (Switzerland), *Atmos. Environ.* **25A**, 1739-1749, 1991.

Tarasick, D. W., D. I. Wardle, J. B. Kerr, J. J. Bellefleur, J. Davies, Tropospheric ozone trends over Canada: 1980-1993,

Tiao, G. C. *et al.*, A statistical trend analysis of ozonesonde data, *J. Geophys. Res.* **91**, 13121-13136, 1986.

Warmbt, W., Ergebnisse Langjahriger messungen des bondennahen ozone in der DDR, *Z. Meteorol.* **29**, 24-31, 1979 (in German).

Chapter 4 Detection of Tropospheric Ozone by Remote Sensing from the Ground

Yibo Jiang, Yuk L. Yung

Division of Geological and Planetary Sciences

California Institute of Technology

Pasadena, CA 91125

and

Stanley P. Sander

Earth and Space Sciences Division

Jet Propulsion Laboratory

California Institute of Technology

Pasadena, CA 91109

Accepted to be published in modified form in *J. Quant. Spectrosc. Radiat. Transf.*, 1997.

Contribution number 5674 from the Division of Geological and Planetary Sciences, California Institute of Technology.

Abstract

Due to larger multiple scattering effects in the troposphere compared to that in the stratosphere, the optical path of tropospheric ozone is markedly enhanced (as compared with that of stratospheric ozone) in the Huggins bands from 310 nm to 345 nm. Model study of the direct and diffuse solar fluxes on the ground shows differences between tropospheric and stratospheric ozone. The characteristic signature of tropospheric ozone enables us to distinguish a change in tropospheric ozone from that of stratospheric ozone. A simple retrieval algorithm is used to recover the tropospheric column ozone from simulated data.

4.1 Introduction

Tropospheric ozone plays a key role in regulating the chemical composition and climate of the troposphere [Logan *et al.*, 1981; Logan, 1994]. There is general agreement that tropospheric ozone has increased globally in recent decades [Fishman *et al.*, 1990; Jiang and Yung, 1996], but the lack of reliable global measurements of tropospheric ozone sets a limit on our ability to predict the variations of this tropospheric chemical species.

Since the tropospheric column ozone is only about 10% of that in the stratosphere, the spectroscopic signal (e.g. in absorption measurements) from tropospheric ozone is usually overwhelmed by the contribution from the much larger stratospheric ozone layer. Therefore, the measurement of the tropospheric ozone by a remote sensing technique has always been a challenge. In this paper, we will investigate the possibility of detecting tropospheric ozone by measuring the atmospheric radiation in the Huggins bands in the range from 310 nm to 345 nm using an interferometric spectrometer [Sander *et al.*, 1993]. In the following we shall assume that the UV instrument will be used to make observations on the ground.

O_3 and SO_2 are the principal absorbing species in the spectral region of the Huggins bands in the Earth's atmosphere. Since the concentration of SO_2 (on the order of 1 ppbv at low altitudes) is much less than that of O_3, and the absorption cross sections are about the same, the absorption of solar radiation by SO_2 can be neglected in this study, except during or immediately after volcanic eruptions. The Huggins bands consist of a series of characteristic alternating absorption minima and maxima as shown in Figure 4.1. The temperature-dependent ozone absorption cross section data (Figure 4.1) in the Huggins bands is from Malicet *et al.* (1995) with resolution of 0.01 nm at 5 temperatures (218K, 228K, 243K, 273K, 295K). As is clearly demonstrated

in this figure, the cross section of ozone in the Huggins bands is strongly dependent on the temperature. In particular, the temperature dependence of the cross section appears to be different for the maxima and the minima, with the minima being more strongly dependent on the temperature.

The underlying principle of the proposed technique is very simple and is based on three facts:

1. UV radiation reaches the surface of the Earth by two pathways: direct propagation from the Sun, and diffuse radiation that has undergone multiple scattering in the atmosphere.

2. Most photons that are absorbed or scattered in the stratosphere have undergone a single scattering process. The photons that are absorbed or scattered in the troposphere have gone through multiple scattering.

3. The ratio of the diffuse radiation to the direct solar radiation provides a useful measure of the multiply to singly scattered photons.

As we shall show later, we can discriminate between tropospheric and stratospheric ozone by making suitable measurements of the diffuse to direct radiation ratio (to be defined later).

4.2 The Radiative Model

To investigate quantitatively the radiative properties of atmospheric ozone in the Huggins bands, we used a radiative transfer model consisting of 80 vertical layers from 0 km to 80 km with vertical resolution 1 km. This model computes accurately multiple

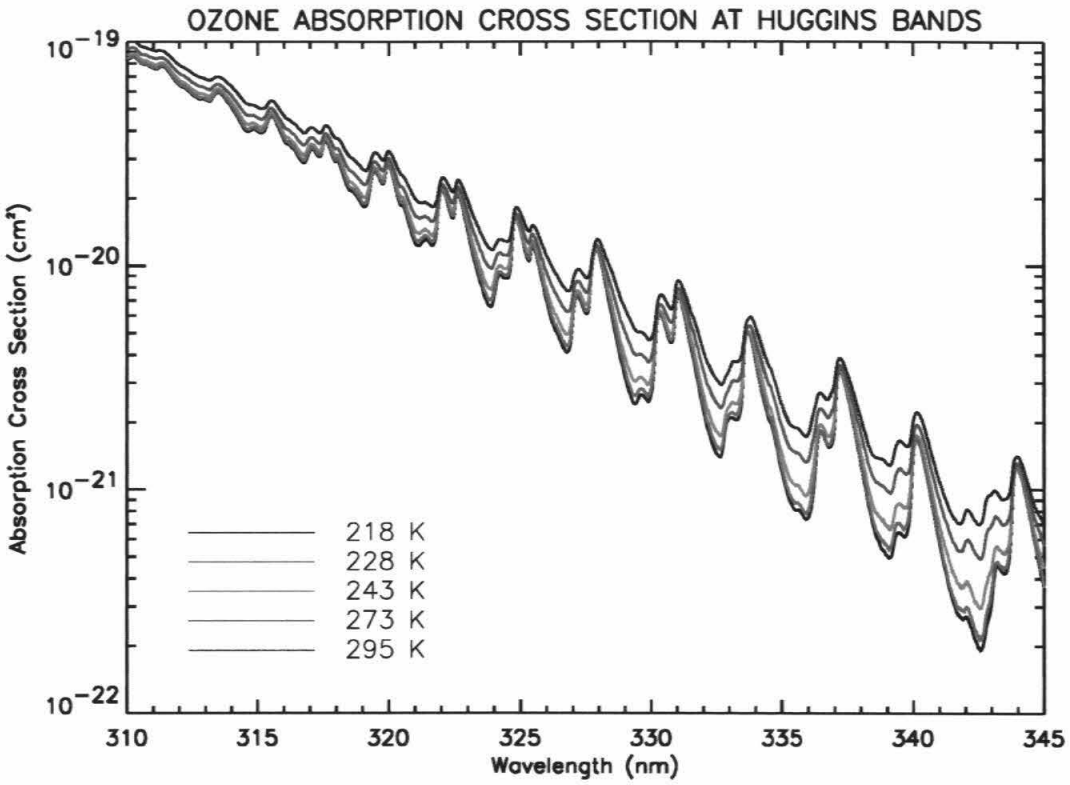

Figure 4.1: Ozone absorption cross section of the Huggins bands in five different temperatures (218K, 228K, 243K, 273K, 295K).

scattering using a method described by Michelangeli *et al.* (1992) and it includes the effects of absorption, Rayleigh and aerosol scattering without polarization.

The vertical profiles of temperature, number density and ozone concentration of the 1976 U.S. Standard Atmosphere (see Figure 4.2) are used in the model. The Standard Atmosphere does not specify on ozone concentration at the ground level. We set it equal to the value of the nearest level (2 km) 6.80×10^{11} cm^{-3} or 26.7 ppmv. We define the tropopause based on the temperature inversion at 12 km. From this definition, the total column ozone density in the atmosphere is 347.22 DU, with 310.34 DU in the stratosphere and 36.88 DU in the troposphere. The aerosol vertical profile (Figure 4.2) and the size distribution are taken from Demerjian *et al.* (1980). The maximum radius of this distribution and the complex refractive index of the particles are 0.07 μm and $1.5–0.1i$, respectively. The earth's surface albedo is set to 0.1 [Eck *et al.*, 1987].

Figure 4.3 shows the total optical depth of this standard atmosphere in the Huggins bands. Rayleigh and aerosol scattering optical depths are nearly constant in the bands. At wavelengths less than 318 nm, the effect of ozone on the absorption spectrum is comparable to the other effects such as Rayleigh and aerosol scattering. The typical total optical depth is around 1.5 and gives rise to considerable scattering and absorption in the troposphere in this wavelength range. At longer wavelengths, the absorption due to ozone is less important.

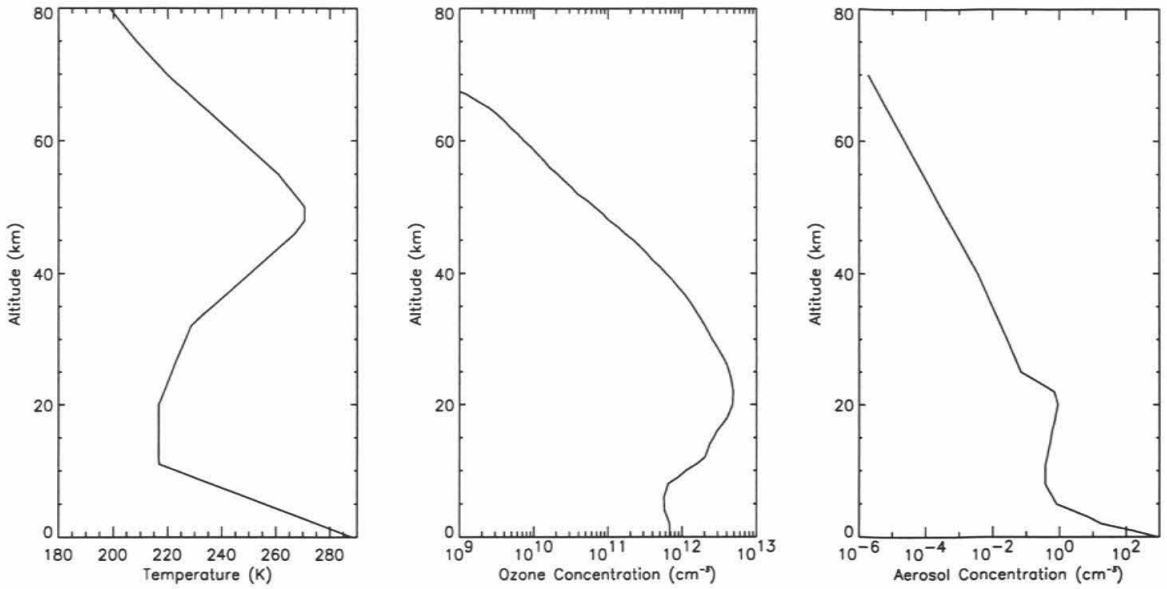

Figure 4.2: Vertical profile of standard temperature, ozone and aerosol number density in the atmosphere.

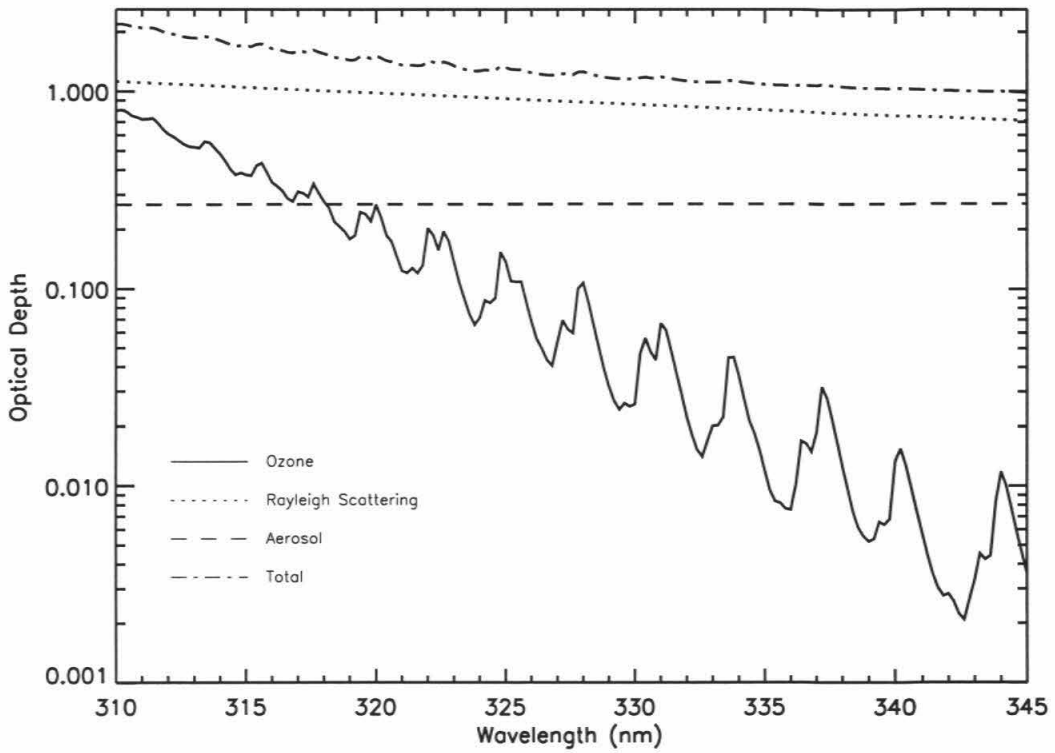

Figure 4.3: Optical depth of ozone, Rayleigh scattering and aerosol in the Huggins bands. Due to the decreasing cross section as wavelength increases, ozone optical depth is much smaller than all the others in longer wavelength.

4.3 Sensitivity Study Of Stratospheric And Tropospheric Ozone Change

In this paper, we will study the transmission of the atmosphere in the Huggins bands using a ground-based measurement. The reference case is defined as a standard ozone profile in the radiative transfer model. In the following study, the azimuth angle is set to 0°.

Solar radiation is both absorbed and scattered in the atmosphere. Single scattering dominates in the middle atmosphere, while multiple scattering becomes important in the troposphere due to the higher concentration of air molecules and aerosols. Therefore, the diffuse solar radiation is greatly enhanced in the troposphere [Bruhl and Crutzen, 1989; Stamnes, 1993]. In this section, we will apply this principle to the study of solar radiation transfer in the Huggins bands and show the the possibility of detecting tropospheric ozone with high accuracy although it is much smaller compared to stratospheric ozone.

First, we will study the sensitivity of diffuse irradiance to tropospheric and stratospheric ozone changes relative to the reference case at different solar zenith angles (SZAs) using contribution function $f_{\lambda,\theta_o}(z)$ of layer z which is defined as

$$f_{\lambda,\theta_o}(z) = \frac{I_{\lambda,\theta_o}(O_3(z) + 5\text{DU}) - I_{\lambda,\theta_o}(O_3(z))}{I_{\lambda,\theta_o}(O_3(z))} \tag{4.1}$$

where $O_3(z)$ is ozone vertical profile and $I_{\lambda,\theta_o}(O_3(z))$ is the reference diffuse irradiance at wavelength λ and solar zenith angle θ_o, $I_{\lambda,\theta_o}(O_3(z)+5\text{DU})$ is the diffuse irradiance when ozone in layer z is increased by 5 DU. Figure 4.4 shows the contribution function for 313.47 nm at SZA 0° and 60° respectively. As shown in Figure 4.4, the contribution function is relatively constant in the stratosphere, but it increases in the troposphere

due to an increase in multiple scattering. The averaged contribution function of the diffuse irradiance in the troposphere is about 1.5 times that of the stratosphere. The change of the SZA (from 0° to 60°) does not significantly change the relative contribution function between troposphere and stratosphere.

Let DIF be the diffuse irradiance specific intensity ($Wnm^{-1}m^{-2}sr^{-1}$) and DIR be the direct solar irradiance ($Wnm^{-1}m^{-2}$). Figure 4.5a shows the ratio DIF/DIR at three viewing angles (relative to zenith) in reference case (solid lines) and in perturbed case (dotted lines) when SZA = 0°. The increase of this ratio at shorter wavelength is due to the greater attenuation of the direct solar beam (DIR). The DIF also decreases at shorter wavelengths, but not as much as DIR. The Huggins bands of ozone are clearly seen in this figure. In the perturbed case tropospheric ozone is decreased in each level proportionally, with total decrease of 10 DU. The dotted lines show this new DIF/DIR ratio.

Figure 4.5b presents the relative change of the perturbed case (tropospheric ozone decreased by 10 DU) as compared to the reference case in the DIF/DIR ratio. Note that the changes become larger at greater viewing angles. The same case is repeated for the decrease of stratospheric ozone by 10 DU. The difference, as shown by the dotted lines in Figure 5b, is very small in the stratospheric case and it remains constant as the viewing angle changes.

The distinction between changing the tropospheric versus stratospheric ozone can be even more easily seen if we consider the difference in the DIF/DIR ratio as a function of viewing angle at a certain wavelength (312 nm here) (Figure 4.6). Again in each perturbed case 10 DU of ozone has been taken out from the troposphere or the stratosphere. We obtain a characteristic profile with a peak at viewing angle around

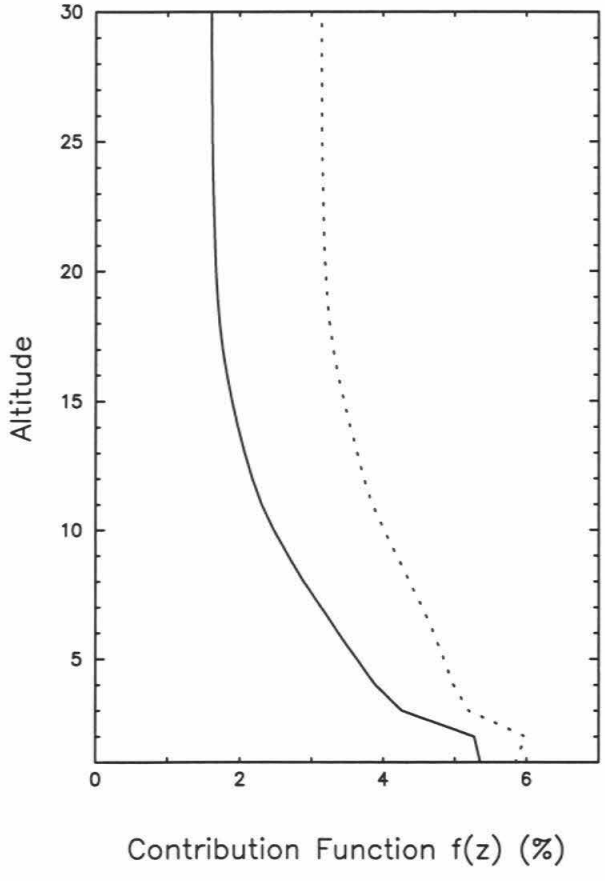

Figure 4.4: Contribution function of diffuse irradiance at wavelength 313.47 nm at SZA 0° (solid line) and 60° (dotted line).

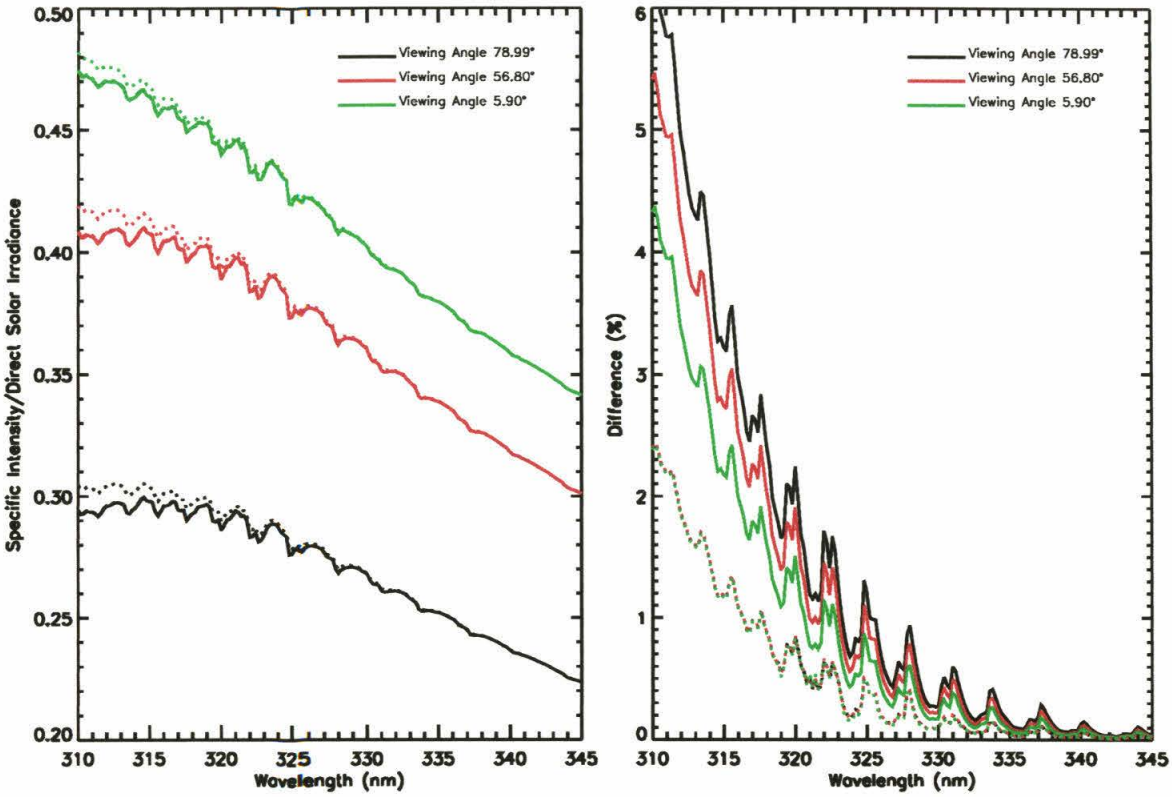

(A) (B)

Figure 4.5: (a) Ratio of specific intensity and direct solar irradiance in three viewing angles (5.90°, 56.80°, 78.99°) at SZA 0° with 0° azimuth angle. Solid line and dotted line represent the reference and perturbed case respectively. (b) Percent difference of the ratio relative to the reference state when either troposphere (solid line) or stratosphere (dotted line) is perturbed.

85° depending on SZA for decreasing tropospheric ozone, while we get a constant value for decreasing stratospheric ozone. The physical reason is as follows. Ozone in the stratosphere contributes to both DIR and DIF only in single scattering. Therefore, the ratio DIF/DIR is independent of viewing angles (as long as we use the same SZA for observing DIF and DIR). Tropospheric ozone contributes to DIR in single scattering, but contributes to DIF in multiple scattering. Since the latter changes with viewing angle, we get a large difference in the DIF/DIR ratio. In these characteristic profiles, we have a way to discriminate between tropospheric and stratospheric ozone. This will constitute the basis for our proposed experiment to measure tropospheric ozone.

4.4 The Retrieval Algorithm

In the last section we have provided a convincing demonstration that with appropriate measurements and modeling there is a sensitive way to distinguish between stratospheric and tropospheric ozone. The retrieval algorithm is based on this line of reasoning. In the absence of real data, we will develop a simple two parameter retrieval scheme. With the acquisition of observed data, we expect to further develop and improve this retrieval scheme.

We shall first make the simple assumption that atmospheric ozone profile $O_3(z)$ may be described as the superposition of two "typical" profiles,

$$O_3(z) = aS_{ref}(z) + bT_{ref}(z) \tag{4.2}$$

where $S_{ref}(z)$ is the reference vertical ozone profile for stratospheric ozone, and $T_{ref}(z)$ that for tropospheric ozone. The constants a and b are equal to unity for the 1976 U.S. Standard Atmosphere. In the retrieval algorithm, we will let a and b be undetermined

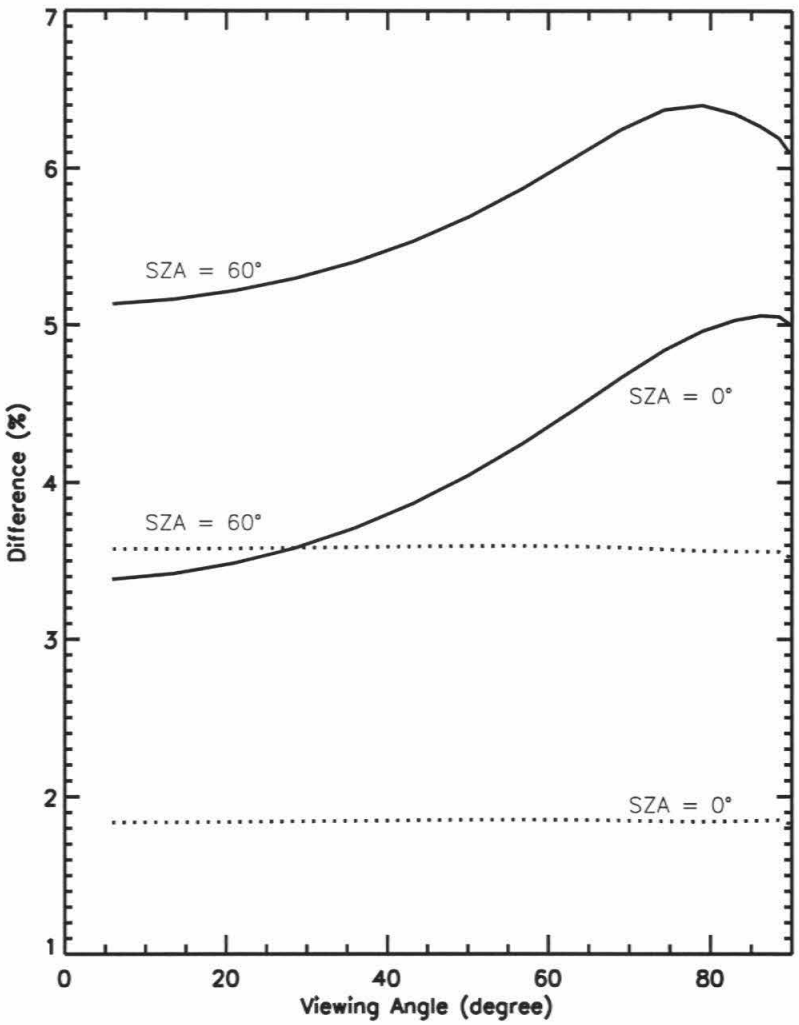

Figure 4.6: Percent difference of the ratio at 312 nm as a function of viewing angle at SZA 0° and 60° when either troposphere (solid line) or stratosphere (dotted line) is perturbed.

parameters that will be chosen by minimizing the least square error between the model predictions of the observations computed using $O_3(z)$ and the actual observations. An example of the retrieval is given in Figures 4.7 and 4.8. Figure 4.7 gives the "synthetic data" (solid line), with artificial "noise" (dash line) added. The "synthetic data" corresponds to $a = 0.934, b = 0.729$ at SZA 60°. Figure 4.8 shows the quality of the "fits" to the "synthetic data" with various sets of values for the parameters a and b. As expected, we get the minimum least square error at $a = 0.934 \pm 0.016, b = 0.729 \pm 0.136$. This very crude retrieval scheme will be used as a first order solution to determine the tropospheric ozone column. As the data become available, we will be exploring new ways to improve upon this scheme so that we can extract more information on the vertical distribution of ozone in the atmosphere by studying the ozone Huggins bands transmission.

Since the difference between single scattering (e.g. in the stratosphere) and multiple scattering (e.g. troposphere) is essential for discriminating stratospheric and tropospheric ozone, we believe that another useful discriminant may be the polarization of the diffuse light. Single scattering of UV radiation by air molecules is strongly polarized. On the other hand, multiple scattering tends to randomize polarization. This may provide another powerful constraint on the origin of the diffuse radiation (whether it is from the stratosphere or troposphere).

In this study, we have not considered the Ring effect [Joiner it et al., 1995]. But our method is not sensitive to this effect, and we can always chose wavelengths at which the Ring effect is minimal.

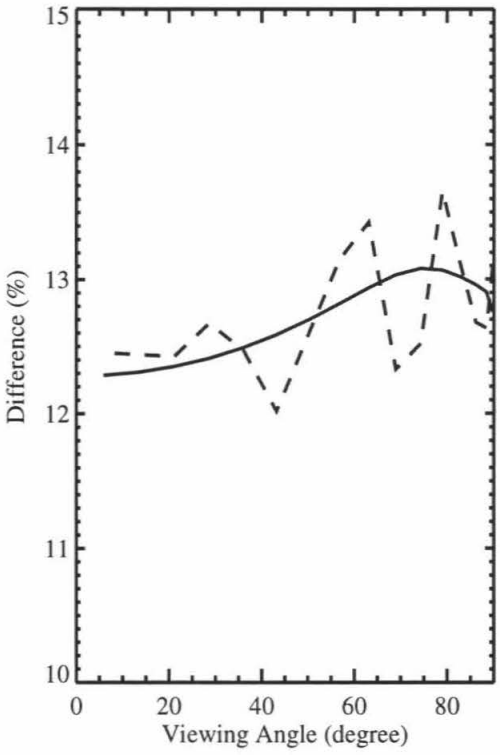

Figure 4.7: Synthetic data (solid line) with artificial "noise" (dash line) added. The synthetic data corresponds to $a = 0.934, b = 0.729$ at SZA 60°.

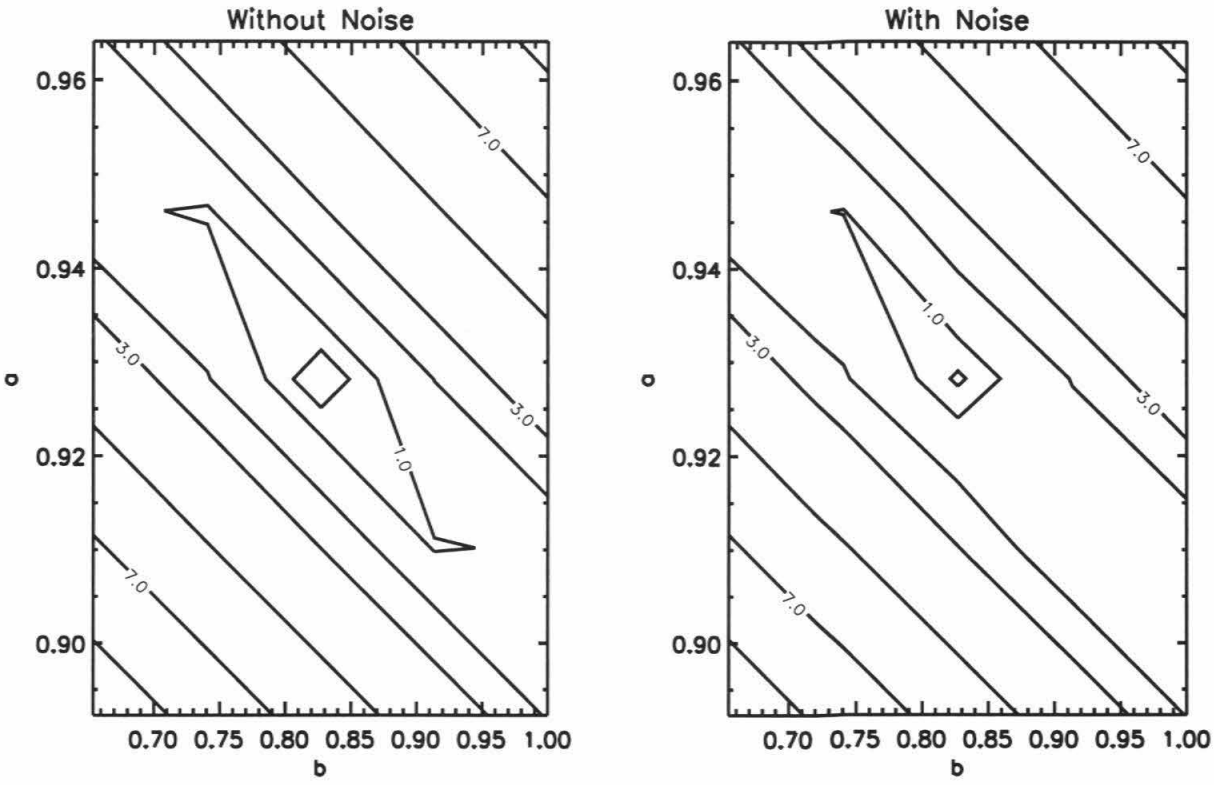

Figure 4.8: Contour plots of the least square error (percentage difference) with and without noise added.

4.5 Conclusions

This paper presents the preliminary results of a novel technique to measure tropospheric ozone by remote sensing from the ground. It provides the theoretical background for future measurement and retrieval of tropospheric ozone. The principal findings in this paper are summarized as follows

1. Due to the multiple scattering of air molecules and aerosols, the signal due to absorption of tropospheric ozone is amplified by as much as 1.5 times compared to that in the stratosphere in the Huggins bands.

2. The characteristic profile (Figure 4.6) related to the tropospheric ozone change is found and this enables us to separate the tropospheric from stratospheric ozone in the transmitted spectrum measurements. The influence of profile shapes for stratospheric and, especially, tropospheric ozone will influence the derived tropospheric column ozone and must be considered in more detail.

3. A simple retrieval algorithm is demonstrated to effectively obtain the tropospheric column ozone.

4.6 Acknowledgements

We thank R. S. Stolarski, R. Cageao, M. Allen, R. McPeters, M. Newchurch and J.-H. Kim for valuable comments. This work was supported by National Science Foundation grant ATM 9526209 and NASA grant NAG1-1806 to the California Institute of Technology. Contribution number 5674 from the Division of Geological and Planetary Sciences, California Institute of Technology. After this work was completed, it

was pointed out to us by R. McPeters that similar ideas were proposed by Green *et al.* (1977).

4.7 References

Bruhl, C., and P. J. Crutzen, On the disproportionate role of tropospheric ozone as a filter against solar UV-B radiation, *Geophys. Res. Lett.* **16**, 703-706, 1989.

Demerjian, K. L., K. L. Schere, and J. T. Peterson, Theoretical estimates of actinic (spherically integrated) flux and photolytic rate constants of atmospheric species in the lower troposphere, *Adv. Environ. Sci. Tech.* **10**, 369 1980.

Eck, T. F., P. K. Bhartia, P. H. Hwang, and L. L. Stowe, Reflectivity of earths surface and clouds in ultraviolet from satellite-observations, *J. Geophys. Res.* **92**, 4287-4296, 1987.

Fishman, J., C. E. Watson, J. C. Larsen, and J. A. Logan, Distribution of tropospheric ozone determined from satellite data, *J. Geophys. Res.* **95**, 3599-3617, 1990.

Green, A. E. S., and K. F. Klenk, *Technical Proceedings of the First International Interactive Workshop on Inversion Methods in Atmospheric Remote Sounding*, 297, 1977.

Jiang, Y., and Y. L. Yung, Concentrations of tropospheric ozone from 1979 to 1992 over tropical Pacific South America from TOMS data, *Science* **272**, 714, 1996.

Joiner, J., P. K. Bhartia, R. P. Cebula, E. Hilsenrath, R. D. McPeters, and H. Park, Rotational Raman scattering (Ring effect) in satellite backscatter ultraviolet measurements, *Appl. Opt.* **34**, 4513-4525, 1995.

Logan, J. A., M. J. Prather, S. C. Wofsy, and M. B. McElroy, Tropospheric chemistry: a global perspective, *J. Geophys. Res.* **86**, 7210-7254, 1981.

Logan, J. A., Trends in the vertical-distribution of ozone - an analysis of ozonesonde data, *J. Geophys. Res.* **99**, 25553-25585, 1994.

Malicet, J., D. Daumont, J. Charbonnier, C. Parisse, A. Chakir, and J. Brion, Ozone UV spectroscopy II. absorption cross-sections and temperature dependence, *J. Atmos. Chem.* **21**, 263-273, 1995.

Michelangeli, D. V., M. Allen, Y. L. Yung, R. L. Shia, and D. Crisp, Enhancement of atmospheric radiation by an aerosol layer, *J. Geophys. Res.* **97**, 865-874, 1992.

Sander, S. P., R. P. Cageao, and R. R. Friedl, *S.P.I.E. Proceedings Series* **1715**, 15, 1993.

Stamnes, K., The stratosphere as a modulator of ultraviolet radiation into the biosphere, *Surveys in Geophysics* **14**, 167-186, 1993.

Appendix A Polarization Modeling of Atmospheric Radiative Transfer

Abstract

Light reflected or transmitted by a planetary atmosphere contains information about the particles and molecules in the atmosphere. Therefore, accurately calculating the radiation field is necessary. In this part, the doubling-adding method for plane-parallel polarized radiative transfer model is studied in detail. A special Fourier expansion leading to a compact notation is developed for the azimuth-dependent quantities. The multi-layer model for a vertically inhomogeneous atmosphere is implemented and several numerical results are presented for verification and comparison. Preliminary runs from this model in the Huggins bands show the distinct features of linear polarization in the reflection spectrum due to the multiple Rayleigh scattering in the troposphere.

A.1 Introduction

The radiation field in a planetary atmosphere is generally polarized, since scattering of radiation changes its state of polarization. Although neglecting the vector nature of light and replacing the rigorous vector radiative transfer equation by its approximate scalar counterpart has no physical background, it is a widely used simplification when the incident light is unpolarized and only the intensity of multiple scattered light is to be computed. The errors in the reflected intensity resulting from the neglect of polarization were examined by Hansen (1971) on the basis of accurate adding-doubling calculations of multiple scattering. He concluded that in most cases the errors in the scalar approximation should be less than or of the order of 1% for light reflected by a cloud of spherical particles with sizes of the order of or larger than the wavelength of light, which makes the scalar approximation applicable in radiance calculations for cloud and aerosol layers. On the other hand, it has been known that the errors can be much larger in the case of a semi-infinite atmosphere with pure Rayleigh scattering. For light reflected by finite Rayleigh atmospheres Adams and Kattawar found errors up to 11.7%. Similar large errors are seen in Table 43 of van de Hulst (1980). Furthermore, polarization of light contains more information which cannot be retrieved just from intensity, such as the aerosol size distribution and composition. Since the linear polarization can be measured to an accuracy of 0.1%, the information related to the polarization can be readily observed. A review of application of linear polarization to studies of planetary atmospheres has been given by Coffeen and Hansen (1974).

A.2 Light Representation

Consider a parallel beam of light of circular frequency ω traveling in a certain direction which we choose to call the positive direction. The components of the electric field in any two mutually perpendicular directions (represented by unit vector **r** and **l**) may be written in terms of the amplitudes (a_l and a_r) and phases (ε_l and ε_r) as

$$\begin{aligned} E_l &= a_l e^{i(\omega t - kz - \varepsilon_l)} \\ E_r &= a_r e^{i(\omega t - kz - \varepsilon_r)} \end{aligned} \tag{A.1}$$

t represents time, and k is wave number, $\mathbf{r} \times \mathbf{l}$ is in the direction of propagation. In problems involving a single scattering event **r** is chosen perpendicular to the plane of scattering, which is defined as a plane containing the directions of incidence and scattering.

Light can be represented by Stokes parameters in the column vector,

$$\mathbf{I} = \begin{pmatrix} I \\ Q \\ U \\ V \end{pmatrix} \tag{A.2}$$

The Stokes parameters are the time averages

$$\begin{aligned} I &= < E_l E_l^* + E_r E_r^* > &&= < a_l^2 + a_r^2 > \\ Q &= < E_l E_l^* - E_r E_r^* > &&= < a_l^2 - a_r^2 > \\ U &= < E_l E_r^* + E_r E_l^* > &&= 2 < a_l a_r \cos\delta > \\ V &= i < E_l E_r^* - E_r E_l^* > &&= 2 < a_l a_r \sin\delta > \end{aligned} \tag{A.3}$$

where $\delta = \varepsilon_l - \varepsilon_r$ and the asterisk represents the complex conjugate. I is the intensity and the other parameters have the same dimension. A constant factor common to

all four parameters is omitted from (A.3) for convenience. The Stokes parameters of a mixture of independent waves are the sums of the respective Stokes parameters of the separate waves.

For monochromatic light, complete polarization satisfies

$$I = (Q^2 + U^2 + V^2)^{1/2} \tag{A.4}$$

For polychromatic light, in general

$$I \geq (Q^2 + U^2 + V^2)^{1/2} \tag{A.5}$$

It is clear that an arbitrary beam of radiation can be mathematically decomposed into two parts, one unpolarized with Stokes parameters,

$$\begin{pmatrix} I - (Q^2 + U^2 + V^2)^{1/2} \\ 0 \\ 0 \\ 0 \end{pmatrix} \tag{A.6}$$

and one elliptically polarized with Stokes parameters,

$$\begin{pmatrix} (Q^2 + U^2 + V^2)^{1/2} \\ Q \\ U \\ V \end{pmatrix}. \tag{A.7}$$

Thus the intensity of polarized light is

$$I_{pol} = (Q^2 + U^2 + V^2)^{1/2} \tag{A.8}$$

and the degree of (elliptical) polarization is

$$\frac{I_{pol}}{I} = \frac{(Q^2 + U^2 + V^2)^{1/2}}{I} \tag{A.9}$$

We further define the intensity of linearly polarized light as

$$I_{lp} = (Q^2 + U^2)^{1/2} \tag{A.10}$$

and the intensity of circularly polarized light as

$$I_{cp} = V \tag{A.11}$$

Thus the degree of linear polarization is I_{lp}/I and the degree of circular polarization is I_{cp}/I.

It is convenient to express the solutions to the multiple scattering problem in terms of 4×4 reflection and transmission matrices such that

$$\begin{aligned} \mathbf{I}_r(\mu, \phi) &= \frac{1}{\pi} \int_0^1 \mu_0 d\mu_0 \int_0^{2\pi} \mathbf{R}(\mu, \mu_0, \phi - \phi_0) \mathbf{I}_0(\mu_0, \phi_0) d\phi_0 \\ \mathbf{I}_t(\mu, \phi) &= \frac{1}{\pi} \int_0^1 \mu_0 d\mu_0 \int_0^{2\pi} \mathbf{T}(\mu, \mu_0, \phi - \phi_0) \mathbf{I}_0(\mu_0, \phi_0) d\phi_0 \end{aligned} \tag{A.12}$$

where

$$\mathbf{I}_0 = \begin{pmatrix} I_0 \\ Q_0 \\ U_0 \\ V_0 \end{pmatrix} \tag{A.13}$$

is the incident light at the top of the atmosphere.

The net flux is defined as

$$\begin{aligned} \pi\mathbf{F} &= \int_0^{2\pi}\int_{-1}^{1}\mathbf{I}(\mu,\phi)\mu d\mu d\phi \\ &= 2\pi\int_{-1}^{1}{}^0\mathbf{I}(\mu)\mu d\mu \end{aligned} \tag{A.14}$$

where ${}^0\mathbf{I}(\mu)$ is the azimuth-independent term in the Fourier expansion of $\mathbf{I}(\mu,\phi)$.

For most problems it is satisfactory to approximate incident sunlight as monodirectional i.e.,

$$\mathbf{I}_0 = \delta(\mu-\mu_0)\delta(\phi-\phi_0)\pi\mathbf{F}_0,$$

Thus in this case

$$\begin{aligned} \mathbf{I}_r(\mu,\phi) &= \mu_0\mathbf{R}(\mu,\mu_0,\phi-\phi_0)\mathbf{F}_0 \\ \mathbf{I}_t(\mu,\phi) &= \mu_0\mathbf{T}(\mu,\mu_0,\phi-\phi_0)\mathbf{F}_0 \end{aligned} \tag{A.15}$$

A.3 The Doubling-Adding Method

A variety of techniques have been developed for computing the intensity and polarization of multiple scattered light. Among them, doubling-adding method is widely used for a plane-parallel atmosphere which is sufficient to cover most applications for light scattering in planetary atmospheres. The scattering is assumed to be 'coherent' in the sense that no change of frequency occurs within the visible region (thus Raman scattering, for example, is excluded). Thermal emission is also excluded, but it can easily be added into the formalism. The essence of the doubling-adding method is simple: if the reflection and transmission is known for each of two layers, the reflection

and transmission from the combined layer can be obtained by computing the successive reflections back and forth between the two layers. If the two layers are chosen to be identical, the results for a thick homogeneous layer can be built up rapidly in a geometric (doubling) manner.

Let τ_a and τ_b be the optical thickness of two layers to be added, with the subscripts a and b referring to the top and bottom layers, respectively (Figure A.1). The equations for the adding method is then

$$\begin{aligned}
\mathbf{Q}_1 &= \mathbf{R}_a^* \mathbf{R}_b \\
\mathbf{Q}_n &= \mathbf{Q}_1 \mathbf{Q}_{n-1} \\
\mathbf{S} &= \sum_{n=1}^{\infty} \mathbf{Q}_n \\
\mathbf{D} &= \mathbf{T}_a + \mathbf{S} e^{-\frac{\tau_a}{\mu_0}} + \mathbf{S}\mathbf{T}_a \\
\mathbf{U} &= \mathbf{R}_b e^{-\frac{\tau_a}{\mu_0}} + \mathbf{R}_b \mathbf{D} \\
\mathbf{R}(\tau_a + \tau_b) &= \mathbf{R}_a + e^{-\frac{\tau_a}{\mu}} \mathbf{U} + \mathbf{T}_a^* \mathbf{U} \\
\mathbf{T}(\tau_a + \tau_b) &= e^{-\frac{\tau_b}{\mu}} \mathbf{D} + \mathbf{T}_b e^{-\frac{\tau_a}{\mu_0}} + \mathbf{T}_b \mathbf{D}
\end{aligned} \tag{A.16}$$

In the above equations, the bold face symbols represent matrices of 4×4. An arbitrary matrix of this type, say $\mathbf{X}$, stands for

$$\mathbf{X} = X^{ij}(\mu, \mu_0, \phi - \phi_0), \qquad i, j = 1, 2, 3, 4,$$

where i and j are the indices for the rows and columns, respectively. The product of two matrices implies matrix multiplication and integration over the adjoining angles, an arbitrary $\mathbf{Z} = \mathbf{XY}$ being defined as

$$Z^{ij}(\mu,\mu_0,\phi-\phi_0) = \frac{1}{\pi}\int_0^1\int_0^{2\pi}\Big(\sum_{k=1}^{4} X^{ik}(\mu,\mu',\phi-\phi')Y^{kj}(\mu',\mu_0,\phi'-\phi_0)\Big)\mu' d\mu' d\phi' \tag{A.17}$$

$\mathbf{R}^*$ and $\mathbf{T}^*$ are the reflection and transmission matrices for layer when it is illuminated from below. In general $\mathbf{R}^* \neq \mathbf{R}$ and $\mathbf{T}^* \neq \mathbf{T}$, but, since we are considering homogeneous layers, the simple relations

$$\begin{aligned} R^*(\mu,\mu_0,\phi-\phi_0) &= R(\mu,\mu_0,\phi_0-\phi) \\ T^*(\mu,\mu_0,\phi-\phi_0) &= T(\mu,\mu_0,\phi_0-\phi) \end{aligned} \tag{A.18}$$

are valid.

The physical basis for these equations can be inferred from Figure A.1. The exponential terms refer to the direct transmission through layer a or b without scattering; $\mathbf{T}$ is the diffuse transmission matrix. Emerging from the bottom of the two layers is the diffuse transmission $\mathbf{T}(\tau_a+\tau_b)$ and the unscattered radiation of flux $\mu_0\pi \mathrm{F}_0 e^{-\frac{\tau_a+\tau_b}{\mu_0}}$ for horizontal areas. The transmission is explicitly divided into its diffuse and direct components because the appearance of a delta function in the total transmission makes it inappropriate for precise numerical integrations. $\mathbf{D}$ and $\mathbf{U}$ are, after multiplication by $\mu_0\mathrm{F}_0$, the diffuse intensities downward and upward at the dividing boundary between the two layers. The indicated summation is over the reflections between the two layers with $n-1$ indicating the number of times the radiation has crossed the dividing boundary going up. In practice this sum is terminated after a small number (≤ 5) of terms, depending on the accuracy desired. Furthermore, the omitted terms may be approximated by a geometric series because the ratio of successive terms approaches a constant value.

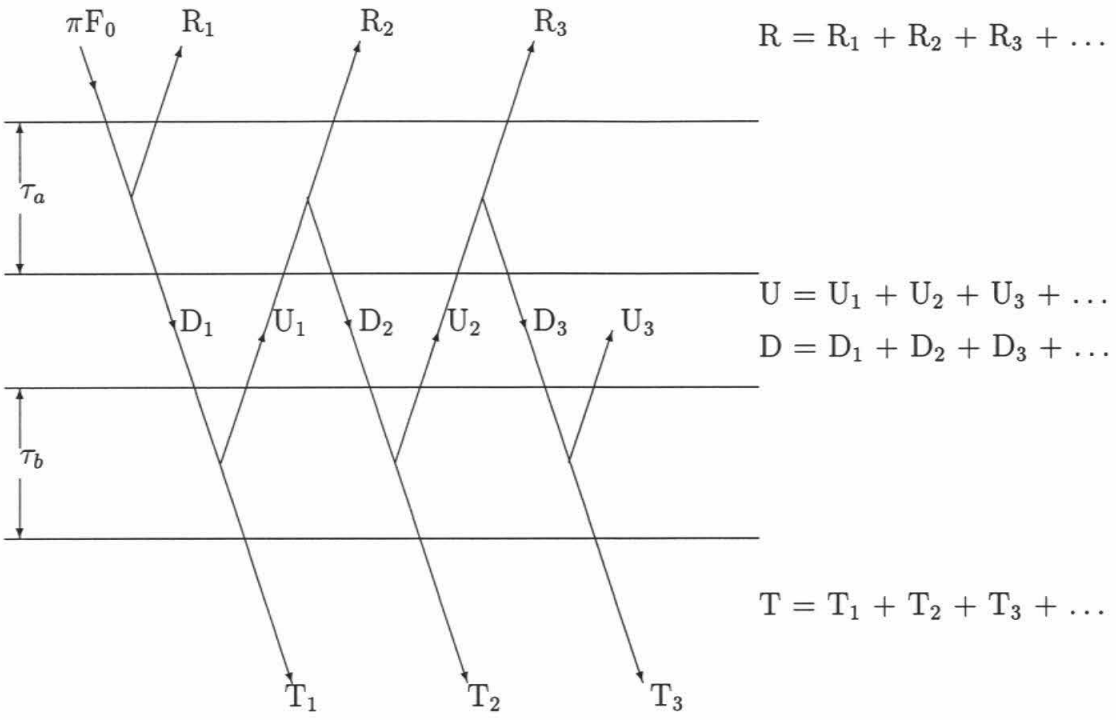

Figure A.1: Schematic representation of the doubling-adding method. The two layers of the atmosphere, of optical thickness τ_a and τ_b, are for convenience illustrated as if they were physically separated.

The numerical computations can be handled efficiently by means of a Fourier series expansion for the azimuth dependence and numerical quadrature for the μ' integrations. Formulae for the Fourier series expansions are given below. The doubling-adding equations remain valid for each Fourier component. Results are thus obtained for all values of $\phi - \phi_0$ and discrete values of μ and μ_0. The number of discrete zenith angles required depends on the anisotropy of the phase matrix and on the accuracy desired. This number of zenith angles can be kept at a moderate value, typically, 5-25, if the phase matrix is normalized for the discrete space of zenith angles.

It is advantageous to expand the azimuth-dependent functions in Fourier series in $\phi - \phi_0$. Each term in the Fourier series may then be treated independently. Let $\mathbf{X}$ represent the phase matrix or any of the matrices in doubling-adding equations. $\mathbf{X}$ may be expanded as

$$\begin{aligned} X^{ij}(\mu, \mu_0, \phi - \phi_0) &= X^{ij}_{c,0}(\mu, \mu_0) \\ &+2 \sum_{m=1}^{\infty} \Big[X^{ij}_{c,m}(\mu, \mu_0) \cos m(\phi - \phi_0) + X^{ij}_{s,m}(\mu, \mu_0) \sin m(\phi - \phi_0) \Big], \end{aligned} \tag{A.19}$$

where

$$\begin{aligned} X^{ij}_{c,m}(\mu, \mu_0) &= \frac{1}{2\pi} \int_0^{2\pi} X^{ij}(\mu, \mu_0, \phi') \cos m\phi' d\phi', \qquad m = 0, 1, 2, ... \\ X^{ij}_{s,m}(\mu, \mu_0) &= \frac{1}{2\pi} \int_0^{2\pi} X^{ij}(\mu, \mu_0, \phi') \sin m\phi' d\phi', \qquad m = 1, 2, ... \end{aligned} \tag{A.20}$$

The rule for matrix multiplication becomes

$$
\begin{aligned}
&Z^{ij}_{c,0}(\mu,\mu_0) = \\
&\quad 2\int_0^1 \sum_{k=1}^{4} X^{ik}_{c,0}(\mu,\mu')Y^{kj}_{c,0}(\mu',\mu_0)\mu' d\mu' \\
&Z^{ij}_{c,m}(\mu,\mu_0) = \\
&\quad 2\int_0^1 \left\{ \sum_{k=1}^{4} \left[X^{ik}_{c,m}(\mu,\mu')Y^{kj}_{c,m}(\mu',\mu_0) - X^{ik}_{s,m}(\mu,\mu')Y^{kj}_{s,m}(\mu',\mu_0) \right] \right\} \mu' d\mu' \\
&Z^{ij}_{s,m}(\mu,\mu_0) = \\
&\quad 2\int_0^1 \left\{ \sum_{k=1}^{4} \left[X^{ik}_{c,m}(\mu,\mu')Y^{kj}_{s,m}(\mu',\mu_0) + X^{ik}_{s,m}(\mu,\mu')Y^{kj}_{c,m}(\mu',\mu_0) \right] \right\} \mu' d\mu'
\end{aligned}
\tag{A.21}
$$

The matrices $\mathbf{R}^*$ and $\mathbf{T}^*$ do not need to be explicitly calculated because they differ from $\mathbf{R}$ and $\mathbf{T}$ only in the sign of the sine coefficients in the Fourier expansions; thus,

$$
\begin{aligned}
R^{*ij}_{c,m}(\mu,\mu_0) &= R^{ij}_{c,m}(\mu,\mu_0) \qquad m = 0,1,2,... \\
T^{*ij}_{c,m}(\mu,\mu_0) &= T^{ij}_{c,m}(\mu,\mu_0) \qquad m = 0,1,2,... \\
&\text{and} \\
R^{*ij}_{s,m}(\mu,\mu_0) &= -R^{ij}_{s,m}(\mu,\mu_0) \qquad m = 1,2,... \\
T^{*ij}_{s,m}(\mu,\mu_0) &= -T^{ij}_{s,m}(\mu,\mu_0) \qquad m = 1,2,...
\end{aligned}
\tag{A.22}
$$

Most computations are made for the special case in which the elements of the 4×4 phase matrix, $P^{ij}(\mu,\mu_0,\phi-\phi_0)$, are even functions of $\phi-\phi_0$ for the 2×2 submatrices $(ij = 11,12,21,22)$ and $(ij = 33,34,43,44)$, and odd functions of $\phi-\phi_0$ for the submatrices $(ij = 13,14,23,24)$ and $(ij = 31,32,41,42)$. Thus in the following we omit the subscript s or c, since the superscript specifying the matrix element determines whether the function is odd or even.

A.4 Model Description

We make computations for the reflection and transmission of solar radiation in a plane-parallel model atmosphere. The atmosphere is allowed to be vertically inhomogeneous and is divided into a sufficient number of layers that each may be approximated as being homogeneous. The monochromatic scattering properties of each homogeneous layer are determined by its optical thickness τ, single scattering albedo ω_0, and phase matrix $P^{ij}(\alpha)$, where α is the scattering angle.

The doubling-adding method requires that the reflection and transmission matrices be known for the layers to be added. These can be obtained from the following analytic expressions for single scattering with the initial optical thickness $\tau_0 \sim 2^{-20}$,

$$\begin{aligned} \mathbf{R}(\tau_0;\mu,\mu_0,\phi-\phi_0) &= \frac{\omega_0\tau_0}{4\mu\mu_0}\left[1-\frac{\tau_0}{2}(\frac{1}{\mu}+\frac{1}{\mu_0})\right]\mathbf{P}(\mu,\mu_0,\phi-\phi_0) \\ \mathbf{T}(\tau_0;\mu,\mu_0,\phi-\phi_0) &= \frac{\omega_0\tau_0}{4\mu\mu_0}\left[1-\frac{\tau_0}{2}(\frac{1}{\mu}+\frac{1}{\mu_0})\right]\mathbf{P}(\mu,\mu_0,\phi-\phi_0) \end{aligned} \tag{A.23}$$

Now we consider a multilayered atmosphere that is a stack of N homogeneous layers. The bottom of the layer n is interface $n+1$ and the top interface n. Thus the bottom of the atmosphere is interface $N+1$ and its top is interface 1. The optical depth at interface n is denoted by τ_n. A homogeneous layer n with optical thickness $d\tau_n = \tau_{n+1} - \tau_n$ has K internal levels. Here we consider levels at optical depths

$$
\begin{aligned}
\tau \;=\; & d\tau_n/2^{K-1}, \\
& d\tau_n/2^{K-2}, \\
& \ldots, \\
& d\tau_n/2^{K-k+1}, \\
& d\tau_n/2^{K-k}, \\
& \ldots, \\
& d\tau_n/2^{2}, \\
& d\tau_n/2^{1}, \\
& d\tau_n/2^{0}
\end{aligned}
\tag{A.24}
$$

The top of the layers is denoted by $k = 1$, the bottom by $k = K + 1$.

Figure A.2 shows the layers from top of the atmosphere to the surface of the earth. The ground is "added" to the atmosphere, as if it were another layer, with the following specifications: $\mathbf{T}_{N+1} = 0$, since no light is transmitted, and $\mathbf{R}_{N+1} = \mathbf{R}_{\mathbf{g}}(\mu, \mu_0)$, the reflection function of the ground in the absence of an atmosphere. If the ground is approximated as a Lambert reflector, $\mathbf{R}_{\mathbf{g}}$ is a constant between 0 and 1.

First the matrices pertaining to each homogeneous layer n are calculated using the doubling method which is started with an optical thin layer $d\tau_n/2^{K-1}$. The exact value of the optical thickness of this starting layer depends on the desired accuracy of the numerical results. The reflection and transmission matrices that emerges from this optically thin atmosphere are given in above equations. After K consecutive steps of the doubling schemes we obtain the reflection and transmission matrices for

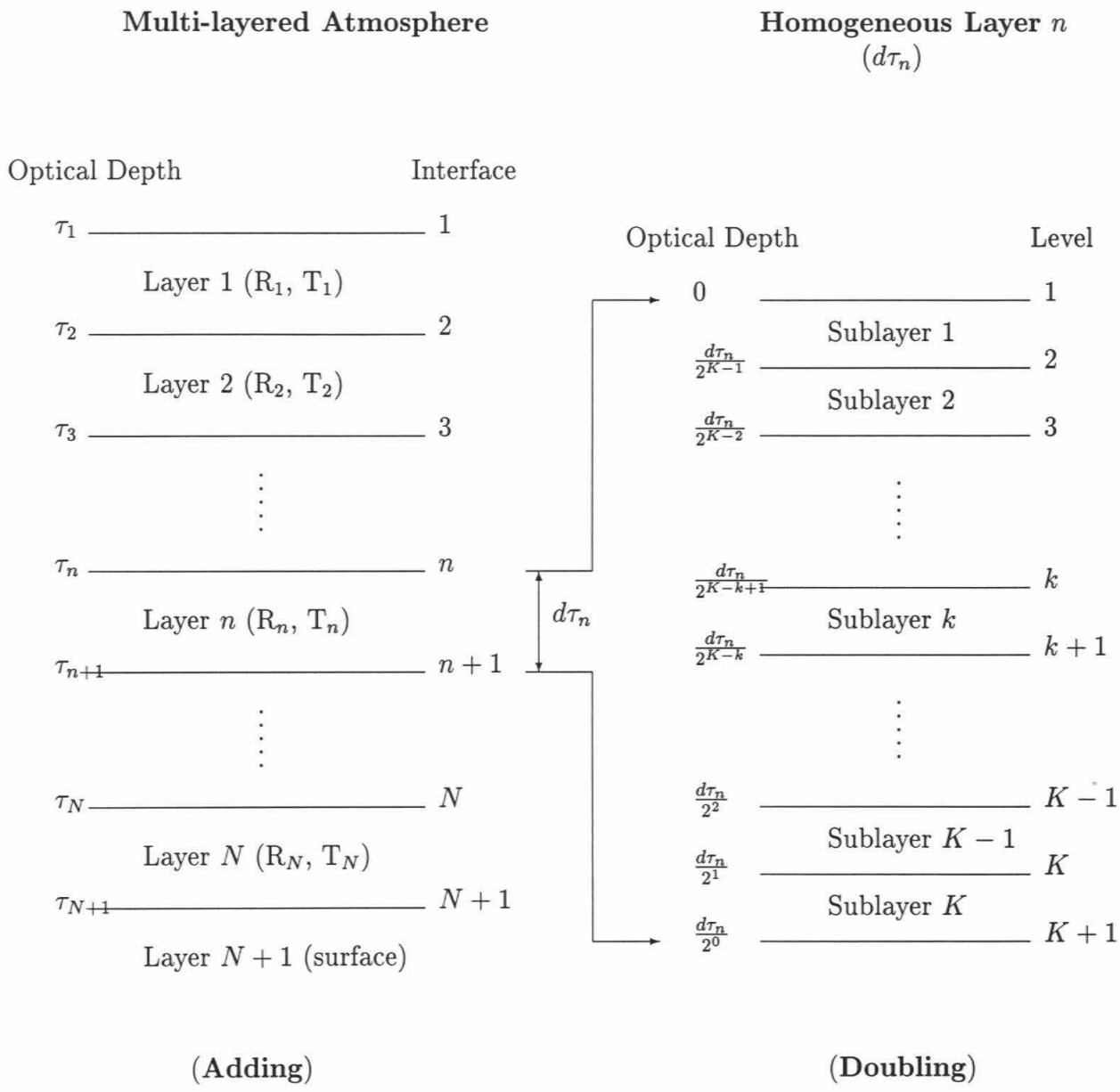

Figure A.2: Schematic representation of the atmospheric model of multi-layered atmosphere (a) and of each homogeneous layer (b).

homogeneous layer n. We then use adding method to add all the homogeneous layers to get the pure reflection and transmission matrices. Finally, the surface layer is added to the pure atmosphere layer, and the final matrices are what we want.

A.5 Checks and Discussion of the Computational Methods

In order to verify the accuracy of the radiative transfer model and to provide examples for comparison with other model, result from one type of the atmosphere is presented which is a Rayleigh scattering atmosphere illuminated by sunlight. The Stokes parameters I and Q of transmission and reflectivity from a single layer with optical depth of 1 and surface albedo = 0, 0.25, and 0.8 respectively are shown in Figure A.3, A.4, A.5, A.6, A.7, A.8 (Coulson *et al.*, 1960). The Rayleigh scattering atmosphere test case was compared with the tables by Coulson *et al.* (1960). Since the sun's vertical - containing the direction of illumination by the sun - is the plane of symmetry of the problem, it is convenient to count the azimuth from the sun's vertical, positive in an counterclockwise direction. Then the direction of the sun's radiation is defined by μ_0 and $\phi_0 = 0$. Comparisons were done for three cases of varying optical depth and solar zenith angle. The radiative transfer model was run with azimuth numbers up to 10. A quadrature scheme that lets the angles be specified and computes the optimal integration weights was used. The transmission at the surface of the earth and the reflection on the top of the atmosphere were compared at azimuth angles of 0, 30, 60, 120, and 180°. Table A.1, A.2 and Figure A.9, A.10, A.11, A.12, A.13, A.14 and A.15 show the comparison results. On average the results agree to the fourth decimal.

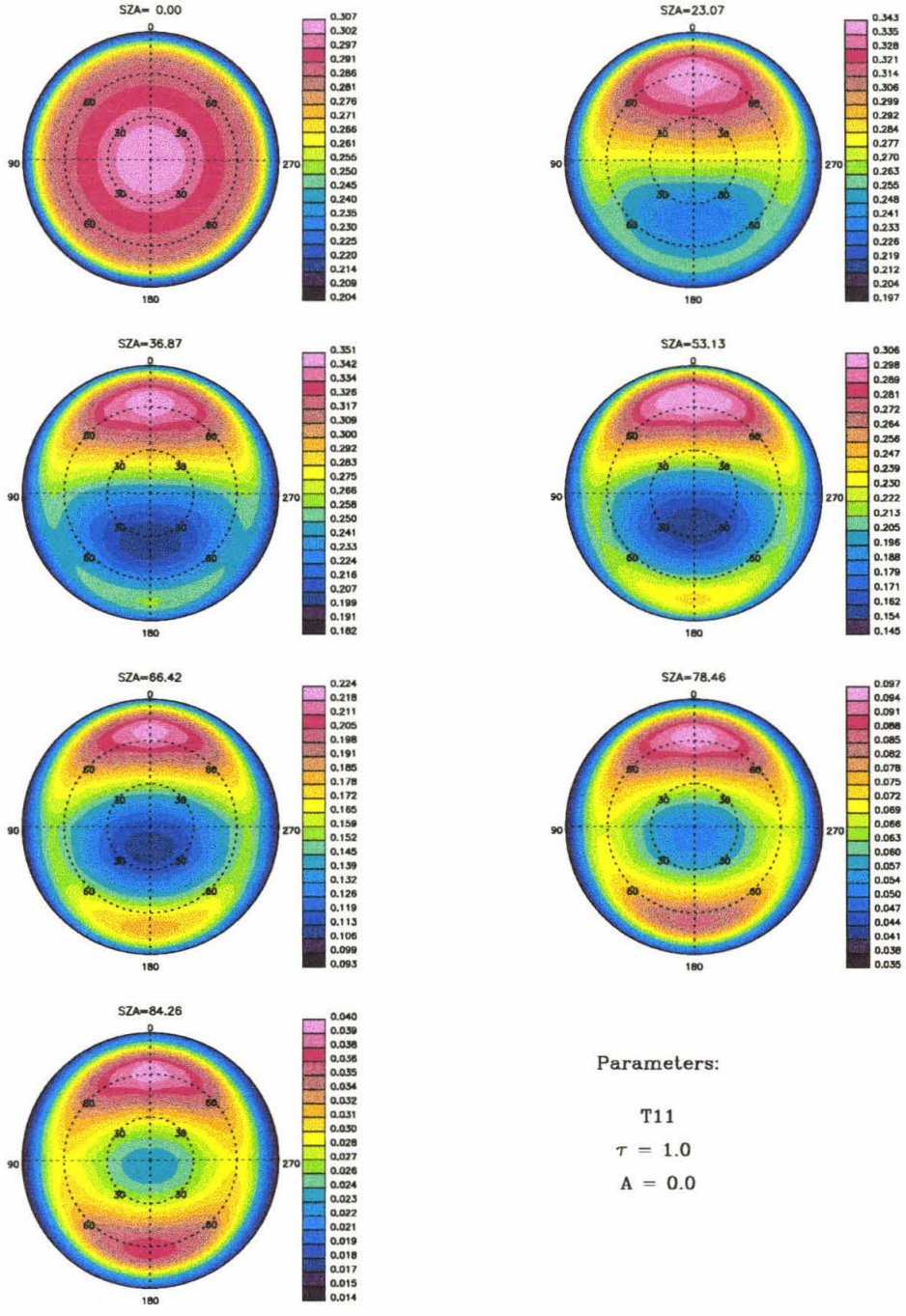

Figure A.3: Rayleigh scattering transmission T_{11} for optical depth $\tau = 1$ and albedo A=0.0 at solar zenith angle (SZA) 0°, 23.07°, 36.87°, 53.13°, 66.42°, 78.46°, 84.26°.

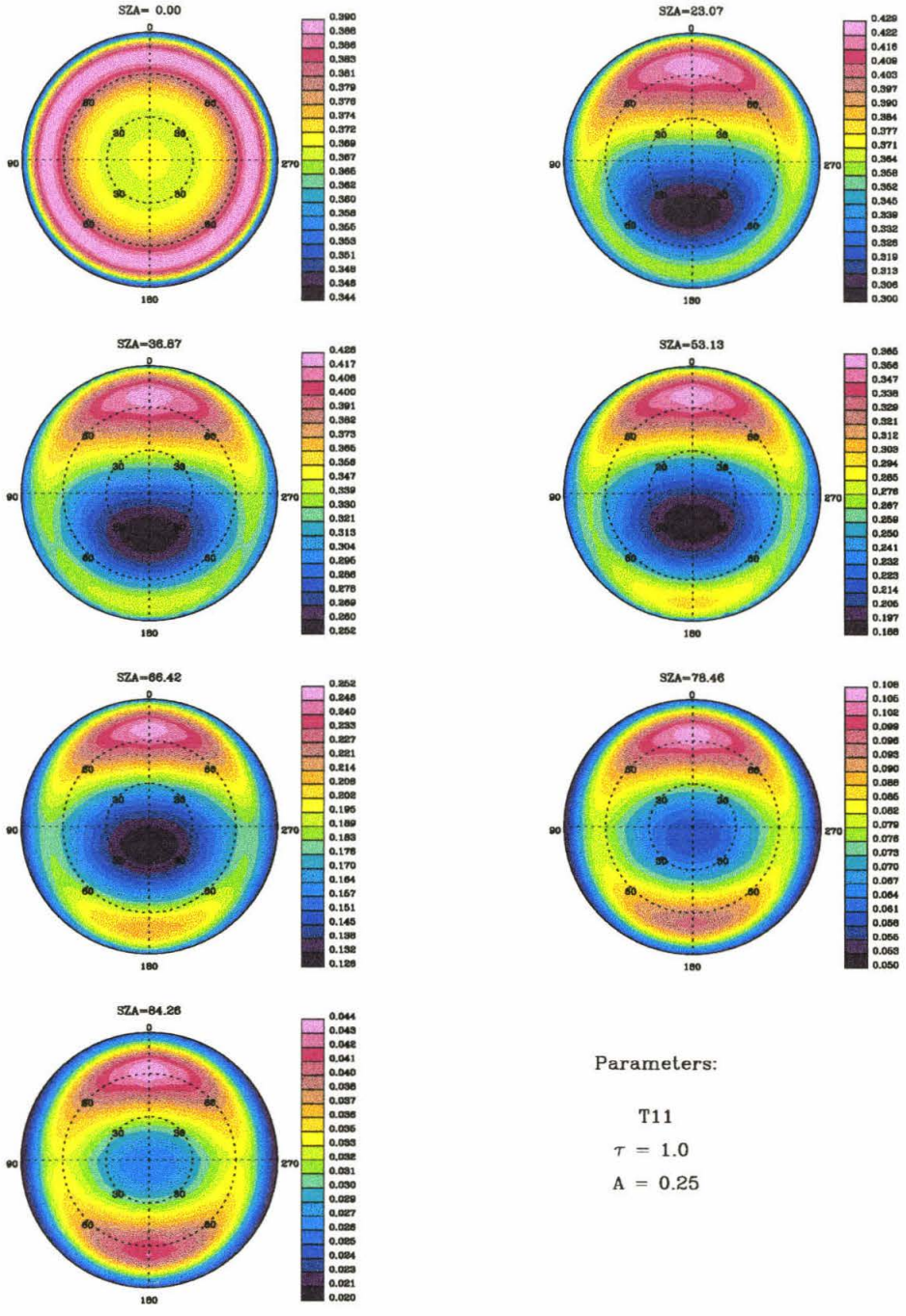

Figure A.4: Rayleigh scattering transmission T_{11} for optical depth $\tau = 1$ and albedo A=0.25 at solar zenith angle (SZA) 0°, 23.07°, 36.87°, 53.13°, 66.42°, 78.46°, 84.26°.

Table A.1: Transmission Comparison: Comparison of model output with the results of Coulson *et al.* for a homogeneous Rayleigh atmosphere of optical depth of 1. The Solar flux is normalized to π, the cosine of the solar zenith angle is 0.8, and the ground albedo is 0.25 (it is 0.0 for U). The transmitted radiance as a function of viewing angle μ for an azimuth of 60° is shown.

	Present Model			Coulson *et al.*		
μ	I	Q	U	I	Q	U
0.02000	0.29471	0.02312	0.08751	0.29475	0.02319	0.08762
0.10000	0.32587	0.01850	0.09783	0.32571	0.01864	0.09789
0.20000	0.35525	0.01201	0.10541	0.35508	0.01215	0.10547
0.32000	0.37008	0.00205	0.10316	0.36993	0.00216	0.10320
0.52000	0.36240	-0.01581	0.08100	0.36230	-0.01573	0.08104
0.72000	0.34035	-0.02942	0.04946	0.34026	-0.02939	0.04947
0.92000	0.31029	-0.03256	0.00829	0.31032	-0.03260	0.000848
0.98000	0.29568	-0.02699	-0.01263	0.29593	-0.02724	-0.01205
1.00000	0.28766	-0.02188	-0.02478	0.28377	-0.01800	-0.03132

A.6 Huggins Bands Modeling

As have been pointed out in Chapter 4 that the polarization of the diffuse light may be effectively used for determining the tropospheric ozone change, cloud and aerosol particles properties, we will report in this section the model results for the Huggins bands. We have not included aerosol scattering and absorbtion in the current model. All the other parameters are the same as that in Chapter 4.

Figures A.16 and A.17 show the transmitted and reflected specific intensity and linear polarization when SZA and viewing angle are both 36.87° for the reference atmosphere. The specific intensity is similar to that from Chapter 4. The transmitted linear polarization does not vary much with respect to the wavelength. But in the reflected light, the short wavelength light can not penetrate deep down to the

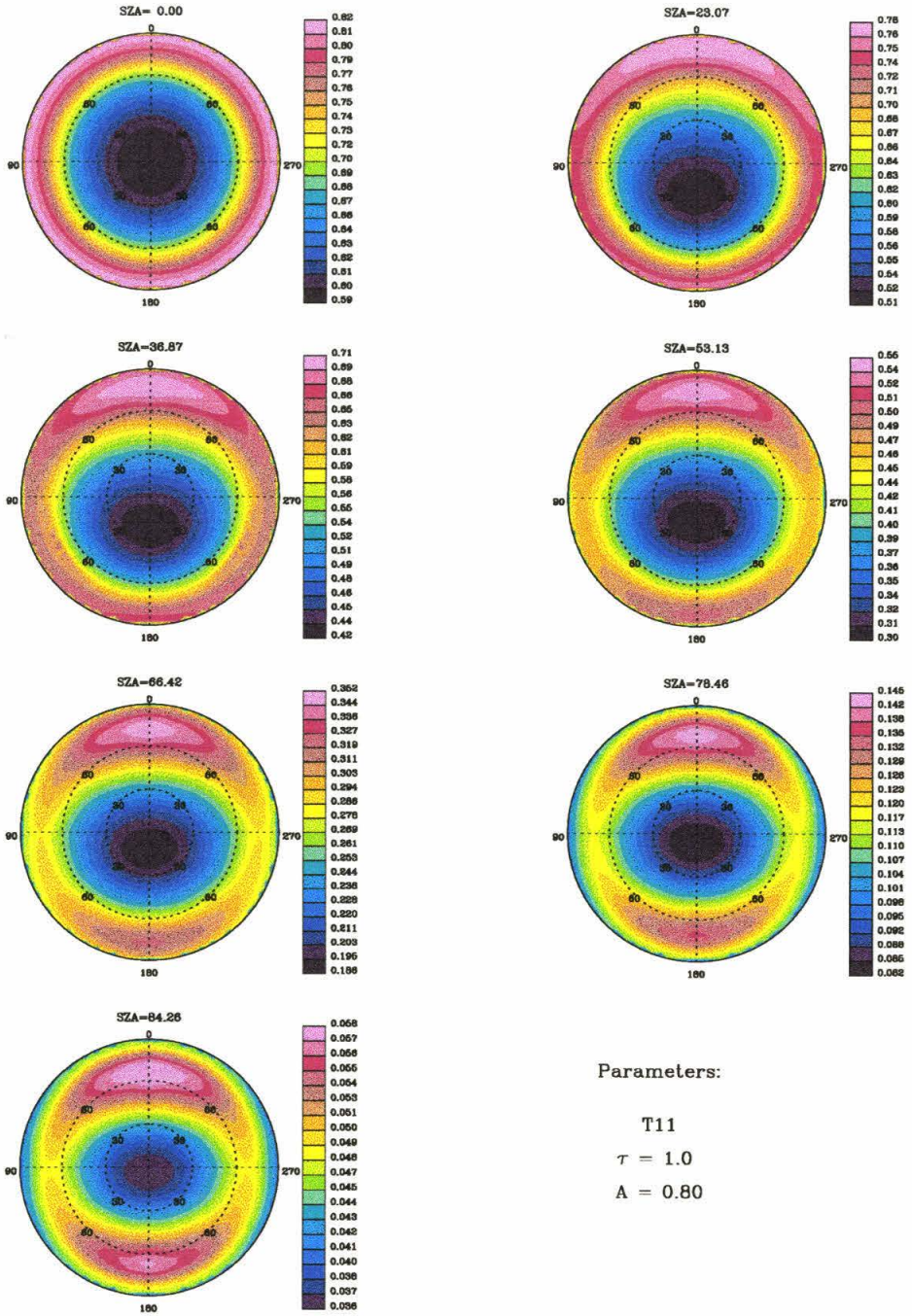

Figure A.5: Rayleigh scattering transmission T_{11} for optical depth $\tau = 1$ and albedo A=0.80 at solar zenith angle (SZA) 0°, 23.07°, 36.87°, 53.13°, 66.42°, 78.46°, 84.26°.

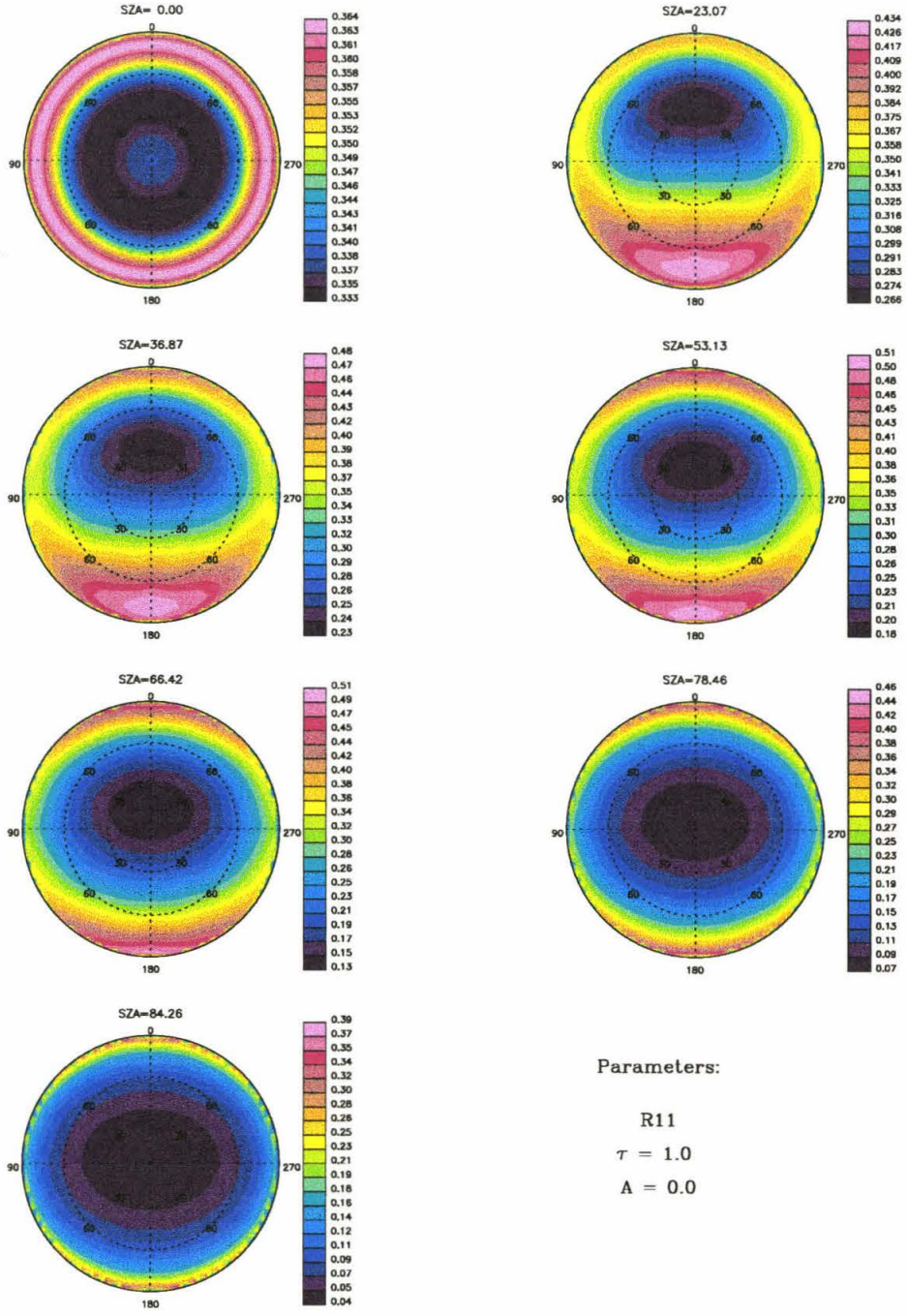

Figure A.6: Rayleigh scattering reflection R_{11} for optical depth $\tau = 1$ and albedo A=0.0 at solar zenith angle (SZA) 0°, 23.07°, 36.87°, 53.13°, 66.42°, 78.46°, 84.26°.

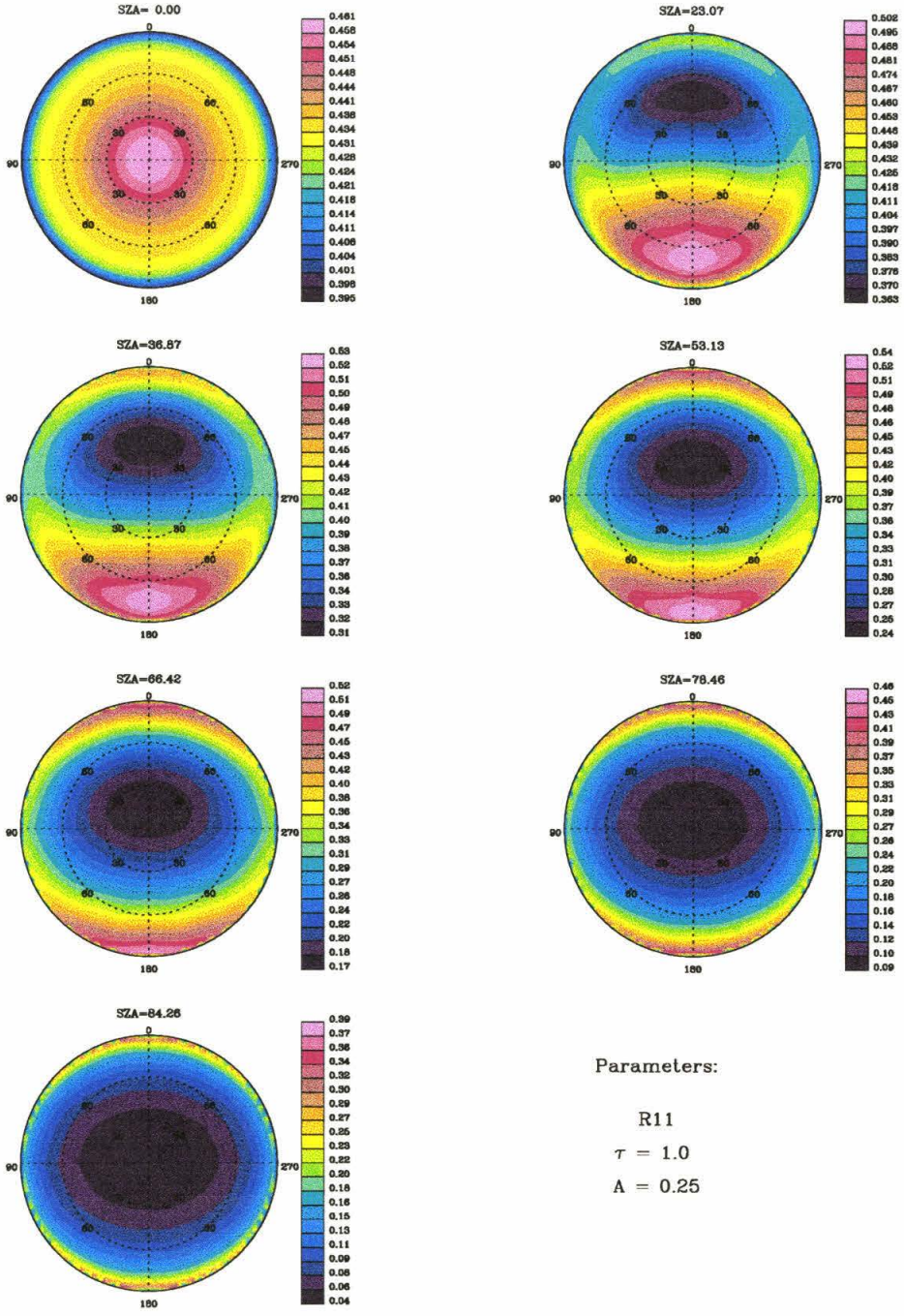

Figure A.7: Rayleigh scattering reflection R_{11} for optical depth $\tau = 1$ and albedo A=0.25 at solar zenith angle (SZA) 0°, 23.07°, 36.87°, 53.13°, 66.42°, 78.46°, 84.26°.

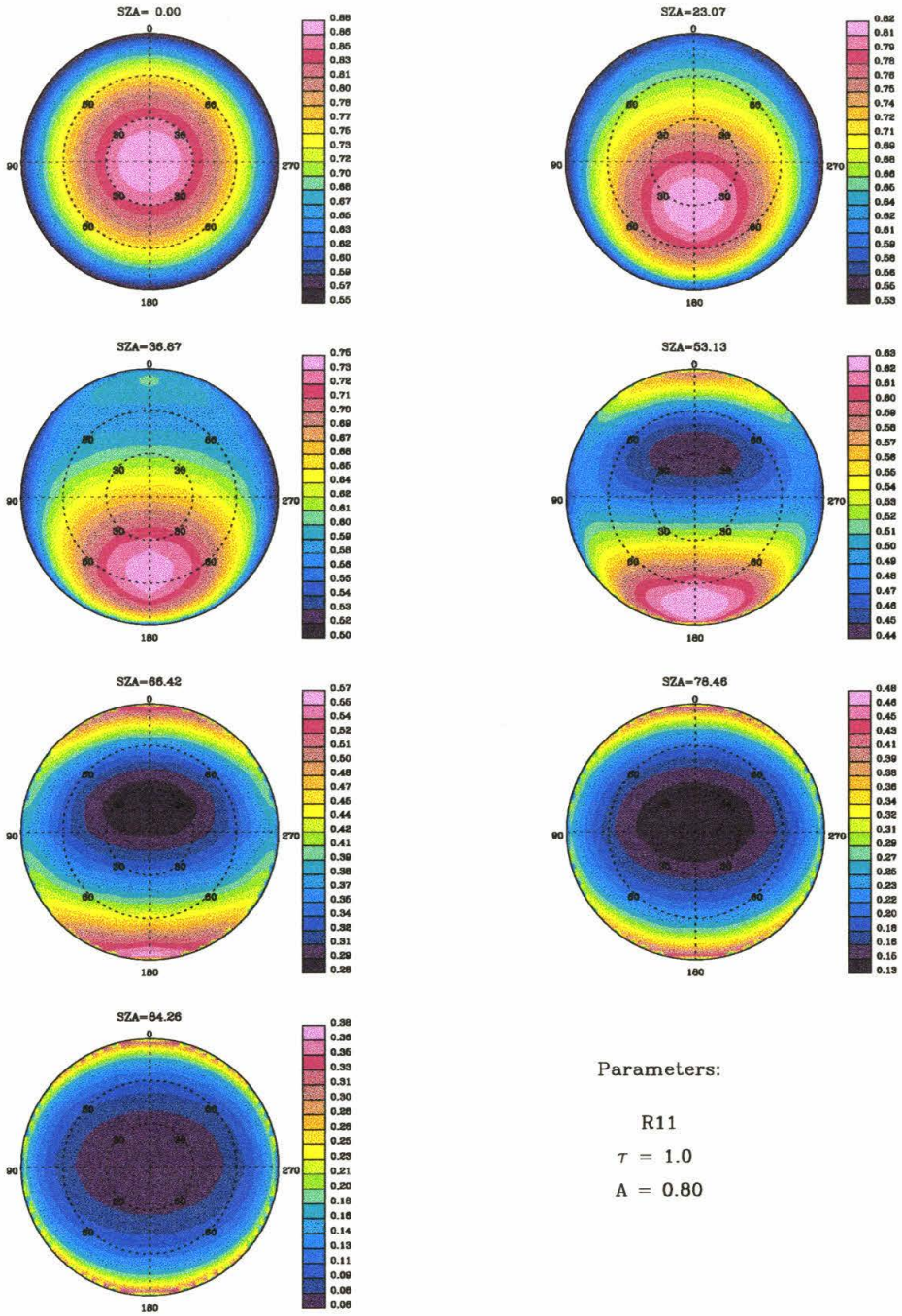

Figure A.8: Rayleigh scattering reflection R_{11} for optical depth $\tau = 1$ and albedo A=0.80 at solar zenith angle (SZA) 0°, 23.07°, 36.87°, 53.13°, 66.42°, 78.46°, 84.26°.

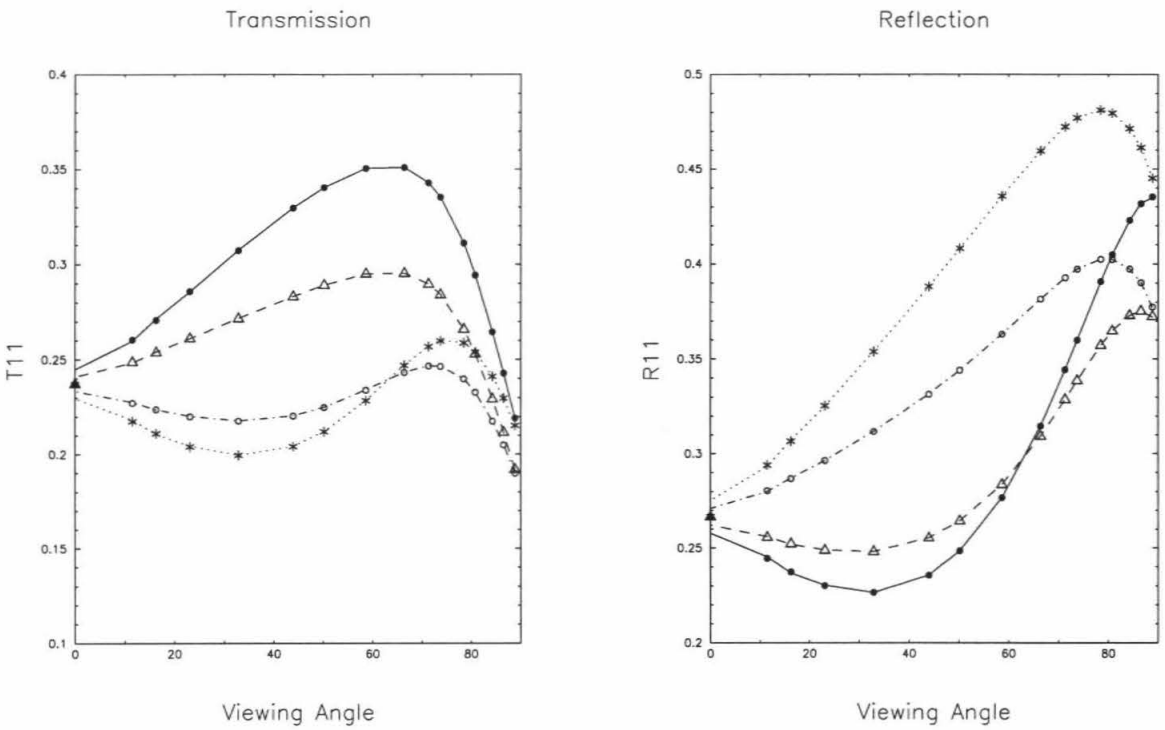

Figure A.9: Comparison of Intensity I between model (lines) and table (points) for optical depth $\tau = 1$, albedo A=0.0, solar zenith angle (SZA) 36.87° and azimuth angle 0° (solid line), 60° (dash line), 120° (dash-dot line), 180° (dotted line) respectively.

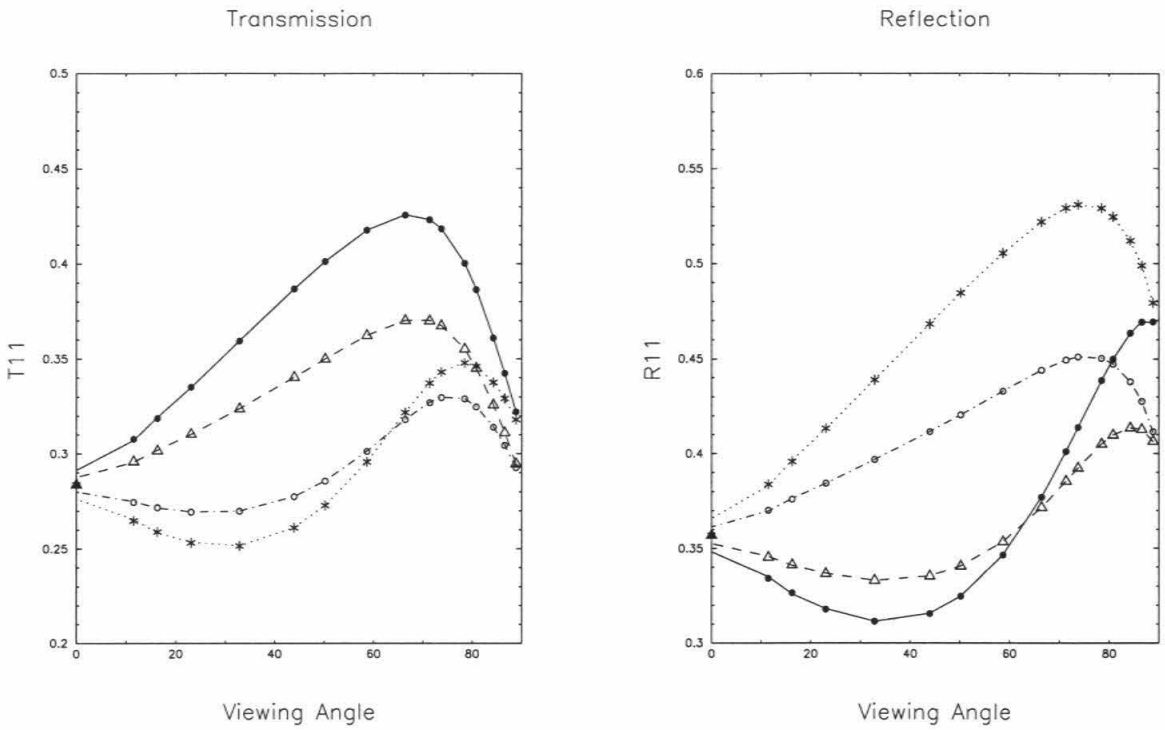

Figure A.10: Comparison of Intensity I between model (lines) and table (points) for optical depth $\tau = 1$, albedo A=0.25, solar zenith angle (SZA) 36.87° and azimuth angle 0° (solid line), 60° (dash line), 120° (dash-dot line), 180° (dotted line) respectively.

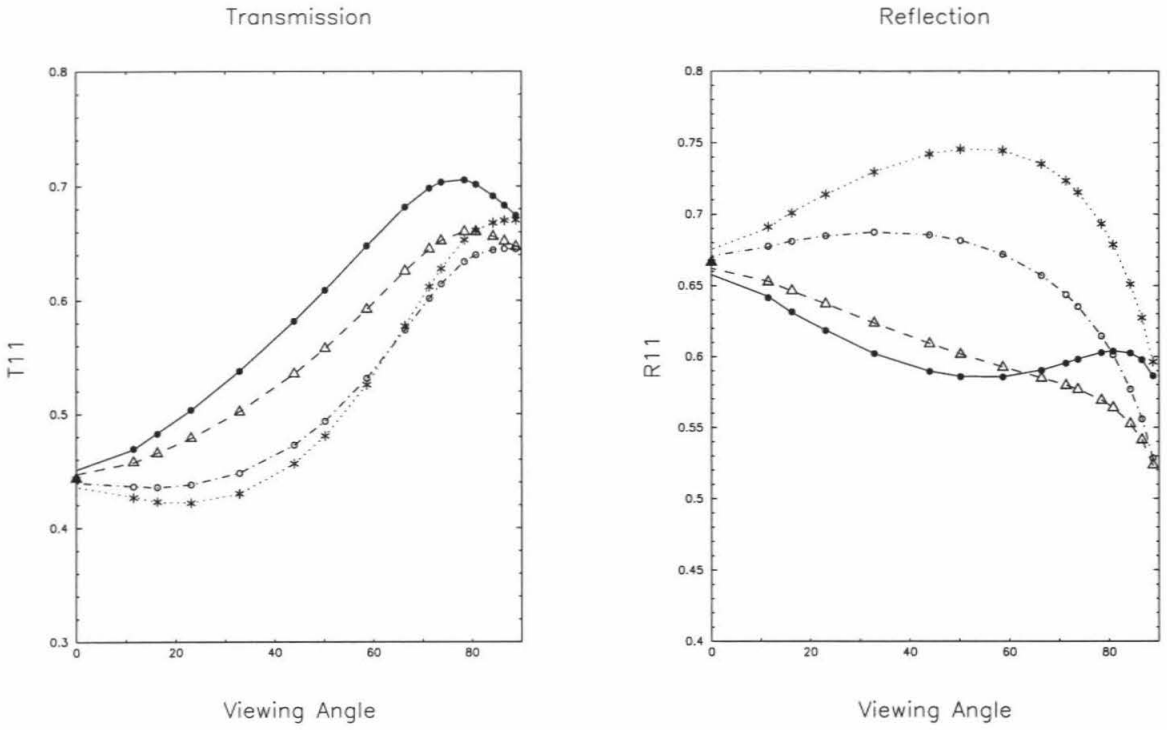

Figure A.11: Comparison of Intensity I between model (lines) and table (points) for optical depth $\tau = 1$, albedo A=0.80, solar zenith angle (SZA) 36.87° and azimuth angle 0° (solid line), 60° (dash line), 120° (dash-dot line), 180° (dotted line) respectively.

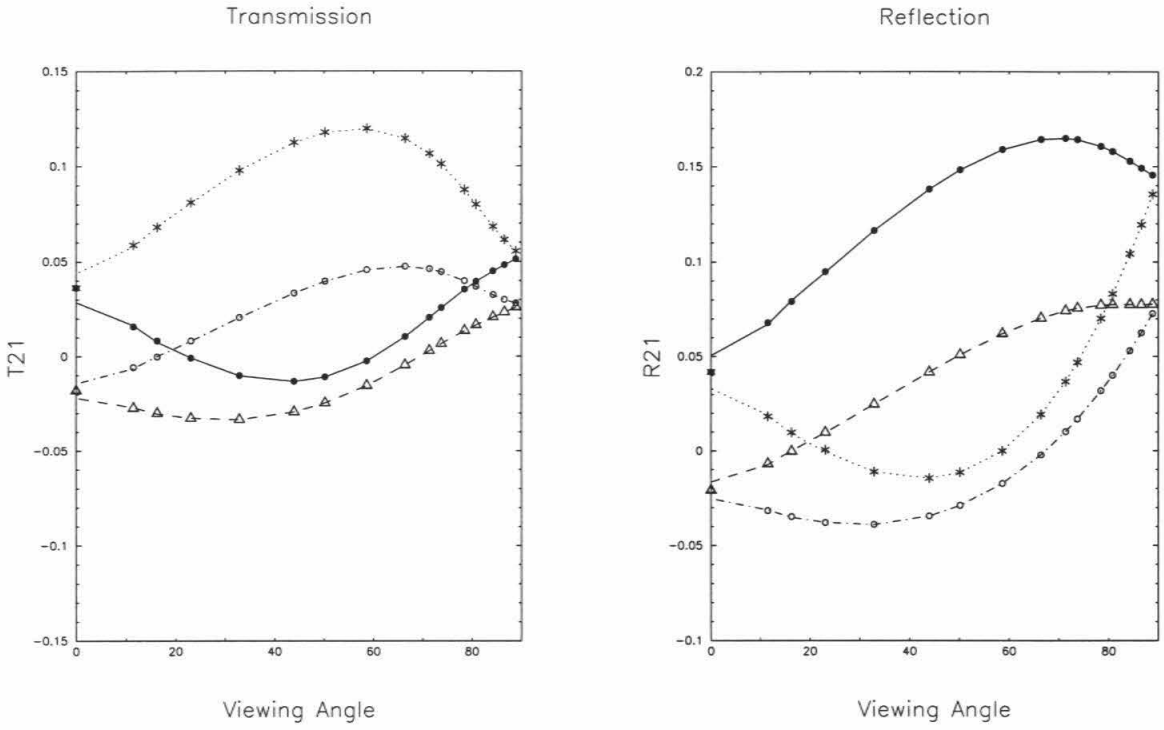

Figure A.12: Comparison of Stokes parameter Q between model (lines) and table (points) for optical depth $\tau = 1$, albedo A=0.0, solar zenith angle (SZA) 36.87° and azimuth angle 0° (solid line), 60° (dash line), 120° (dash-dot line), 180° (dotted line) respectively.

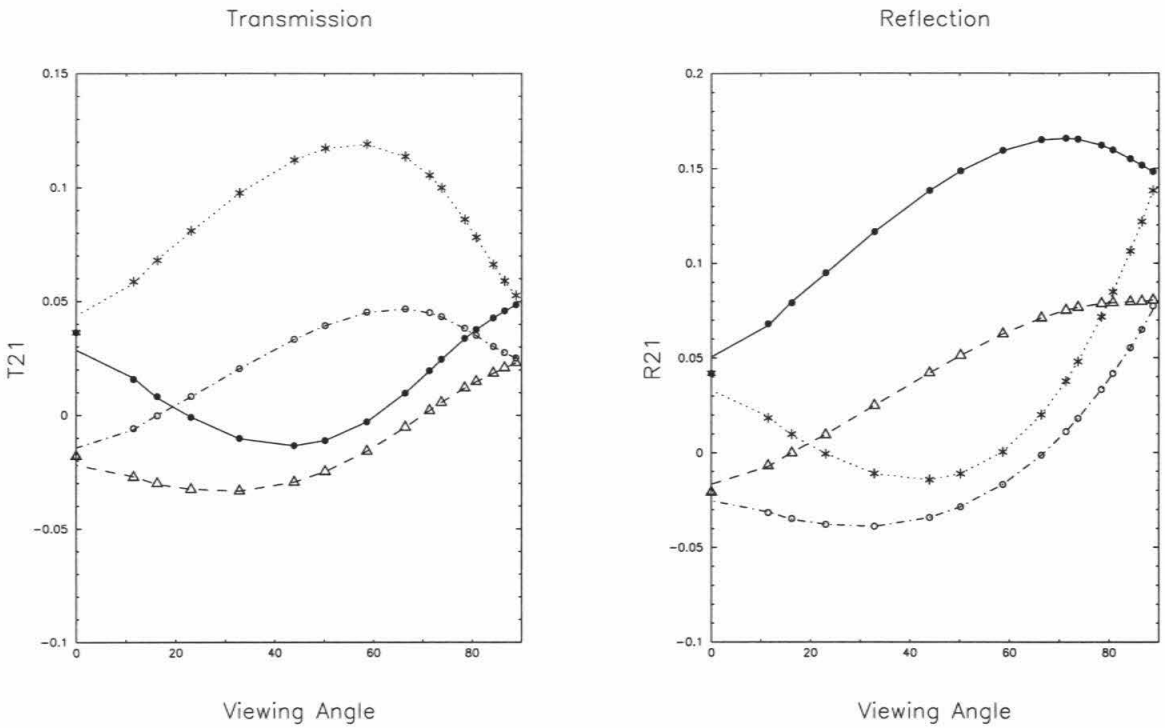

Figure A.13: Comparison of Stokes parameter Q between model (lines) and table (points) for optical depth $\tau = 1$, albedo A=0.25, solar zenith angle (SZA) 36.87° and azimuth angle 0° (solid line), 60° (dash line), 120° (dash-dot line), 180° (dotted line) respectively.

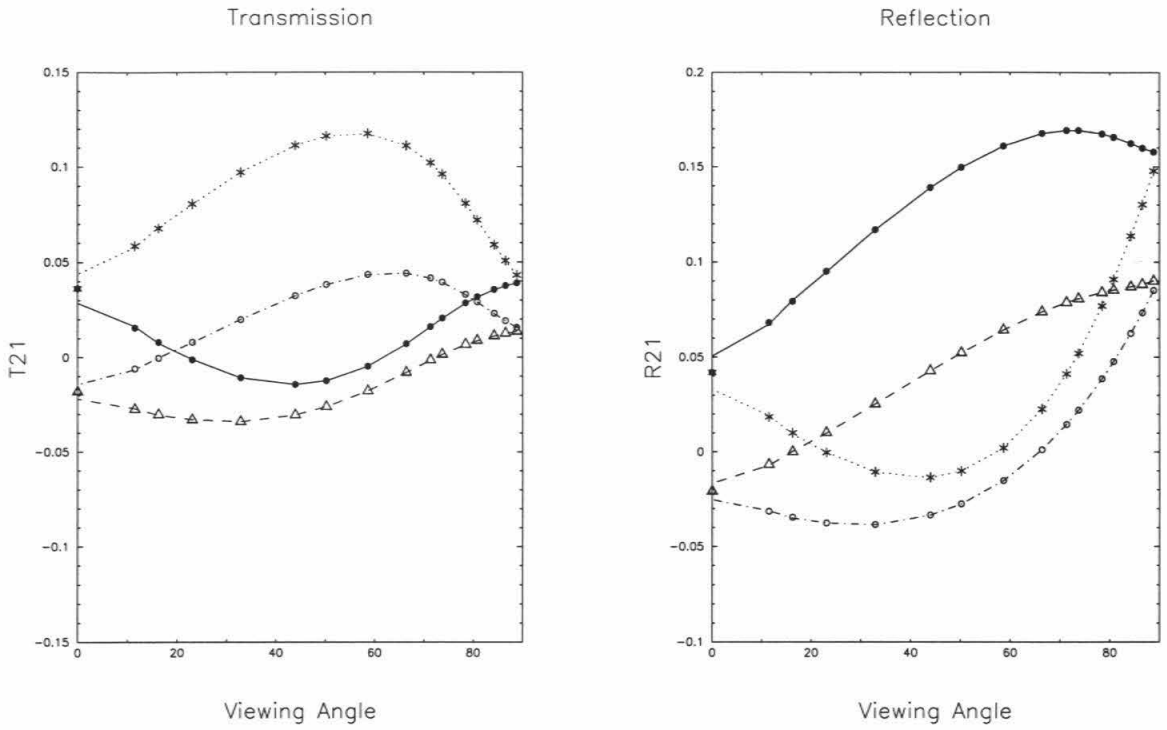

Figure A.14: Comparison of Stokes parameter Q between model (lines) and table (points) for optical depth $\tau = 1$, albedo A=0.80, solar zenith angle (SZA) 36.87° and azimuth angle 0° (solid line), 60° (dash line), 120° (dash-dot line), 180° (dotted line) respectively.

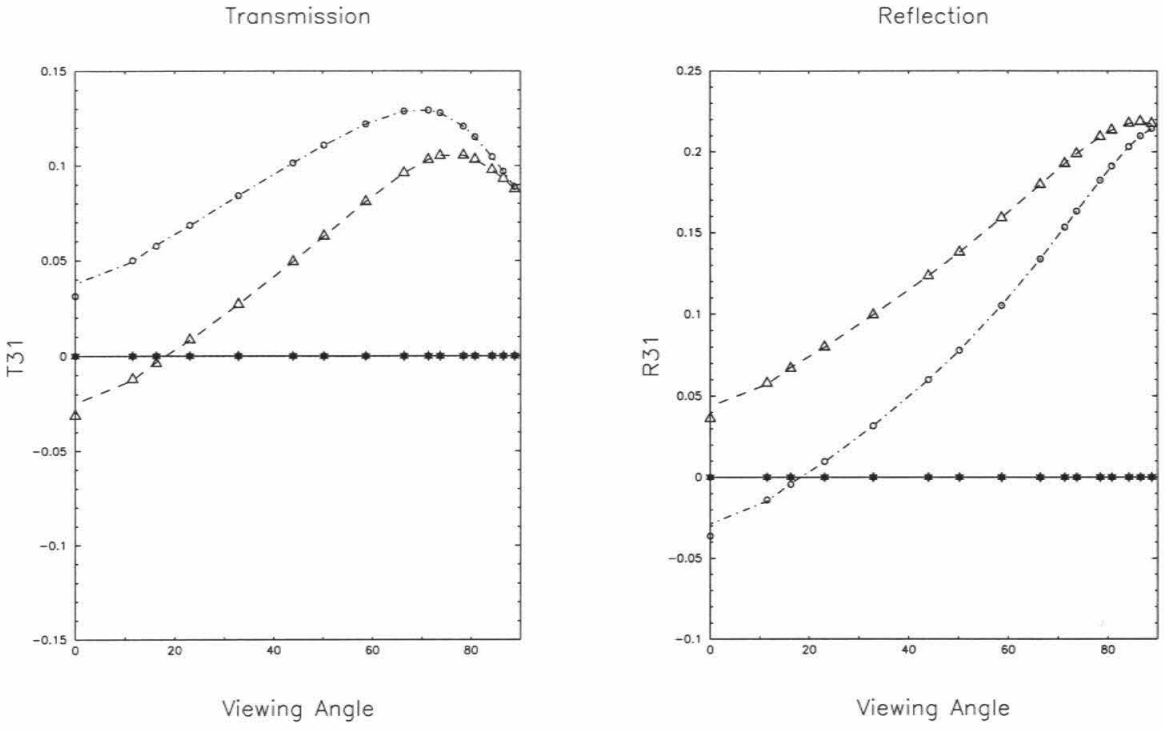

Figure A.15: Comparison of Stokes parameter U between model (lines) and table (points) for optical depth $\tau = 1$, albedo A=0.0, solar zenith angle (SZA) 36.87° and azimuth angle 0° (solid line), 60° (dash line), 120° (dash-dot line), 180° (dotted line) respectively.

Table A.2: Reflectivity Comparison: Comparison of model output with the results of Coulson *et al.* for a homogeneous Rayleigh atmosphere of optical depth of 1. The Solar flux is normalized to π, the cosine of the solar zenith angle is 0.8, and the ground albedo is 0.25 (it is 0.0 for U). The reflected radiance as a function of viewing angle μ for an azimuth of 60° is shown.

	Present Model			Coulson *et al.*		
μ	I	Q	U	I	Q	U
0.02000	0.40622	0.08048	0.21731	0.40653	0.08046	0.21758
0.10000	0.41356	0.07958	0.21761	0.41356	0.07957	0.21774
0.20000	0.40513	0.07866	0.20937	0.40504	0.07866	0.20946
0.32000	0.38553	0.07518	0.19277	0.38540	0.07519	0.19285
0.52000	0.35355	0.06258	0.15917	0.35342	0.06261	0.15923
0.72000	0.33541	0.04203	0.12351	0.33529	0.04208	0.12355
0.92000	0.33685	0.00972	0.07987	0.33661	0.00991	0.08011
0.98000	0.34585	-0.00721	0.05724	0.34534	-0.00676	0.05793
1.00000	0.35265	-0.01656	0.04376	0.35694	-0.02088	0.03626

troposphere due to the higher absorption cross section, therefore, the lack of higher multiple scattering in the troposphere will not smooth out the polarization. From this plot, it is clear that the light in the range 310 to 325 nm does not go through troposphere and the light in the range 325 to 345 nm has been multiple scattered in the troposphere.

Figures A.18 and A.19 show the transmitted and reflected specific intensity percentage change and linear polarization change relative to the reference atmosphere when tropospheric column ozone was decreased by 10 DU while A.20 and A.21 show the change when stratospheric column ozone was decreased by 10 DU. Again the intensity change in the reflected light is much higher than that in the transmitted light. There is not much difference in the intensity between tropospheric ozone change and

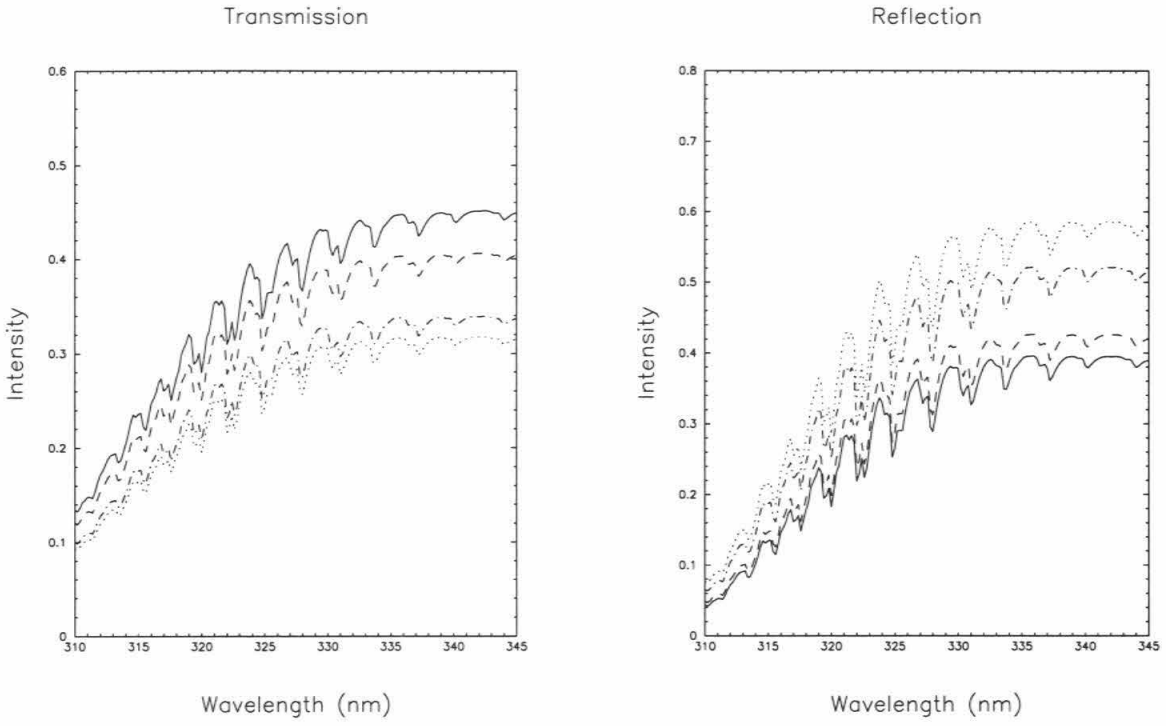

Figure A.16: Transmitted and reflected specific intensity when SZA and viewing angle are both 36.87° for the reference atmosphere at four azimuth angles 0° (solid line), 60° (dash line), 120° (dash-dot line) and 180° (dotted line).

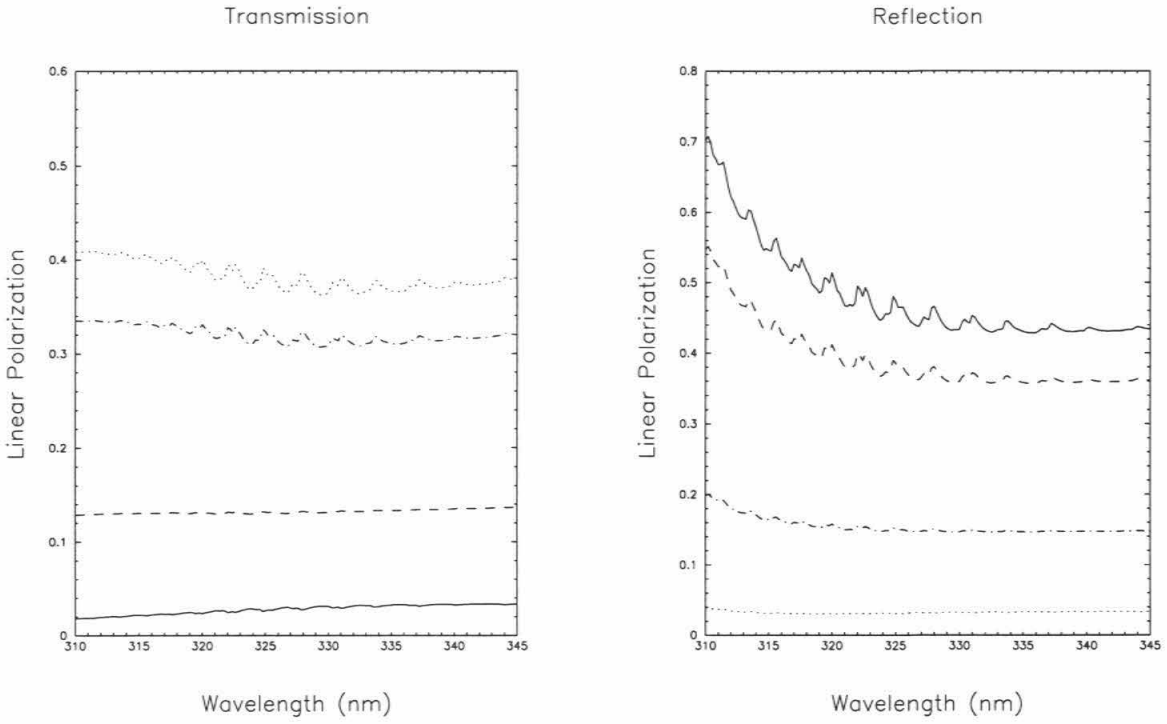

Figure A.17: Transmitted and reflected linear polarization when SZA and viewing angle are both 36.87° for the reference atmosphere at four azimuth angles 0° (solid line), 60° (dash line), 120° (dash-dot line) and 180° (dotted line).

stratospheric ozone change. In the transmitted light, the linear polarization does not change very much in the short and long wavelength region when the stratospheric column ozone was decreased by 10 DU. There is a maximum decrease in the middle of the Huggins band which is not understood yet. Meanwhile, there is a relatively larger change when the tropospheric column ozone was decreased by 10 DU with a increase when azimuth angle is less than 90° and decrease when azimuth angle is bigger than 90°. In the reflected light, the linear polarization has only decreased up to 0.01 for the shorter wavelength when the stratospheric column ozone was decreased by 10 DU while there is a significant decrease up to 0.02 when the tropospheric column ozone was decreased by 10 DU at azimuth angle 0°. The reason for the decrease of linear polarization following the decrease of column ozone is simple. The light is less absorbed as the ozone is decreased, therefore, there is higher probability that the light will be scattered by atmosphere to smooth out the polarization. The decrease of tropospheric ozone is more efficient in decreasing the polarization as shown in these figures.

A.7 Conclusions

We have described and developed a multi-layer radiative transfer model with the state of polarization fully taken into account by using the doubling-adding method. Excellent agreement was found when we compared the model results with those obtained from Coulson *et al.* (1960). The model is designed for passive atmospheric remote sensing applications, whether reflection or transmission based. Preliminary runs from this model in the Huggins bands show the distinct features of linear polarization in

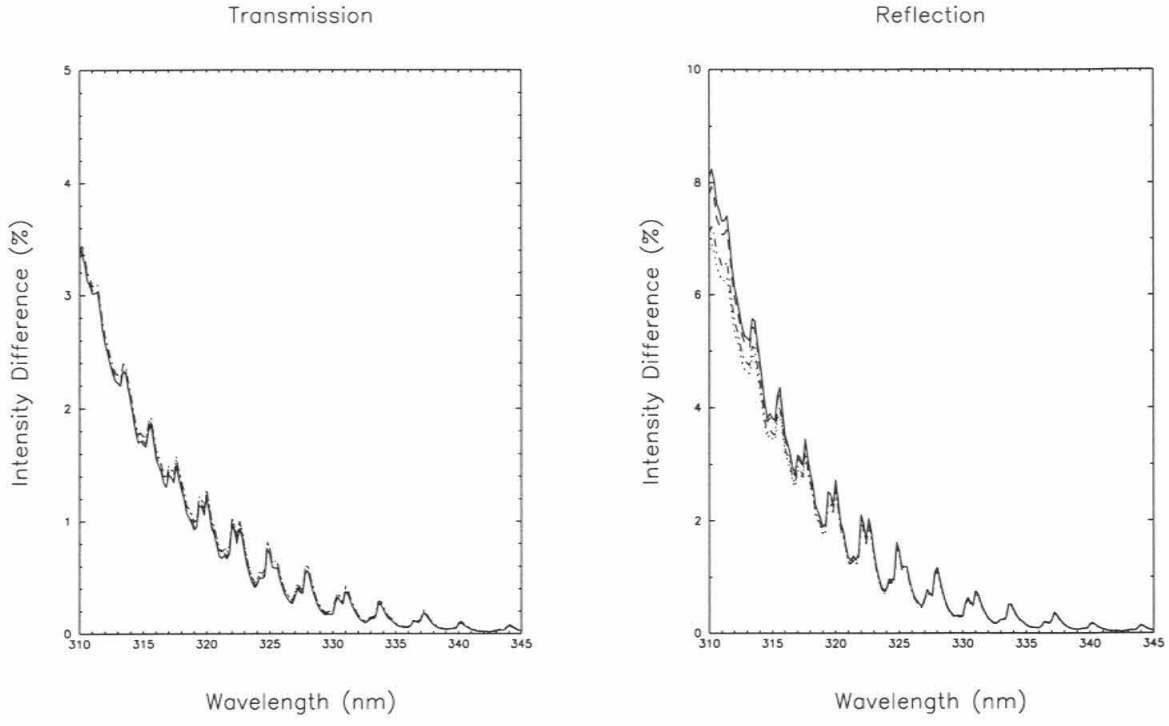

Figure A.18: Transmitted and reflected specific intensity percentage change relative to the reference atmosphere when tropospheric column ozone was decreased by 10 DU at four azimuth angles 0° (solid line), 60° (dash line), 120° (dash-dot line) and 180° (dotted line). The SZA and viewing angle are both 36.87°.

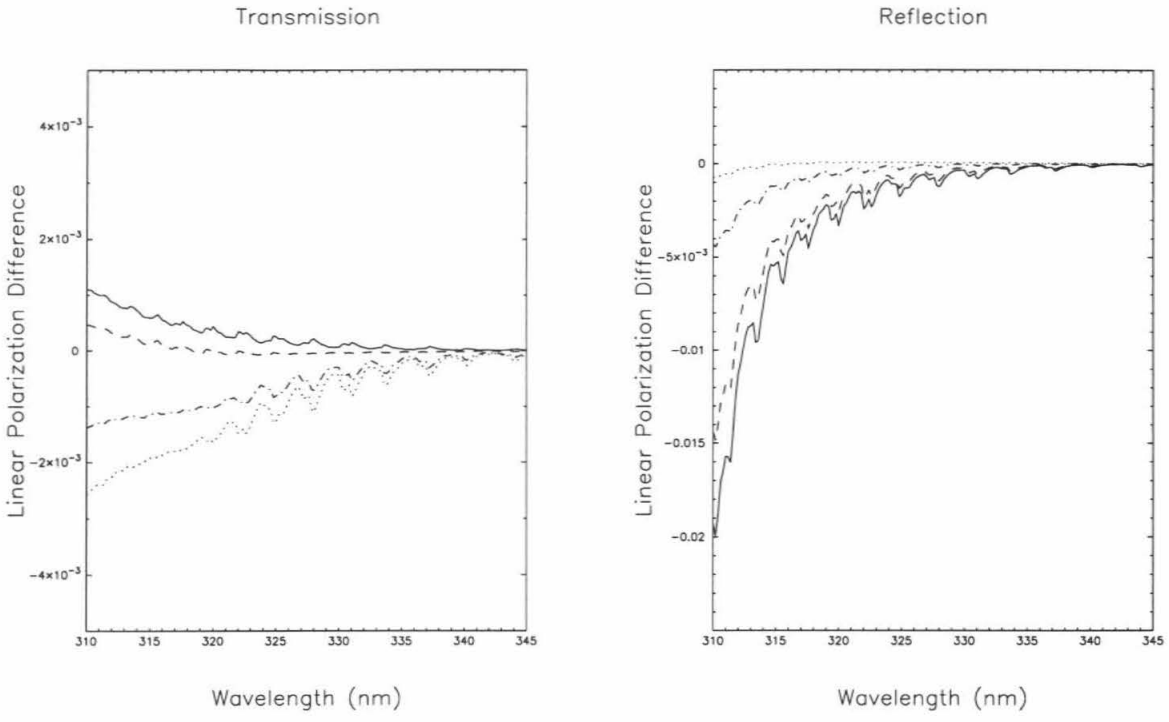

Figure A.19: Transmitted and reflected linear polarization change relative to the reference atmosphere when tropospheric column ozone was decreased by 10 DU at four azimuth angles 0° (solid line), 60° (dash line), 120° (dash-dot line) and 180° (dotted line). The SZA and viewing angle are both 36.87°.

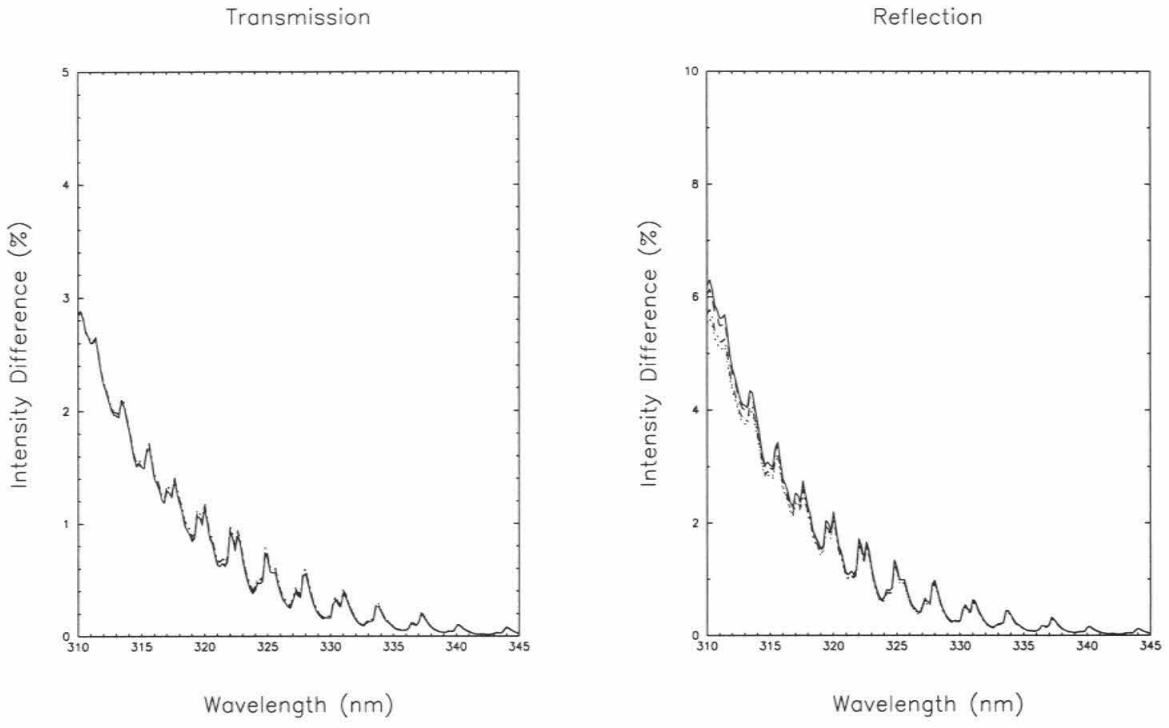

Figure A.20: Transmitted and reflected specific intensity percentage change relative to the reference atmosphere when stratospheric column ozone was decreased by 10 DU at four azimuth angles 0° (solid line), 60° (dash line), 120° (dash-dot line) and 180° (dotted line). The SZA and viewing angle are both 36.87°.

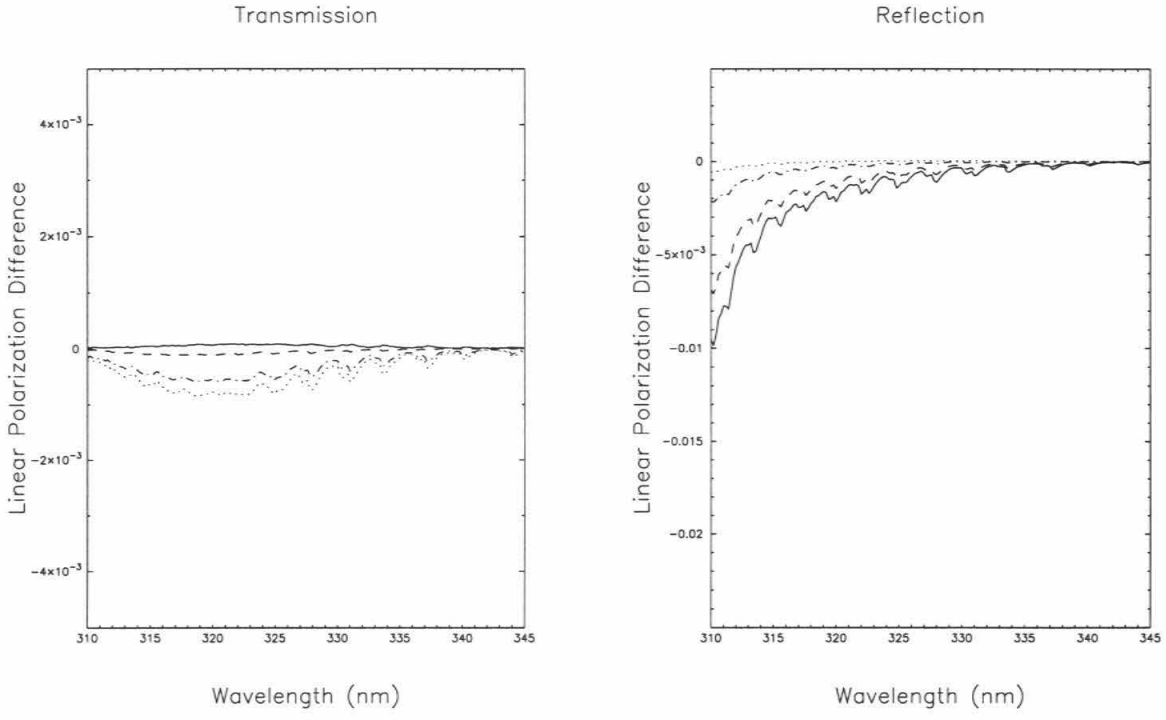

Figure A.21: Transmitted and reflected linear polarization change relative to the reference atmosphere when stratospheric column ozone was decreased by 10 DU at four azimuth angles 0° (solid line), 60° (dash line), 120° (dash-dot line) and 180° (dotted line). The SZA and viewing angle are both 36.87°.

the reflection spectrum due to the multiple Rayleigh scattering in the troposphere. Further study will be continued in order to find the signal from the troposphere ozone.

A.8 Acknowledgements

We would like to express our appreciation to Larry D. Travis for sending his one layer doubling-adding model to us. This work was supported principally by NASA grant NAGW 2204 to the California Institute of Technology and was carried out there and at JPL, under contract with NASA.

A.9 References

Chandrasekhar, S., Radiative transfer, Clarendon Press, London (1950).

Coffeen, D. L., and J. E. Hansen, in T. Gehrels (ed.), Planets, stars and nebulae studied with photopolarimetry, Univ. Arizona Press, Tucson, p. 518.

Coulson, K. L., J. V. Dave, and Z. Sekera, Tables related to radiation emerging from a planetary atmosphere with Rayleigh scattering, University of California Press, Berkeley & Los Angeles, CA (1960).

Dave, J. V., Multiple scattering in a non-homogeneous, Rayleigh atmosphere, *J. Atmos. Sci.* **22**, 273-279 (1965).

Demerjian, K. L., K. L. Schere, and J. T. Peterson, Theoretical estimates of actinic (spherically integrated) flux and photolytic rate constants of atmospheric species in the lower troposphere, *Adv. Environ. Sci. Tech.* **10**, 369 (1980).

Evans, K. F., and G. L. Stephens, A new polarized atmospheric radiative transfer model, *J. Quant. Spectrosc. Radiat. Transfer* **46**, 413-423 (1991).

Hansen, J. E., Multiple scattering of polarized light in planetary atmospheres, Part I. The doubling method, *J. Atmos. Sci.* **28**, 120-125 (1971).

Hansen, J. E., and L. D. Travis, Light scattering in planetary atmospheres, *Space Science Reviews* **16**, 527 (1974).

Hovenier, J. W., Multiple scattering of polarized light in planetary atmospheres, *Astron. & Astrophys.* **13**, 7-29 (1971).

Jiang, Y., Y. L. Yung, and S. P. Sander, Modeling of atmospheric radiation in the O_3 Huggins bands, *J. Quant. Spectrosc. Radiat. Transfer*, in press (1996).

Lacis, A. A., and J. E. Hansen, A parameterization for the absorption of solar radiation in the Earth's atmosphere, *J. Atmos. Sci.* **31**, 118-133 (1974).

Malicet, J., D. Daumont, J. Charbonnier, C. Parisse, A. Chakir, and J. Brion, Ozone UV spectroscopy. II. absorption cross-sections and temperature dependence, *J. Atmos. Chem.* **21**, 263 (1995).

Michelangeli, D. V., M. Allen, Y. L. Yung, R. L. Shia, and D. Crisp, Enhancement of atmospheric radiation by an aerosol layer, *J. Geophys. Res.* **97**, 865 (1992).

Mishchenko, M. I., A. A. Lacis, and L. D. Travis, Errors induced by the neglect of polarization in radiance calculations for Rayleigh-scattering atmosphere, *J. Quant. Spectrosc. Radiat. Transfer* **51**, 491 (1994)

van de Hulst, H. C., Light scattering by small particles, New York, Wiley, 470pp (1957).

van de Hulst, H. C., Multiple scattering in planetary atmospheres, *J. Quant. Spectrosc. Radiat. Transfer* **11**, (1971).

van de Hulst, H. C., Multiple light scattering, Academic Press, New York, NY (1980).

Wauben, W. M. F., J. F. de Haan, and J. W. Hovenier, A method for computing visible and infrared polarized monochromatic radiation in planetary atmospheres, *Astron. Astrophys.* **282**, 277-290 (1994)